Fetal programming of adipocyte development by exposure to an obesogenic intrauterine milieu

Inaugural-Dissertation

zur Erlangung des Doktorgrades
der Mathematisch-Naturwissenschaftlichen Fakultät
der Heinrich-Heine-Universität Düsseldorf

vorgelegt von

Marten Schouwink
aus Moers

Düsseldorf, Juni 2024

aus dem Institut für Molekulare Ernährung,
Klinik für Allgemeine Pädiatrie, Neonatologie und Kinderkardiologie,
Universitätsklinikum Düsseldorf, Medizinische Fakultät an der
Heinrich-Heine-Universität Düsseldorf

Gedruckt mit der Genehmigung der
Mathematisch-Naturwissenschaftlichen Fakultät der
Heinrich-Heine-Universität Düsseldorf

Berichterstatter:

1. Herr Univ.-Prof. Dr. rer. nat. Hadi Al-Hasani

2. Frau Univ.-Prof. Dr. med. Regina Ensenauer

Tag der mündlichen Prüfung: 16.12.2024

Table of contents

Abstract

The escalating prevalence of overweight and obesity, affecting 55% of women and 67% of men, and up to 38% and up to 40% of girls and boys aged 5-19 years in high-income western countries, respectively, underscores a pressing public health concern with profound implications for future generations. Maternal factors such as gestational weight gain, gestational diabetes mellitus, and increased pre-pregnancy weight negatively affect offspring health. Furthermore, previous studies on mouse models of our research group revealed sex-specific impacts of maternal obesity on adipose tissue development, with disturbances, particularly in females. Processes that cause these effects are called *fetal programming* and include epigenetic alterations like DNA methylation.

This thesis aims to study underlying mechanisms by which the intrauterine obesogenic environment influences offspring adipocyte development focusing on embryonic female adipocytes. Utilizing an NMRI mouse model for maternal obesity in pregnancy established in our group, *ex vivo* differentiated E13.5 mouse embryonic fibroblasts were analyzed regarding their adipogenic differentiation capacity, transcriptome, proteome, and methylome. Subsequently, candidate genes' role in adipogenesis was investigated *in vitro* in the 3T3-L1 preadipocyte cell line using RNA interference-mediated knockdown.

Maternal obesity during pregnancy altered female fetal adipocytes' transcriptome, proteome, and methylome, affecting genes and proteins associated with regulating commitment to the adipogenic lineage and lipid metabolism. Transcriptomic analysis revealed a downregulation of several genes including aldehyde dehydrogenase family 1 subfamily A7 (Aldh1a7) in female fetal adipocytes by maternal obesity. Remarkably, analysis of the time course of expression and knockdown experiments during adipogenic differentiation uncovered *Aldh1a7* as a novel regulator of adipogenesis and showed its downregulation in female adipose tissue also in adulthood.

These findings highlight the early onset of maternal obesity's impact on female offspring adipocyte development, predisposing offspring to adverse fat tissue development, obesity, and long-term adverse health consequences. In this context, the identification of targets such as *Aldh1a7* offers avenues for intervention such as nutritional modifications to alleviate the intergenerational transmission of metabolic dysfunction associated with maternal obesity. In conclusion, this thesis supports the development of preventive interventions aimed at improving health development of future generations by further understanding the intricate sex specific molecular mechanisms underlying adipocyte development and dysregulation in the context of maternal obesity.

Zusammenfassung

Die rasant zunehmende Prävalenz von Übergewicht und Adipositas, von der 55% der Frauen und 67% der Männer sowie bis zu 38% beziehungsweise 40% der Mädchen und Jungen im Alter von 5-19 Jahren in westlichen Ländern mit hohem Einkommen betroffen sind, unterstreicht ein dringendes Problem für die öffentliche Gesundheit mit weitreichenden Folgen für künftige Generationen. Mütterliche Faktoren wie Gewichtszunahme während der Schwangerschaft, Schwangerschaftsdiabetes und ein erhöhtes Gewicht vor der Schwangerschaft wirken sich nachteilig auf die Gesundheit der Kinder aus. Darüber hinaus ergaben frühere Studien an Mausmodellen aus unserer Arbeitsgruppe geschlechtsspezifische Auswirkungen der mütterlichen Adipositas auf die Entwicklung des Fettgewebes insbesondere in weiblichen Nachkommen. Die Prozesse, die diese Auswirkungen verursachen, werden als fetale Programmierung bezeichnet und umfassen unter anderem epigenetische Veränderungen wie die DNA-Methylierung.

Ziel dieser Arbeit ist es, die zugrundeliegenden Mechanismen zu untersuchen, durch die eine intrauterine adipogene Umgebung die Adipozytenentwicklung der Nachkommen beeinflusst. Dabei liegt der Schwerpunkt auf embryonalen weiblichen Adipozyten. Unter Verwendung eines in unserer Arbeitsgruppe etablierten NMRI-Mausmodells für mütterliche Adipositas während der Schwangerschaft wurden e*x vivo* differenzierte E13.5 embryonale Fibroblasten der Maus bezüglich ihrer adipogenen Differenzierungskapazität und ihres Transkriptoms, Proteoms und Methyloms analysiert. Anschließend wurde die Rolle der Kandidatengene bei der Adipogenese weitergehend untersuchen, indem *in vitro* RNA Interferenz vermittelte Knockdown-Experimente in der 3T3-L1 Präadipozyten-Zelllinie durchgeführt wurden.

Mütterliche Adipositas während der Schwangerschaft veränderte das Transkriptom, das Proteom und das Methylom der fötalen weiblichen Adipozyten der Nachkommen, wobei insbesondere Gene und Proteine betroffen sind, die mit der Regulierung der Commitment-Phase der Adipogenese und dem Fettstoffwechsels in Verbindung stehen. Transkriptomische Analysen ergaben neben der Dysregulation anderer Gene eine Herunterregulation der Aldehyd-Dehydrogenase-Familie 1 Unterfamilie A7 *(Aldh1a7)* durch mütterliche Adipositas in weiblichen fötalen Adipozyten. Die Untersuchungen zur mRNA Expression und Knockdown-Experimente während der Adipogenese enthüllten *Aldh1a7* als neuartigen Regulator der Adipogenese und zeigten, dass er auch im adulten weiblichen Fettgewebe herabreguliert ist.

Diese Ergebnisse verdeutlichen, dass sich die mütterliche Adipositas schon früh auf die Entwicklung der Adipozyten der weiblichen Nachkommen auswirkt und diese zu einer ungünstigen Entwicklung des Fettgewebes führt, und für Fettleibigkeit prädisponiert, was sich langfristig negativ auf die Gesundheit auswirkt. In diesem Zusammenhang bietet die Identifizierung von Zielgenen wie *Aldh1a7* Möglichkeiten zur präventiven Intervention zum

Beispiel mittels nutritiver Modifikationen, um die intergenerationale Weitergabe von Stoffwechselstörungen im Zusammenhang mit mütterlicher Fettleibigkeit zu verringern. Insgesamt tragen die Ergebnisse dieser Arbeit dazu bei, das Design präventiver Strategien zur Verbesserung der gesundheitlichen Entwicklung künftiger Generationen zu unterstützen, indem die komplexen geschlechtsspezifischen molekularen Mechanismen, die der Entwicklung und Dysregulation von Adipozyten im Zusammenhang mit mütterlicher Adipositas zugrunde liegen, weiter aufgeklärt werden.

1 Introduction

1.1 The role of adipose tissue in obesity and diabetes mellitus

1.1.1 Metabolic diseases: overweight, obesity, and diabetes mellitus

Overweight and obesity are defined by an increase in body mass index (BMI). BMI is calculated by dividing the body weight by the squared height. The World Health Organization (WHO) defines BMI cutoffs for the diagnosis of overweight (BMI 25-29.9 kg/m²) and obesity (BMI ≥ 30 kg/m²) in adults. In children, overweight and obesity are diagnosed using the BMI z-score, which defines age- and sex-dependent cutoffs using the standard deviation of WHO growth standards (Gomes et al., 2022). Overweight is defined as a BMI-for-age between 2 and 3 (age 0-4 years) or 1 and 2 (age 5-19 years) standard deviations of the respective WHO growth standards. Likewise, obesity is defined as a BMI-for-age 3 (age 0-5 years) and 2 (age 5-19 years) standard deviations above the respective WHO growth standards (World Health Organization, 2023).

The number of patients suffering from overweight and obesity has risen from 43.5% and 54.5% in 1990 to 56.3% and 67.0% in 2022 of women and men in high-income western countries, respectively, having overweight or obesity (Phelps et al., 2024). The prevalence of overweight and obesity in children is increasing too from 21% - 29% and 20% - 30% in 1990 to 27% - 38% and 29% - 40% in 2022 of girls and boys aged 5-19 years in high-income western countries, respectively. Furthermore, increased BMI during childhood increases the risk of suffering from overweight or obesity in adolescence and adulthood (Riedel et al., 2014; Simmonds et al., 2016). This leads to over 1 billion patients (men: 374 million; women: 504 million; boys: 94 million, girls: 65 million) worldwide having obesity, and according to estimations a high BMI, a high BMI contributed to 4 million deaths globally in 2015, mainly by contributing to cardiovascular disease and diabetes mellitus (Afshin et al., 2017; Phelps et al., 2024).

Diabetes mellitus is a chronic disease characterized by increased blood glucose levels caused by deficient insulin secretion, insulin action, or a combination of both. There are more than 530 million people affected by type 1 (T1D) or type 2 diabetes mellitus (T2D) worldwide (International Diabetes Federation, 2021) and approximately 12 per 100 000 11- to 18-year-old children are suffering from T2D in Germany to date (Rosenbauer et al., 2019). Overall, diabetes is categorized into T1D, T2D, and gestational diabetes mellitus (GDM) depending on disease etiology (World Health Organization, 2023). While T1D is caused by an autoimmune reaction leading to insulin deficiency, T2D results from insulin resistance or insulin deficiency mostly associated with overweight or obesity (Committee, 2021). Lastly, GDM is defined as increased fasting blood glucose or glucose intolerance first recognized during pregnancy. However, diabetes mellitus is a very heterogeneous disease with differing disease progressions and pathologies. Therefore, recent research used data-driven clustering of

common disease parameters to postulate a new classification of adult-onset diabetes into five different groups instead of the former classification into T1D and T2D (Ahlqvist et al., 2018). These new classification clusters are reproducible in different cohorts and can allow better and more precise treatment of patients with diabetes mellitus in the future (Ahlqvist et al., 2018).

1.1.2 Body weight regulation

The brain tightly regulates energy intake and expenditure to keep body weight constant by integrating feedback signals from different peripheral organs (Jais & Brüning, 2022). As depicted in Figure 1, ghrelin, glucagon-like peptide 1 (GLP-1), cholecystokinin (CCK), leptin, adiponectin and insulin act on the brain, specifically the hypothalamic arcuate nucleus and influence the balance between energy intake and expenditure (Friedman, 2019; Könner et al., 2007; Suyama et al., 2016; Wang et al., 2014). Leptin is secreted by adipose tissue and its circulating concentrations positively correlate with adipose tissue mass (Friedman, 2019). It is a key regulator of body weight inhibiting energy intake via its action on both pro-opiomelanocortin (POMC) and agouti-related protein (AGRP) neurons in a negative feedback loop in times of increased energy availability and storage in adipose tissue. Similarly, insulin is secreted by the pancreatic beta cells, and suppresses food intake via POMC and AGRP neurons (Könner et al., 2007). Adiponectin's impact on the energy balance depends on the glucose concentration as it inhibits food intake in a high-glucose brain environment and increases it in a low-glucose environment (Suyama et al., 2016). Furthermore, circulating ghrelin levels are constantly rising until food is consumed and decrease afterward (Spiegel et al., 2011). Hence, it is proposed as a hunger signal influencing AGRP neurons in the arcuate nucleus promoting energy intake (Wang et al., 2014). Lastly, GLP-1 and CCK are both increasingly secreted by the intestine during meals and act as a satiety signal on the brain reducing food intake (Andermann & Lowell, 2017; Müller et al., 2019; Steinert et al., 2017). However, in individuals with obesity, disturbances in body weight regulation are evident, marked by both leptin and insulin resistance as well as altered neuroplasticity and neuronal circuitry (Friedman, 2019; Heni, 2024; Matikainen-Ankney & Kravitz, 2018).

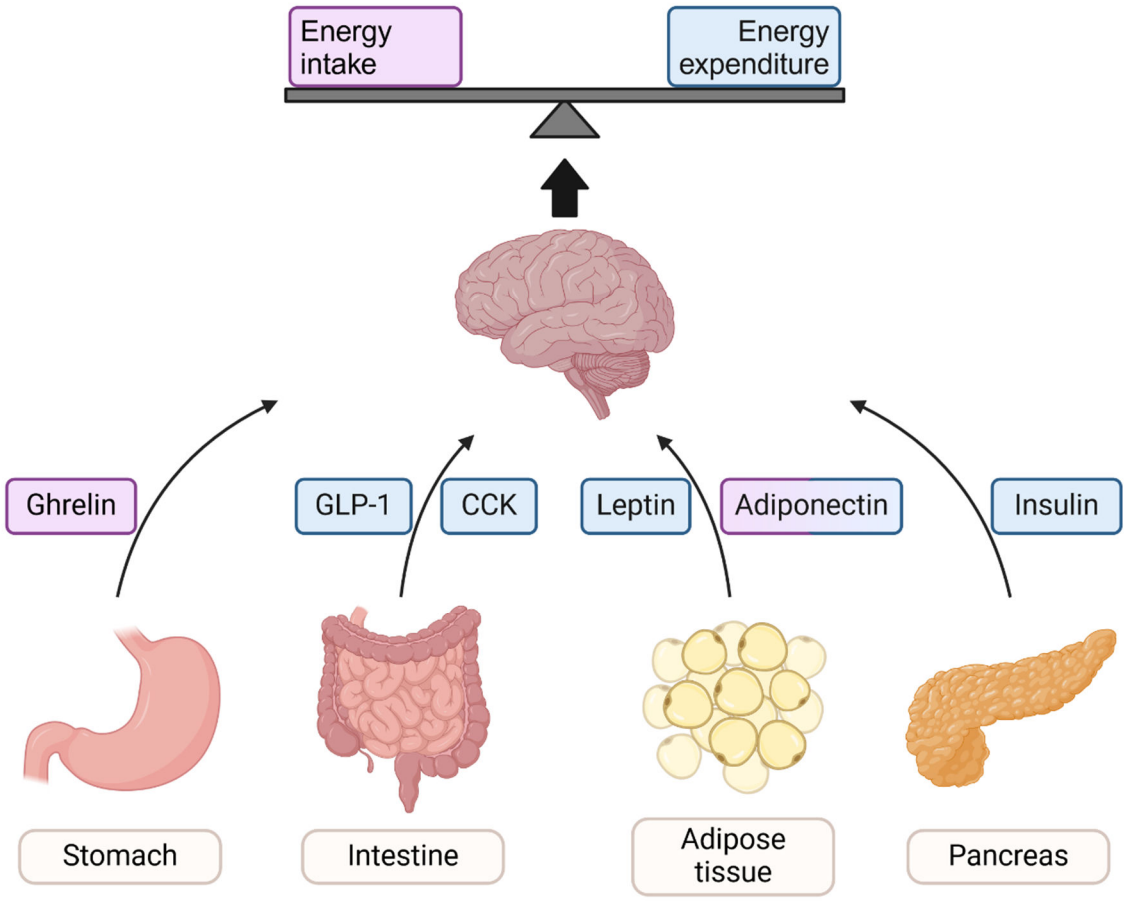

Figure 1: Simplified illustration of body weight regulation.
The brain tightly regulates body weight impacted by signaling molecules like ghrelin, glucagon-like peptide 1 (GLP-1), cholecystokinin (CCK), leptin, adiponectin, and insulin secreted from different peripheral organs. While ghrelin promotes energy intake, GLP-1, CCK, leptin, and insulin inhibit it, thereby benefitting energy expenditure. Depending on glucose concentration, adiponectin either promotes (low glucose) or inhibits (high glucose) energy intake. Signaling molecules that promote food intake are displayed in purple, while those that inhibit food intake or increase energy expenditure are displayed in blue. M. Schouwink generated this figure based on (Barsh & Schwartz, 2002). Created with BioRender.com.
GLP-1 = Glucagon-like peptide 1; CCK = Cholecystokinin

1.1.3 The genetic background of obesity

Past research investigating the genetic background of obesity revealed 19 monogenetic obesity-associated syndromes like Bardet-Biedl syndrome and Prader-Willi syndrome and further non-syndromic monogenetic forms of obesity, e.g. caused by mutations in the leptin or leptin receptor genes (Kaur et al., 2017). However, they only account for around 5% of total obesity in adults indicating a polygenetic background for the majority of human obesity (Ranadive & Vaisse, 2008). Accumulating genome-wide association studies (GWAS) associated variations in more than 1100 gene loci with different obesity traits to date (Loos & Yeo, 2022). Follow-up investigations revealed an association between a genetic variant in the fat-mass and obesity-related (FTO) gene identified by GWAS and differences in food intake supporting a genetic background of obesity (Frayling et al., 2007; Smemo et al., 2014). Further

studies revealed proteins mainly expressed in the central nervous system like *ectonucleoside* triphosphate diphosphohydrolase *(Entpd6)*, acetylcholinesterase *(Ache)* and melanocortin 4 receptor *(Mc4r)* to be associated with obesity supporting its key role described above (Turcot et al., 2018). However, only 6% of BMI variation can be explained by all associated genetic variants with single gene variants, only explaining 0.005 - 0.011% of BMI variation each (Loos & Yeo, 2022; Turcot et al., 2018). Even though these percentages are expected to rise with larger GWAS sample sizes in the future, this data demonstrates that only a small part of obesity is explainable by genetic background enhancing the need for further research investigating obesity development.

1.1.4 Adipose tissue dysfunction and its role in T2D

In Germany, 63% of people with T2D also had overweight or obesity indicating an association between these diseases (Szendroedi et al., 2016). Furthermore, overweight and obesity were revealed as key risk factors for developing T2D (Langenberg et al., 2014; Narayan et al., 2007). However, recent studies indicates that increased body fat by itself does not cause adipose tissue dysfunction, but every person has an individual threshold above which adverse comorbidities emerge (Scheidl et al., 2023; Taylor et al., 2023). The so-called “adipose tissue expandability hypothesis” proposes that after reaching its individual storage capacity, subcutaneous adipose tissue (SAT) fails to store more lipids leading to lipid spillover into circulation, causing inflammation, ectopic, or visceral adipose tissue lipid storage (Figure 2). This in turn causes insulin resistance and dysfunction of insulin-producing beta cells, two key characteristics of T2D (Kawai et al., 2021; Nowotny et al., 2013; Xourafa et al., 2024). Different factors like inflammation but also fetal programming can influence maximum adipocyte size and progenitor recruitment impairing personal SAT storage capacity (Scheidl et al., 2023). Taylor and coworkers demonstrated in the ReTUNE study that not BMI but the personal fat threshold is indicative of T2D and weight loss regardless of BMI can ameliorate diabetic symptoms (Taylor et al., 2023). Hence, further knowledge of adipose tissue development is important in understanding obesity and its pathology.

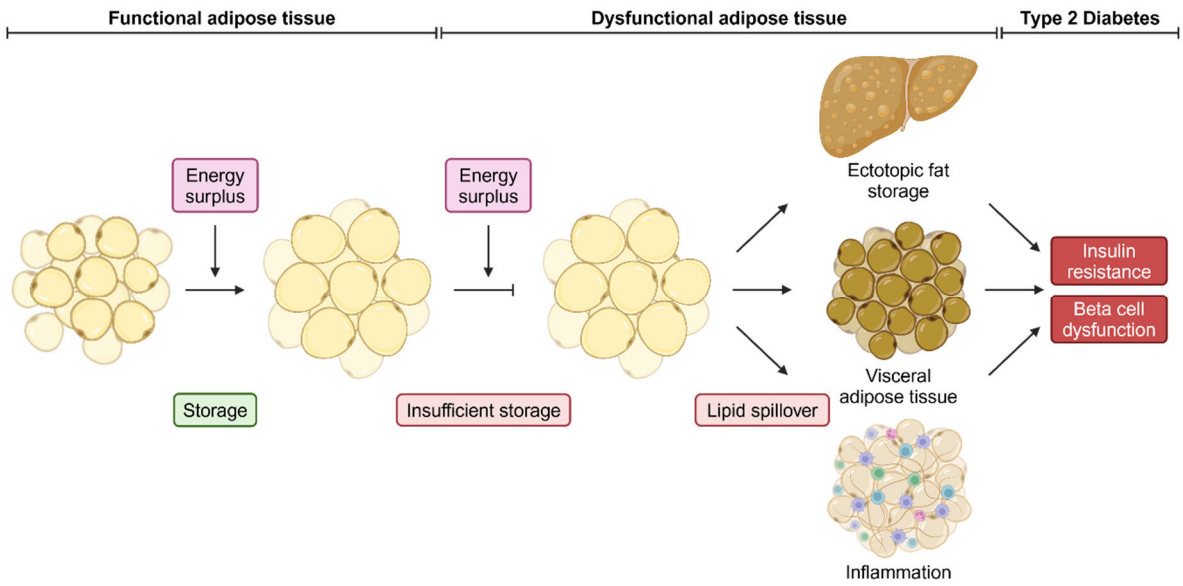

Figure 2: Adipose tissue expandability hypothesis.
The adipose tissue expandability hypothesis describes that insufficient storage capability causes adipose tissue to become dysfunctional leading to lipid spillover into other organs causing ectotopic fat storage, increased visceral adipose tissue growth and adipose tissue inflammation. Thereby their function is impaired causing type 2 diabetes. M. Schouwink generated this figure based on (Scheidl et al., 2023). Created with BioRender.com.

1.1.5 Adipocyte development

Adipose tissue mainly consists of adipocytes which develop from mesenchymal stem cells (Ghaben & Scherer, 2019). This process, also called adipogenesis, can be divided into two phases: First, mesenchymal stem cells commit themselves to the adipocyte lineage in the commitment phase. Next, these committed preadipocytes differentiate into adult adipocytes. Commitment of stem cells to the adipocyte lineage primarily takes place early in development, and gestation is crucial for adipose tissue development (Lecoutre et al., 2023). In mice, adipocyte progenitor cells are detectable as early as embryonic day 10.5 (E10.5) (Jiang et al., 2014).

As displayed in Figure 3, adipogenesis is regulated by different transcription factors with Peroxisome proliferator-activated receptor gamma (*Pparg*) being the key regulator of adipogenesis (Mota de Sa et al., 2017). CCAAT/enhancer-binding protein beta *(Cebpb)* and delta *(Cebpd)* are activated early on in adipogenic regulation and subsequently activate *Cebpa* and *Pparg* (Mota de Sa et al., 2017). *Cebpa* and *Pparg* further activate each other and primarily drive adipogenic differentiation (Moseti et al., 2016). *Pparg* activity is further induced via the transcription factor sterol regulatory element binding transcription factor 1 (*Srebf1c)* (Fajas et al., 1999). It also directly induces *fatty acid synthase (Fasn)* and acetyl-Coenzyme A carboxylase alpha *(Acaca)* together with nuclear receptor subfamily 1, group H, member 3 *(Nr1h3)* which is induced by *Cebpa* and *Pparg (Chen et al., 2016; Joseph et al., 2002; Laurencikiene & Ryden, 2012).* FASN and ACACA are two crucial enzymes in *de novo*

lipogenesis (DNL) of palmitic acid from acetyl CoA, a key function of adipocytes (Kusunoki et al., 2006). Similarly, fatty acid trafficking and lipolysis are central functions of adipocytes and are mainly performed by fatty acid binding protein 4 *(Fabp4),* fatty acid translocase *(Cd36),* cell death-inducing DNA fragmentation factor, alpha subunit-like effector A *(Cidea),* and peroxisome proliferative activated receptor, gamma, coactivator 1 alpha *(Pgc-1a)*, whose expression is initiated by *Cebpa* and *Pparg* (Furuhashi et al., 2014; Gao et al., 2017; Hwang et al., 2011; P. Liu et al., 2015; Moseti et al., 2016; Puigserver et al., 1998; Puri et al., 2008). Adipogenesis also increases the production and secretion of the two adipokines leptin and adiponectin, which are key players in the regulation of satiety and energy homeostasis (Fasshauer & Bluher, 2015; Moseti et al., 2016; Zhang & Chua, 2017). Overall, adipogenesis is a complex process coordinated and regulated by several genes, many of whom remain unknown. Hence, more research is needed to unravel further regulators of adipogenesis involved for example in fetal programming of maternal obesity.

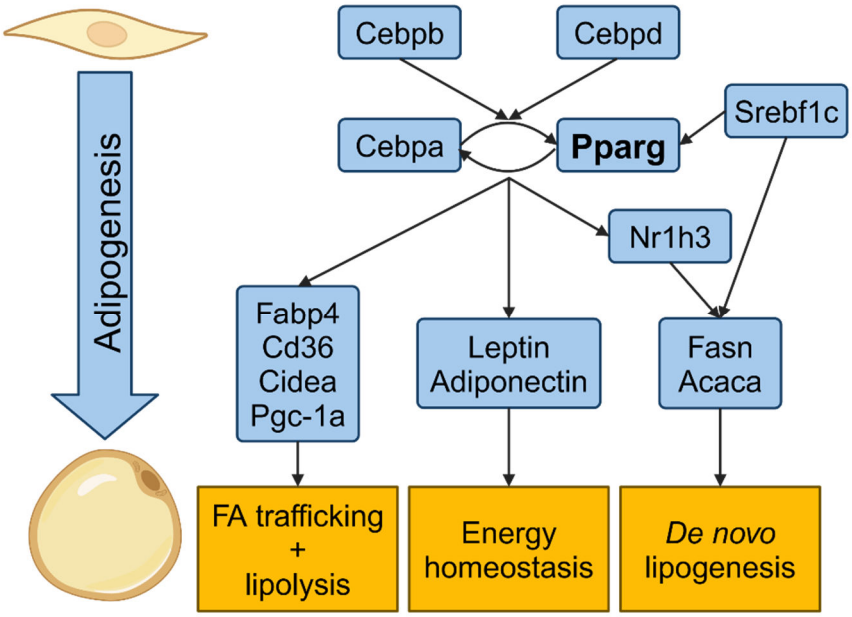

Figure 3: Simplified illustration of the transcriptional regulation of adipogenesis.
Adipogenic differentiation is regulated by different transcription factors. At the beginning of differentiation, *Cebpb* and *Cebpd* induce the expression of *Cebpa* and *Pparg* which are the main regulators of adipogenesis. They induce the expression of different sets of genes responsible for key adipocyte functions, namely fatty acid trafficking and lipolysis (*Fabp4, Cd36 Cidea, Pgc-1a*), energy homeostasis (*Leptin, Adiponectin*), and *de novo* lipogenesis (*Fasn, Acaca)*. M. Schouwink generated this figure. Created with BioRender.com.
Cebpb = CCAAT/enhancer-binding protein beta; *Cebpd* = CCAAT/enhancer-binding protein delta; *Pparg* = Peroxisome proliferator-activated receptor; *Cebpa* = CCAAT/enhancer-binding protein alpha; *Srebf1c* = sterol regulatory element-binding transcription factor 1c; *Fasn* = fatty acid synthase; FA = fatty acid; *Acaca* = acetyl-Coenzyme A carboxylase alpha; *Nr1h3* = nuclear receptor subfamily 1, group H, member 3; *Fabp4* = fatty acid binding protein 4; *Cd36* = fatty acid translocase; *Cidea* = cell death-inducing DNA fragmentation factor, alpha subunit-like effector A

Transcriptional regulation of preadipocyte differentiation into adipocytes has been mainly studied *in vitro* using the murine 3T3-L1 preadipocyte cell line (Dufau et al., 2021), which was

generated from mouse fibroblasts in 1974 (Dufau et al., 2021; Green & Kehinde, 1974). Recently, the protocol used to differentiate 3T3-L1 cells into adult adipocytes over two weeks was optimized by adding rosiglitazone alongside dexamethasone, 3-isobutyl-1-methylxanthine (IBMX), and insulin (Zebisch et al., 2012). Mouse embryonic fibroblasts (MEFs) obtained from murine embryos at different ages can be adipogenically differentiated using a similar protocol and represent a primary cell model for the investigation of adipogenesis (Dastagir et al., 2014). Furthermore, the 2001 characterized preadipocyte cell line derived from an infant with Simpson-Golabi-Behmel syndrome (SGBS) can also be differentiated into adipocytes *in vitro* to investigate human adipogenesis (Wabitsch et al., 2001).

1.1.6 Obesity treatment options and need for prevention

Current clinical guidelines focus on managing diet, physical activity, and behavioral changes to reduce body weight (Deutsche Adipositas-Gesellschaft e.V., 2014). However, previous studies revealed that only stringent intervention protocols result in significant weight loss that is maintained long-term (Kheniser et al., 2021). Currently, bariatric surgery is the most effective obesity treatment causing a 20% reduction in weight loss up to 20 years after surgery (O'Brien et al., 2019). Nevertheless, this type of surgical intervention is bound to strict eligibility criteria like BMI, age, and health status and poses the risk of several complications (Eisenberg et al., 2023; Schulman & Thompson, 2017). Already available single (e.g. semaglutide) and upcoming dual (e.g. tirzepatide) and triple agonists (e.g. retatutride) against GLP-1, glucose-dependent insulinotropic polypeptide and glucagon receptors respectively lead to weight loss of 15% - 20% of total body weight after one year of continuous application once a week (Jastreboff et al., 2022; Jastreboff et al., 2023; Wilding et al., 2021). However, besides side effects like nausea, diarrhea, and vomiting patients regain weight after treatment stops (Kubota et al., 2023; Wilding et al., 2022). Hence, long-term treatment of obesity remains difficult supporting the need for prevention strategies.

1.2 Pregnancy as a critical time window for early origins of metabolic disease

1.2.1 Risk factors during pregnancy

A growing body of evidence acknowledges pregnancy as a critical time window for early origins of obesity and T2D. Different factors influencing the fetus during pregnancy are discussed as risk factors for later disease development (Figure 4). Among these, excessive gestational weight gain (GWG), GDM, smoking during pregnancy, and increased maternal pre-pregnancy weight show strong influences on children’s health trajectories (Albers et al., 2018; Ensenauer et al., 2013; Gomes et al., 2022; Perschbacher et al., 2022; Voerman et al., 2019).

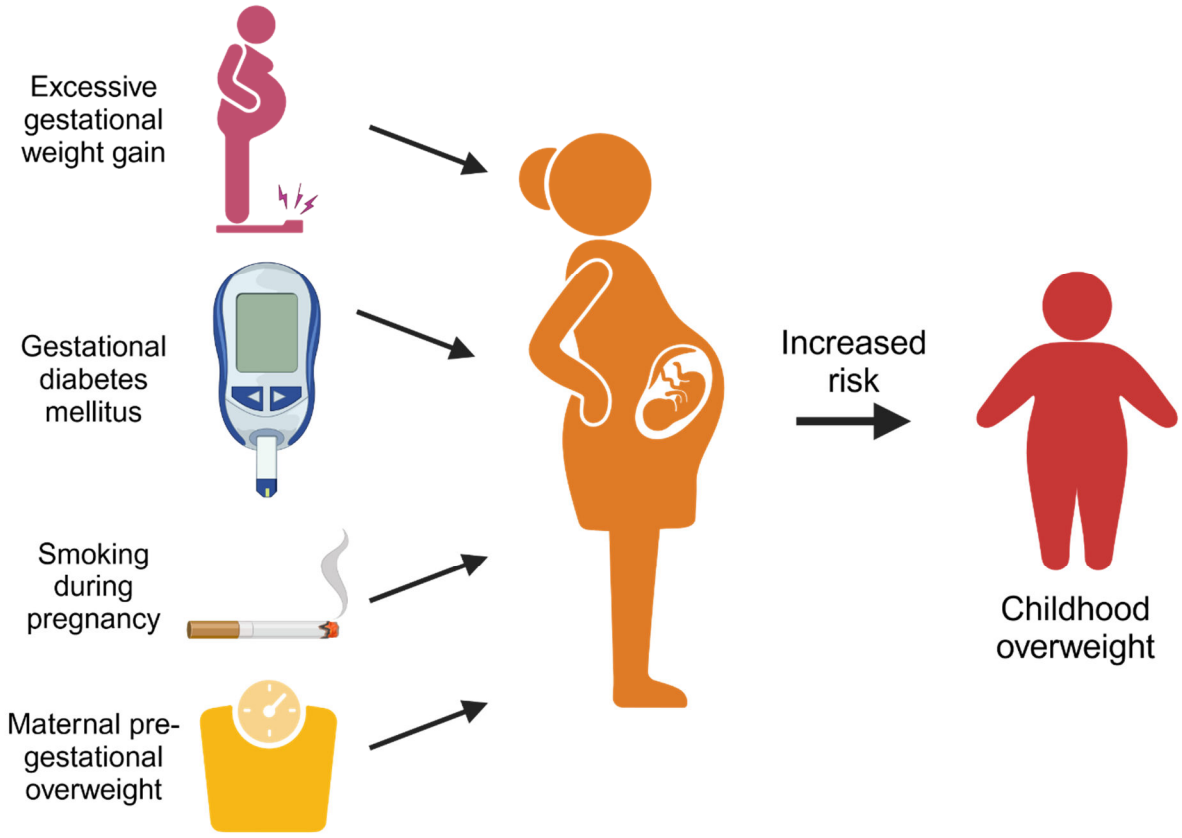

Figure 4: Major risk factors during pregnancy for childhood overweight.
The risk for childhood overweight is increased by the different factors during pregnancy like excessive gestational weight gain, gestational diabetes mellitus, smoking during pregnancy, and maternal pre-gestational overweight (Perschbacher et al., 2022). M. Schouwink generated this figure. Created with BioRender.com.

1.2.1.1 Excessive gestational weight gain

In 2009, the US National research council reexamined the guidelines for the optimal gestational weight gain (GWG) depending on maternal pre-pregnancy BMI to minimize negative health consequences for both mother and child (National Research Council, 2009). Mothers with normal pre-pregnancy weight (BMI 18.5-24.9 kg/m²) are advised to gain 11.5-16.0 kg during pregnancy, but mothers with pre-pregnancy overweight (BMI 25.0-29.9 kg/m²) or obesity (BMI 30.0-34.9 kg/m²) are advised to limit GWG to 7.0-11.5 kg and 5.0-9.0 kg, respectively (National Research Council, 2009). However, research of our group revealed that GWG above recommendations ("excessive GWG") is common, as shown in a large German cohort study, with more than half of mothers (53.6%) who had gained weight above the advised range (Ensenauer et al., 2013). Additionally, excessive GWG increased the offspring's risk of developing overweight (odds ratio (OR): 1.57) and abdominal adiposity (OR: 1.39) in this study. Further studies unveil increased body fat percentages in children of mothers with increased GWG (Castillo et al., 2015). Additionally, Voerman and coworkers were able to show a gradual increase in children's overweight risk with increasing GWG. They found that the OR for

childhood overweight or obesity increased by 1.14-1.16 for each standard deviation increase in GWG relative to reference charts (Voerman et al., 2019). Furthermore, they attributed 11.4-19.2% of childhood (2-18 years) overweight and obesity to excessive GWG depending on children's age, with older children (10-18 years) having the highest risk for childhood obesity attributed to excessive GWG. Von Kries and coworkers provided further strong evidence for the influence of GWG on childhood overweight, as a return to recommended GWG during late pregnancy lowers the overweight risk in children at school entry (von Kries et al., 2013)

1.2.1.2 Gestational diabetes mellitus

Gestational diabetes mellitus (GDM) is defined as an increased fasting blood glucose or a glucose intolerance first diagnosed during pregnancy and is one of the most prevalent pregnancy complications with long-term ramifications for both mother and child (Reitzle et al., 2021). Since 2012, GDM screening is performed in Germany reporting a prevalence of 9.41% in 2022 (IQTIG, 2023; Reitzle et al., 2021). It is challenging to discern the impact of GDM on offspring's health development from the effects of an increased pre-pregnancy BMI. Nonetheless, studies revealed an effect of GDM on an increased BMI in children irrespective of maternal pre-pregnancy BMI (Hu et al., 2019; Nehring et al., 2013; Wang et al., 2019). Another study also showed a relationship between GDM and increased BMI in different childhood age groups, but this effect was reduced in all age groups after adjusting for maternal pre-pregnancy BMI and only remained significant for early childhood BMI (Patro Golab et al., 2018). Additionally, dysglycemia in the last trimester, identified by increased HbA1c values at birth, despite a previously negative GDM test result, increased the offspring's risk of being born large-for-gestational-age and for a high BMI at 4 years of age (Ensenauer et al., 2015; Gomes et al., 2018). Interestingly, two studies found an influence of offspring's sex on the susceptibility to the long-term effects of GDM as they showed an increased risk of developing overweight only in boys but not in girls (Le Moullec et al., 2018; Li et al., 2017). Furthermore, maternal GDM has not just been shown to increase the offspring's risk of developing overweight but also to increase the child's plasma glucose and HbA1c values, potentially priming children to develop T2D themselves (Scholtens et al., 2019).

1.2.1.3 Smoking during pregnancy

Between 2007 and 2016, 10.9% of pregnant women in Germany smoked during pregnancy (Kuntz et al., 2018). Among other harmful effects, e.g. disturbed developmental and growth processes, smoking increases the offspring's risk to develop overweight or obesity (Toschke et al., 2003). Additionally, smoking during pregnancy increases the offspring's risk of developing overweight in a dose-dependent manner, which provides a higher level of evidence for a direct influence of smoking on offspring's health development (Albers et al., 2018).

1.2.1.4 Maternal pre-gestational weight

As the prevalence of overweight and obesity in western societies rises, also the percentage of women starting pregnancy with an elevated body weight has increased in the last years. In Germany, 44% of women have overweight (25%) or obesity (19%) at the beginning of pregnancy (IQTIG, 2023). High maternal body weight during pregnancy not only increases the risk for severe pregnancy complications such as preterm birth, fetal death, or stillbirth (Catalano & Shankar, 2017). It also negatively impacts child's longer-term health development until adulthood (Mannino et al., 2022). Children influenced by maternal pre-pregnancy overweight or obesity have a 264% increased risk of developing obesity during childhood (Heslehurst et al., 2019). Furthermore, even within maternal BMI groups, there is a gradual increase in offspring's overweight and obesity risk with every 1 kg/m² increase in maternal BMI (Voerman et al., 2019). Additionally, 11.5% - 20.1% of childhood overweight and obesity can be attributed to maternal pre-pregnancy overweight, depending on age. Furthermore, 10-18-year-old children have a higher risk of developing overweight and obesity compared to younger children. The role of the intrauterine environment in the offsprings' risk of developing overweight or obesity is further reinforced by studies revealing a decreased risk in children born after maternal bariatric weight loss surgery compared with their siblings born before surgery (Smith et al., 2009). Additionally, weight loss surgery was associated with decreased birth weight, increased insulin sensitivity, and improved lipid profile in children aged 10-16 years. Moreover, maternal overweight and obesity during pregnancy also increased the child's risk of developing T2D later in life (Lahti-Pulkkinen et al., 2019).

Even though several studies report varying effects of maternal overweight and obesity in pregnancy on boys and girls, results remain conflicting. Some studies described a stronger effect of maternal overweight or obesity during pregnancy in boys as their body fat percentage was increased while girls' body fat percentage remained unchanged (Andres et al., 2015; Castillo et al., 2015). However, another study reported a stronger impact on daughters regarding increased BMI after influence of maternal overweight during pregnancy (Dias et al., 2021). Further studies will be needed to elucidate sex-specific effects in offspring.

Importantly, studies that investigate several prenatal risk factors describe maternal pre-gestational weight as the strongest risk factor for impaired child health development (Hu et al., 2019; Patro Golab et al., 2018; Perschbacher et al., 2022; Voerman et al., 2019). Mechanisms underlying the intrauterine effect of different risk factors e.g. maternal pre-pregnancy BMI are still not completely understood.

1.2.2 Impact of maternal obesity in pregnancy on offspring development

The developmental origins of health and disease (DOHaD) concept describes adverse effects of environmental factors during critical developmental periods on childrens' health

development (Gillman, 2005). Many studies investigated mechanisms underlying intrauterine processes influencing offspring's health, which are called "fetal programming" (Seneviratne & Rajindrajith, 2022). Because of the large variability in environmental factors and the difficulties to obtain maternal and fetal tissue in human cohort studies, preclinical mouse models are used to investigate underlying mechanisms. Commonly, mice are fed diets rich in calories (high caloric diet, HCD) stemming mainly from fat and carbohydrates causing them to develop an overweight or obesity phenotype compared to mice fed a low-caloric control diet (CD) (Dahlhoff et al., 2014; Schoonejans & Ozanne, 2021). In our research group, a pregnancy mouse model was established that included transfer of offspring to CD foster dams, to limit an HCD influence on offspring to the gestation period only (Dahlhoff et al., 2014).

1.2.2.1 Sex-specific changes in offspring

Different studies investigating sex-specific effects of maternal obesity on offspring described a higher susceptibility to adverse effects in male offspring. Male offspring of HCD fed dams showed increased body weight, body fat, and increased visceral adipose tissue percentage (Savva et al., 2021). Female offspring on the other hand were protected from these adverse effects. Additionally, male offspring developed insulin resistance and reduced insulin signaling in adipose tissue which was not found in females (Savva et al., 2022). Furthermore, transcriptomic analysis of offspring's fat depots revealed sex- and adipose depot specific changes in transcriptome induced by maternal HCD feeding (Savva et al., 2022). Another study described changes in fat mass in offspring of HCD fed dams of both sexes, but only male offspring displayed an increased body weight compared to offspring of CD fed dams (Schoonejans et al., 2022). Using outbred Naval Medical Research Institute (NMRI) mice, my research group revealed sex-specific effects of maternal HCD feeding only during gestation on offsprings' adipose tissue development (Dahlhoff et al., 2014). While male offspring had increased body fat percentages and body weight, female offspring displayed reduced body fat percentages, reduced visceral adipose tissue size, and smaller adipocyte size. These studies imply an important role of the intrauterine environment in the effect of maternal obesity on offspring development.

1.2.2.2 Possible mechanisms involved in fetal programming

During pregnancy, the placenta is the sole connection between mother and fetus and provides the fetus with necessary nutrition and hence, plays a key role in the healthy development of the fetus *in utero* (Griffiths & Campbell, 2014). Gauster et al. revealed disturbed lipid transport across the placenta in mothers with obesity and GDM (Gauster et al., 2011). Additionally, the placenta displays sex-specific differences in its structure and function (Rosenfeld, 2015), and in mothers with obesity, female placentae exhibited a stronger increase in signs of inflammation than male placentae (Leon-Garcia et al., 2016). Furthermore, mRNA expression of genes related to placental fatty acid trafficking is altered sex-specifically in response to

maternal high caloric feeding with diets differing in fatty acid composition (Gimpfl et al., 2017). Overall, these studies suggest an important role of the placenta in fetal *in utero* development and in fetal programming effects of maternal obesity.

Changes in DNA methylation induced by maternal obesity are investigated in the context of fetal programming. Methylation and demethylation of DNA especially in gene promotor regions can activate or silence gene expression without changing DNA sequence (Lavebratt et al., 2012). Increased maternal BMI and GDM are connected to changes in DNA methylation patterns of genes linked to adipose tissue development in humans (El Hajj et al., 2013; Gemma et al., 2009). Moreover, preadipocytes of patients with obesity together with and without T2D displayed distinct DNA methylation patterns, which correlated with adipogenic differentiation capacity (Andersen et al., 2019), and differential DNA methylation of mesenchymal stem cells was connected to their adipogenic differentiation capacity (Collas, 2010). Furthermore, early nutrition is crucial for DNA methylation during development as it depends on methyl donors stemming from the one-carbon metabolism and hence deficiency in nutrients like methionine, choline, folic acid, and vitamin B12 impair early development (Waterland & Jirtle, 2004). Uteroplacental insufficiency was shown to alter DNA methylation via impaired one-carbon metabolism (MacLennan et al., 2004), and varying omega-3 to omega-6 ratios in diet during gestation and lactation altered offspring DNA-methylation in liver associated with fatty acid metabolism (Niculescu et al., 2013). Thus, offspring's DNA methylation patterns can be altered by maternal diet and obesity, and can influence adipose tissue development, exposing a possible mechanism of fetal programming.

Another epigenetic mechanism possibly involved in fetal programming are microRNAs (miRNAs), which are small non-coding RNAs that inhibit mRNA translation via covalent binding and are involved in the regulation of many processes like adipose tissue development (Brandao et al., 2017). Studies revealed differential expression of miRNA connected to adipogenesis regulation in offspring exposed to maternal obesity including sex-specific alterations (Gaytán-Pacheco et al., 2021; Méndez-Mancilla et al., 2018). Maternal obesity also causes differential miRNA expression in placentas, which were associated with low birth weight and increased postnatal weight gain (Carreras-Badosa et al., 2017). Hence, altered miRNA expression induced by maternal obesity may influence offspring development and constitute a potential mechanism involved in fetal programming.

As DNA is wrapped around histones, their modifications (acetylation, methylation, phosphorylation, ubiquitylation, and sumoylation) cause changes in chromatin structure and thereby influence gene expression (Şanlı & Kabaran, 2019). Maternal HCD-feeding can cause changes in histone acetylation and methylation in fetal leptin and adiponectin promotors linked with changes in their expression and an obesity phenotype (Masuyama & Hiramatsu, 2012).

Furthermore, uteroplacental insufficiency in rats also alters histone acetylation similarly to DNA methylation described above (MacLennan et al., 2004). Therefore, alterations in histone modifications are another epigenetic mechanism potentially involved in fetal programming by maternal obesity.

1.3 Research gap

Over one billion people are affected by obesity, which significantly increases their risk of developing type 2 diabetes and cardiovascular diseases (Afshin et al., 2017; Phelps et al., 2024). Additionally, nearly every second woman in Germany starts pregnancy with overweight or obesity (IQTIG, 2023) and thereby increases their child's risk of also developing overweight and associated comorbidities (Lahti-Pulkkinen et al., 2019; Voerman et al., 2019). Mouse studies have identified pregnancy as a key time window for adipogenic exposures affecting the early origins of offspring disease development (fetal programming) (Seneviratne & Rajindrajith, 2022). Furthermore, studies of our group revealed sex-specific effects of maternal obesity during pregnancy on offspring adipose tissue development with females showing disturbances including reduced body fat percentage and adipocyte size (Dahlhoff et al., 2014). Underlying mechanisms targeting female embryonic adipocyte development in an obesogenic intrauterine environment are not yet identified. Furthermore, the impact of maternal obesity on the transcriptome, proteome, and DNA methylome in offspring embryonic adipocytes unveiling possible mechanisms of fetal programming of later overweight and obesity remain unknown.

1.4 Research question and aim

The overall research question of this thesis is how an intrauterine obesogenic environment programs alterations in fat cell development in the fetal offspring. Developing fat cells of female embryos obtained using an NMRI mouse model for diet-induced maternal obesity will be investigated to address these specific aims:

1. Establishing an NMRI mouse model for diet-induced maternal obesity in the laboratory of our research group based in Düsseldorf
2. Investigating the impact of maternal HCD feeding on the adipogenic differentiation capacity of offsprings' developing adipocytes by adipogenically differentiating E13.5 mouse embryonic fibroblasts *ex vivo* and generating adipocyte-enriched samples of these differentiated cells from female mat-HCD and mat-CD offspring.
3. Analyzing the transcriptome of MEF derived adipocyte samples by RNA sequencing to identify candidate genes altered by maternal diet, and followed by validation using RT-qPCR and western blotting.
4. Establishing an optimized protocol for adipogenically differentiating 3T3-L1 cells in our research group and assessing its suitability for our research on a morphological as well as mRNA and protein expression level.

5. Investigating obtained candidate genes for their role in adipogenesis using siRNA-mediated knockdown in murine 3T3-L1 cells and expression profiles in human SGBS cells.
6. Determining molecular candidate pathways and targets altered by exposure to mat-HCD feeding *in utero* through analysis of the proteome and methylome of female E13.5 adipocytes using mass spectrometry and reduced representative bisulfite sequencing respectively.

2 Material and Methods

2.1 Materials

2.1.1 Animal diets

Table 1: Animal diets

Name	Product	Product number	Manufacturer
High caloric diet (HCD)	D12492 high-fat diet	E15741-34	Ssniff
Control diet (CD)	Control diet to D12492	E15747-044	Ssniff

2.1.2 Laboratory instruments

Table 2: Laboratory instruments

Instrument	Name	Manufacturer
Capillary electrophoresis instrument	Fragment Analyzer	Agilent
Chromatography column	Aurora C18 column (AUR2-25075C18A)	IonOpticks
Fluorescence Microscope	Axio Observer 7	Zeiss
Gel and blot detection system	ChemiDoc Touch imaging system or ChemiDoc MP Imaging System	Bio-Rad Laboratories
Ion Source	Nanospray Flex Ion Source	Thermo Scientific
Mass spectrometer	Orbitrap Fusion Lumos Tribrid Mass Spectrometer	Thermo Scientific
Microplate reader	Infinite M200	Tecan
Microscope camera	Axiocam 7012 mono digital Camera	Zeiss
Next-generation sequencing platform	Illumina NovaSeq6000	Illumina
Objectives	Plan-Apochromat 10x/0.45 M27 objective	Zeiss
PCR cycler	Biometra TRIO	Analytikjena
RT-qPCR machine	StepOnePlus Real-Time PCR System	Applied Biosystems
Sequencing System	HiSeq 3000/4000 system	Illumina
Ultrasonic homogenizer	Sonoplus	Bandelin Electronic

2.1.3 Consumables

Table 3: Consumables

Product	Product number	Manufacturer
Acclaim PepMap C18-LC-column	164946	Thermo Scientific
Cell culture flask T-25, standard	83.3910	Sarstedt
Cell culture flask T-75, standard	83.3911	Sarstedt
Cell culture flask T-175, standard	83.3912	Sarstedt
Cell culture plate, 6 well, Cell+	83.3920.300	Sarstedt
Cell culture plate, 12 well, Cell+	83.3921.300	Sarstedt
Cell culture plate, 24 well, Cell+	83.3922.300	Sarstedt
Cell culture plate, 48 well, Cell+	83.3923.300	Sarstedt
Cell culture plate, 96 well, Cell+	83.3924.300	Sarstedt
Microvette CB 300 Lithium heparin	16.443	Sarstedt
S-Trap micro columns		ProtiFi

2.1.4 Cell culture media and additives

Table 4: Cell culture media and additives

Product	Product number	Manufacturer
3,3′,5-Triiodo-L-thyronine sodium salt (Triiodothyronine)	T6397-250 mg	Sigma-Aldrich
3-Isobutyl-1-methylxanthine	I5879-250mg	Sigma-Aldrich
apo-Transferrin human	T2252-100MG	Sigma-Aldrich
Biotin	B4639-100MG	Sigma-Aldrich
Dexamethasone	D4902-25MG	Sigma-Aldrich
DMEM, high glucose, GlutaMAX™ Supplement, pyruvate	31966021	Gibco
DMEM/F12, HEPES	11330-032	Gibco
D-Pantothenic acid hemicalcium salt (Panthotenat)	P5155-100G	Sigma-Aldrich
Fetal bovine serum	10270106	Gibco
Hydrocortisone (Cortisol)	H0888-1G	Sigma-Aldrich
Insulin (bovine, for 3T3-L1 cells)	I1882-100MG	Sigma-Aldrich
Insulin (human, for MEFs)	I9278-5ML	Sigma-Aldrich
Insulin (human, for SGBS cells)	12585-014	Thermo Fisher Scientific
Newborn calf serum	16010159	Gibco
Opti-MEM I Reduced Serum Medium	31985070	Gibco
Penicillin-Streptomycin	P0781-100ml	Sigma-Aldrich
Rosiglitazone	CAYM71740-25	Cayman Chemical Company
RPMI 1640 Medium	11835063	Gibco
Trypsin-EDTA (0.05%)	25300-062	Gibco

2.1.5 Kits and chemicals

Table 5: Kits and chemicals

Product	Product number	Manufacturer
AMPure XP reagent	A63882	Beckman Coulter
BM Chemiluminescence-Western-Blot-Substrate (POD)	11500694001	Roche
BODIPY 493/503	D3922	Invitrogen
Collagenase D	11088866001	Roche
CompleteTM	11697498001	Roche
Dispase II	37045800	Roche
DNeasy Blood & Tissue Kit	69504	Qiagen
DNF-488 High Sensitivity genomic DNA Analysis Kit	DNF-488-1000	Agilent
DNF-474 NGS fragment kit	DNF-474-0500	Agilent
Dulbecco's Phosphate Buffered Saline	14190144	Gibco
EZ-PCR Mycoplasma Detection Kit	20-700-20	Sartorius
Formaldehyde solution 4% (PFA)	1.00496.8350	Merck
GeneChip Mouse Gene 1.0 ST Array	901168	Affymetrix
GeneChip WT cDNA Synthesis and Amplification Kit	900813	Affymetrix
GeneChip WT Terminal labeling and Controls Kit	901524	Affymetrix
GoTaq®G2 Hot Start Green Master Mix (G2M Master Mix)	M7422	Promega
HiMark Pre-Stained HMW Protein Standard	LC5699	Invitrogen

Hoechst 33342, Trihydrochloride, Trihydrate	H3570	Invitrogen
Illumina® Stranded Total RNA Prep, Ligation with Ribo-Zero Plus	20040525	Îllumina
Ilumina TotalPrep RNA Amplification Kit	IL1791	Ambion
Lipofectamine RNAiMAX	13778-075	Invitrogen
MES SDS Running Buffer	NP0002	Invitrogen
miRNeasy Mini Kit	217004	Qiagen
Nitrocellulose Membrane, Precut, 0.2 µm, 7 x 8.4 cm	1620146	Bio-Rad Laboratories
NuPAGE 4-12% Bis-Tris gel	NP0336BOX	Invitrogen
NuPAGE 7% Tris-Acetate gel	EA03585BOX	Invitrogen
NuPAGE Antioxidant	NP0005	Invitrogen
NuPAGE LDS Sample Buffer (4x)	NP0007	Invitrogen
NuPAGE Sample Reducing Agent (10x)	NP0009	Invitrogen
NuPAGE Transfer buffer (20x)	NP0006-1	Invitrogen
Page Ruler Plus Prestained Protein ladder 10 to 250 kDa	26620	Thermo Scientific
Phosphatase inhibitor cocktail 3	P0044-1ML	Sigma-Aldrich
Pierce BCA Protein Assay Kit	23227	Thermo Scientific
Pierce Quantitative Peptide Assays & Standards	23290	Thermo Scientific
Pierce RIPA Buffer	89900	Thermo Scientific
Ponceau S	P-3504	Sigma-Aldrich
Premium RRBS kit V2	C02030036	Diagenode
Protease Inhibitor Cocktail	P8340-1ML	Sigma-Aldrich
QuantiTect Reverse Transcription Kit	205313	Qiagen
QuantiTect SYBR Green PCR Kit	204145	Qiagen
Qubit dsDNA High Sensistivity (HS) Assay kit	Q32851	Invitrogen
Qubit RNA High Sensitivity (HS) Assay Kit	Q32852	Invitrogen
QuickExtract DNA Extraction Solution 1.0	QE09050	LGC Biosearch Technologies
RNase-Free DNase Set (RNA isolation)	79254	Qiagen
RNeasy Micro kit	74004	Qiagen
RQ1 RNase-Free Dnase (embryo digestion mix)	M6101	Promega
Skim Milk Powder	70166-500G	Sigma-Aldrich
Tris-Acetate SDS Running Buffer	LA0041	Invitrogen
Tris-Buffered-Saline (TBS-10x)	12498	CellSignaling
TRIzol reagent	15596026	Invitrogen
Trypsin/Lys-C Mix	V5071	Promega
Tween 20	P1379-500ml	Sigma-Aldrich
Ultra Sensitive Rat Insulin ELISA	90062	Crystel Chem
UltraPure™ Agarose	16500500	Invitrogen

2.1.6 siRNAs

Table 6: siRNAs

Product	**Product number**	**Target mRNA**	**Assay ID**	**Manufacturer**
Silencer Select Negative Control #1 siRNA	4390843	Control		Ambion
Silencer Select Pre-designed siRNA	4390771	Aldh1a1	s62236	Ambion
Silencer Select Pre-designed siRNA	4390771	Aldh1a7	s211625	Ambion
Silencer Select Pre-designed siRNA	4390771	Scand1	s234227	Ambion

2.1.7 Primers

2.1.7.1 Primers – murine genes

Table 7: Primers for murine genes

Gene	Primer	Sequenz
Acaca	for	CAGACTGATCGCAGAGAAAG
	rev	CTCAGGCTCACATCTGCTAC
Actb	for	GGCTGTATTCCCCTCCATCG
	rev	CCAGTTGGTAACAATGCCATGT
Adipoq	for	ATCCTGCCCAGTCATGCCGA
	rev	AGGACCAAGAAGACCTGCATCTCC
Aldh1a1	for	GCACTCAATGGTGGGAAAGT
	rev	CCAAATGAACATGAGCATTG
Aldh1a7	for	ACTGCTATTTGGCTGTCCCT
	rev	CCATGTTCGCCCAGTTCTCG
CD36	for	CATGATTAATGGCACAGACG
	rev	TCCGAACACAGCGTAGATAG
B2m	for	TTGGATTTCAATGTGAGGC
	rev	GGTCTTTCTGGTGCTTGTCT
Cebpa	for	CCGAGATAAAGCCAAACAACGCA
	rev	CGTGTCCAGTTCACGGCTCA
Cidea	for	TGCTCTTCTGTATCGCCCAGT
	rev	GCCGTGTTAAGGAATCTGCTG
Fabp4	for	CATGAAAGAAGTGGGAGTGG
	rev	AGTACTCTCTGACCGGATGG
Fasn	for	AGATCCTGGAACGAGAACAC
	rev	TCGTGTCAGTAGCCGAGTC
Gapdh	for	AAGGTCATCCCAGAGCTGAA
	rev	CTGCTTCACCACCTTCTTGA
H2-Q2	for	TTTTGGGGAGGAGCCTAGAT
	rev	CCAATGATGATCACAGCTCC
Hprt	for	CTGGATTACATTAAAGCACTGAA
	rev	TCAAGACATTCTTTCCAGTTAAAG
IL6	for	TCACAGAGGATACCACTCCCAACA
	rev	TCTGCAAGTGCATCATCGTTGT
Kdm5c/d	for	TGAAGCTTTTGGCTTTGAG
	rev	CCGCTGCCAAATTCTTTGG
Lep	for	ATCCCAGGGAGGAAAATGTGCTG
	rev	TACCGACTGCGTGTGTGAAATGTC
Mcp1	for	GGCTCAGCCAGATGCAGTTAACG
	rev	TCCTTCTTGGGGTCAGCACAG
Nr1h3	for	GGATAGGGTTGGAGTCAGCA
	rev	GCTCAGCACGTTGTAATGGA
Pparg1	for	GTGAGACCAACAGCCTGAC
	rev	TTCACCGCTTCTTTCAAATC
Pparg2	for	TCCTGTTGACCCAGAGCAT
	rev	TGCGAGTGGTCTTCCATCA
Pgc-1a	for	CTGGTTGCCTGCATGAGTGT
	rev	CTGCACATGTCCCAAGCCAT
Scand1	for	CTGTCGTGTCCGACTTGTCC
	rev	CTCGCCTGCGTCTCGACC

Srebf1c	for	AGGCGATCGGCGGGCTTTA
	rev	GCAATCCATGGCTCCGTGG
Tbp	for	ATGTGGTCTTCCTGAATCCCT
	rev	CAAACCCAGAATTGTTCTCCTT
Ube2d2a	for	CACAGTGGTCTCCAGCACTA
	rev	CATTCCCGAGCTATTCTGTT
Ucp1	for	ACTTTGGAAAGGGACGACCCCTAA
	rev	GCAAAACCCGGCAACAAGAGC

2.1.7.2 Primers – human genes

Table 8: Primers for human genes

Gene	Primer	Sequenz
ALDH1A1	for	CTGCCGGGAAAAGCAATCTG
	rev	CAACAGCATTGTCCAAGTCGG
ALDH1A2	for	AGGAGATCTTTGGCCCTGTT
	rev	TGAATCCCCCAAAGGGGCTC
ALDH1A3	for	TCTCGACAAAGCCCTGAAGT
	rev	CCGCCTTTCCTTCAGGGGTT
B2M	for	GACTTGTCTTTCAGCAAGGA
	rev	TGCTGCTTACATGTCTCGAT
CEBPA	for	TATAGGCTGGGCTTCCCCTT
	rev	AGCTTTCTGGTGTGACTCGG
FABP4	for	AACTGGTGGTGGAATGCGT
	rev	GGTCAACGTCCCTTGGCTTA
FASN	for	GCAAGCTGAAGGACCTGTCT
	rev	AATCTGGGTTGATGCCTCCG
GAPDH	for	TGCACCACCAACTGCTTAG
	rev	GAGGCAGGGATGATGTTC
PPARG1	for	AGAAGCCAACACTAAACCACAA
	rev	ACCATGGTCATTTCGTTAAAG
PPARG2	for	TCTTTTAACGGATTGATCTTTTGCT
	rev	GTGTCAACCATGGTCATTTCTTGT
PPIB	for	GGCCTACATCTTCATCTCCA
	rev	ACGCAACATGAAGGTGCT
UBE2D2	for	CATTCCCGAGCTATTCTGTT
	rev	CACAGTGGTCTCCAGCACTA

2.1.8 Antibodies

Table 9: Antibodies

Target Protein	Product number	Manufacturer	Predicted MW (kDa)	Host species	Incubation time	Lot
ACACA	3676S	Cell Signaling	280	Rabbit	Over night	05/2016 8
ADIPONECTIN	2789S	Cell Signaling	27	Rabbit	Over night	06/2024 3
ALDH1A1	12035S	Cell Signaling	54	Rabbit	Over night	04/2025 2
FABP4	3544S	Cell Signaling	15	Rabbit	Over night	03/2016 2
FASN	3180S	Cell Signaling	273	Rabbit	Over night	08/2016 2
PPARG1/ PPARG2	2435S	Cell Signaling	G1:53. G2:57	Rabbit	Over night	08/2016 4
Anti-Rabbit (HRP secondary antibody)	NA934V	Cytiva		Donkey	1 h	067K6071

2.1.9 Software

Table 10: Software

Software	Version	Manufacturer
CLC Genomics Workbench	22.0.2	Qiagen
GenomeStudio	V2010.1	Illumina
GraphPad Prism	7.05	GraphPad Software
Image Lab	6.0.1	Bio-Rad Laboratories
Magellan pro	V7.4	Tecan
NovaSeq Control Software	1.7.5	Illumina
Proteome Discoverer	3.0	Thermo Scientific
R	4.3.2	The R Foundation for Statistical computing
RStudio	2023.12.1	Posit Software
StepOne Software	2.3	Applied Biosystems
ZEN blue	3.6	Zeiss

2.2 Methods

2.2.1 Mouse handling

Mice experiments were approved by the Ethics Committee of the State Ministry of Agriculture, Nutrition and Forestry (State of North Rhine-Westphalia, Germany, License #81-02.04.2020.A086). A mouse model for maternal obesity was used, that was previously established in my working group (Dahlhoff et al., 2014). Mice experiments were performed in cooperation with Celina Uhlemeyer from the Institute for Vascular and Islet Cell Biology of the German Diabetes Center Düsseldorf.

Wildtype Naval Medical Research Institute (NMRI) mice were obtained from Janvier (Le Genest-Saint-Isle, France) at 3 weeks of age and housed at the animal facility of the German Diabetes Center at a 12h-12h light-dark cycle. Female mice had *ad libitum* access to water and food and were fed either a high caloric diet (HCD; energy derived from fat: 60 energy percent (E%), carbohydrates: 21 E%, protein: 19 E%) or a control diet (CD; energy derived from fat: 13 E%, carbohydrates: 60 E%, protein: 27 E%) ad libitum starting from week 3 of age. Male mice were fed a standard chow diet. Body weight and non-fasted blood glucose were measured every week. At 10 weeks of age, an intraperitoneal glucose tolerance test (ipGTT) was performed after a 16-hour fasting period. Mice received an intraperitoneal injection of glucose at a dosage of 2 g/kg. Glucose levels were assessed before the injection and subsequently every 20 minutes for a duration of up to 120 minutes following the injection. Additionally, blood samples for insulin quantification were drawn at 0-, 20-, and 120-minutes using heparin-coated microvettes, centrifuged at 2000 xg for 5 min, and plasma was stored at -80 °C in a new tube for later analysis. Plasma insulin levels were determined using an ELISA according to the manufacturer's protocol. To optimize mating efficiency, female mice at 12 weeks of age were visually inspected for the estrous state (Byers et al., 2012), and proestrus

and estrus mice were mated with males for 12-16 hours in a dark cycle overnight. Vaginal plug check was performed afterwards for determination of gestational age, and depending on estrous state, mice were mated again after 3-6 days to increase chances of successful conception. At embryonic age 13.5 days (E13.5) dams were sacrificed and embryos were isolated for cell isolation (see 2.2.2.1).

Several adipose tissue samples and data from mice experiments previously performed by the research group from Prof. Ensenauer were used in this thesis (unpublished data). These experiments had been approved by the Animal Ethics Committee (Bavaria, Germany). For these experiments, dams had been treated as described above until mating (Dahlhoff et al., 2014; Gimpfl et al., 2017). Additionally, foster dams were maintained on chow diet for each experimental group. At 12 weeks of age, mice were mated and checked for vaginal plugs every 12 hours, and fetal palpation was performed at 7.5 days post-coitum. Throughout pregnancy, mice remained on their respective diets, and all were allowed to deliver naturally. Offspring were grouped based on the maternal diet during pregnancy, labeled as mat-CD or mat-HCD. Within 12 hours of birth, pups from the experimental groups were transferred to foster dams fed CD during lactation. After weaning, offspring received CD and were sacrificed at 6, 16, and 20 weeks of age, respectively. Animals were anesthetized, bled from the retroorbital plexus, and euthanized by cervical dislocation. Organs were dissected, dried, and weighed. Abdominal adipose tissue, including omental and perigonadal fat depots, was excised from the entire visceral cavity, and stored frozen at -80 °C until analysis.

2.2.2 *Ex vivo* cell culture work

2.2.2.1 Mouse embryonic fibroblasts isolation, differentiation, harvest, and enrichment

Mouse embryonic fibroblasts (MEFs) were isolated from the torso of murine embryos at embryonic age 13.5 (E13.5) and differentiated into lipid loaden mature adipocytes by adding insulin, isobutyl-1-methylxanthine (IBMX), and dexamethasone as previously described (Yang et al., 2013).

Embryos were sacrificed by decapitation and maternal tissue, inner organs, tail, and limbs were removed. The tail or head was used for genotyping (see 2.2.2.2). The trunk of the embryo was transferred into a 15 ml tube containing 1 ml digestion mix (RPMI 1640 medium, 1 mg/ml collagenase D, 1 mg/ml dispase, 0.1% DNAse) and minced by pipetting up and down using a 1 ml pipette tip for around 45 seconds. Following incubation in the digestion mix for 25 minutes at 37 °C while shaking with additional homogenization steps after 10 and 20 minutes via pipetting, digestion was stopped by adding 4 ml standard medium (Dulbecco's Modified Eagle Medium (DMEM) high glucose Glutamax, 15% fetal bovine serum (FBS), 100 U/ml penicillin, and 0.1 mg/ml streptomycin) and by storing tubes on ice. Next, cells were filtered through a 70 µm cell strainer, counted, and seeded out at a density of ~ 90 000 cells/cm^2.

Adipogenic differentiation was initiated one day post-isolation using a combination of 0.5 mM IBMX, 1 µM dexamethasone, and 5 µg/ml insulin in DMEM high glucose supplemented with 15% FBS, 100 U/ml penicillin, and 0.1 mg/ml streptomycin. Cells were cultured under these conditions for eight days. Subsequently, medium was switched to DMEM high glucose with 10% FBS, 100 U/ml penicillin, 0.1 mg/ml streptomycin, and 5 µg/ml insulin for an additional four days. During differentiation, medium was replaced every two days.

After differentiation, lipid droplets were stained for 15 minutes with 0.4 µg/ml Bodipy 493/503 diluted in Dulbecco's phosphate buffered saline (DPBS). Afterwards, cells were harvested using 1 mg/ml collagenase and 1 mg/ml dispase diluted in RPMI 1640 medium and layered on a 50% PBS-50% Lymphoprep mixture in a 15 ml tube (Figure 7) and centrifuged for 30 minutes at 200 xg with low acceleration and no brakes. Adipocytes containing top fractions (Figure 7) were collected and proportions of lipid droplet-containing cells (mature adipocytes) were assessed using flow cytometry.

2.2.2.2 Embryo genotyping

To determine the sex of the isolated embryos the XY chromosome dependent lysine demethylase 5C *(Kdm5c)* and lysine demethylase 5D (*Kdm5d)* expression was utilized. The DNA was isolated from the embryonic tail or head using 30µl QuickExtract and 5-minute incubation at 65 °C and shaking. After digestion was stopped by heating samples to 98 °C for 2 minutes, DNA was diluted with 300 µl water and vortexed strongly for 10-20 seconds. Kdm5c/d genes were amplified in a PCR reaction mixing 1 µl sample with 3.5 µl water, 5 µl 2x G2M Master Mix, and 0.5 µl of 10 µM Primer mix (sequences depicted in Table 7). Male and female samples from previous mouse cohorts were used as controls. PCR was run with the following protocol on a Biometra TRIO PCR cycler:

Table 11: PCR program used for embryo genotyping.

Temperature	Time	Cycles
94 °C	3 min	1
94 °C 57 °C 72 °C	30 sec 30 sec 1 min	29
72 °C	2 min	1
4 °C	hold	1

Afterwards, samples were run for 30-45 minutes at 120 V on a 2% agarose gel to separate the DNA fragments. Gels were imaged using ChemiDoc MP Imaging System and the expected product length from the PCR are 330 bp for Kdm5c (X-chromosome) and 301 bp for Kdm5d (Y-chromosome).

2.2.3 *In vitro* cell culture work

2.2.3.1 Murine 3T3-L1 adipocytes

The 3T3-L1 preadipocyte cell line was obtained from the American Type Cell Culture Laboratories and subjected to cultivation and differentiation following previously established protocols (Zebisch et al., 2012). Cells were cultured in standard cell culture flasks in a humidified atmosphere at 37 °C with 5% CO_2 using DMEM supplemented with 10% newborn calf serum (NBCS), 100 U/ml penicillin, and 0.1 mg/ml streptomycin. Passaging was performed using 0.05% Trypsin-EDTA before reaching confluency, and the medium was refreshed three times per week.

After seeding at a density of ~ 68 000 cells/cm² in Cell+ cell culture plates at day -3 of differentiation, 100% confluency was checked the next day. After two more days, differentiation was initiated using differentiation medium 1 (DM1: DMEM with 10% FBS, 100 U/ml penicillin, 0.1 mg/ml streptomycin, 0.5 mM IBMX, 0.25 µM dexamethasone, 1 µg/ml insulin, and 1 µM rosiglitazone) indicating day 0 of differentiation. After two days, the medium was changed to differentiation medium 2 (DM2: DMEM with 10% FBS, 100 U/ml penicillin, 0.1 mg/ml streptomycin, and 1 µg/ml insulin). On day four of differentiation, the medium was further changed to basal medium 2 (BM2: DMEM with 10% FBS, 100 U/ml penicillin, and 0.1 mg/ml streptomycin). Subsequently, cells were sustained in BM2, with medium replacements on days 7, 9, 11, and 14 of differentiation.

2.2.3.2 Human Simpson-Golabi-Behmel syndrome (SGBS) preadipocyte cell line

Human Simpson-Golabi-Behmel syndrome (SGBS) preadipocyte cells, kindly provided by Prof. Wabitsch from the Department of Pediatrics and Adolescent Medicine, University of Ulm, Germany, were cultured and adipogenically differentiated following established methods (Fischer-Posovszky et al., 2008). Cells were cultured in DMEM/F12 supplemented with 10% FBS, 33 µM panthotenat, 17 µM biotin, 100 U/ml penicillin, and 0.1 mg/ml streptomycin in standard cell culture flasks and passaged before reaching confluency using 0.05% Trypsin-EDTA. After growing cells to 80% confluency in Cell+ cell culture plates, adipogenic differentiation was initiated using DMEM/F12 containing 33 µM panthotenat, 17 µM biotin, 100 U/ml penicillin, 0.1 mg/ml streptomycin, 0.01 mg/ml transferrin, 20 nM insulin, 100 nM cortisol, 0.2 nM triiodothyronine (T3), 2.5 µM dexamethasone, 250 µM IBMX, and 2 µM rosiglitazone for four days. Subsequently, the medium was changed to DMEM/F12 containing 33 µM panthotenat, 17 µM biotin, 100 U/ml penicillin, 0.1 mg/ml streptomycin, 0.01 mg/ml transferrin, 20 nM insulin, 100 nM cortisol, 0.2 nM T3 for 17 days, with medium changes twice a week.

All cells were regularly checked for mycoplasma contamination using the EZ-PCR Mycoplasma Detection Kit according to manufacturer's instructions.

2.2.3.3 siRNA mediated gene knockdown

Gene specific knockdown was induced by RNA interference using Lipofectamine™ RNAiMAX and pre-designed Silencer Select small interfering RNAs (siRNA, Table 6), following the forward transfection protocol outlined by Thermo Fisher Scientific. A mixture of 23.4 pmol Silencer Select siRNA and 0.39 µl Lipofectamine RNAiMAX in 468 µl Opti-MEM I Reduced Serum Medium per 1 cm² of cell culture surface was prepared, resulting in a final concentration of 50 nM Silencer Select siRNA. This mixture was then added to the cells for 24 hours on day prior to the induction of differentiation (day -1 of differentiation).

2.2.3.4 Lipid droplet staining, imaging, and quantification

After differentiation, cells were fixed using 4% formaldehyde (PFA) and stained using 0.4 µg/ml Bodipy 493/503 (lipid droplets; Invitrogen, Waltham, MA, USA) and 1 µg/ml Hoechst 33342 (nuclei; Invitrogen) for 30 minutes in DBPS. Lipid droplets were quantified by measuring Bodipy fluorescence using an Infinite M200 microplate reader running Magellan pro V7.4 software at an excitation wavelength of 493 ± 9 nm and emission wavelength of 525 ± 20 nm. Cells were imaged using an Axio Observer 7 fluorescence microscope equipped with an Axiocam 7012 mono digital Camera, a Plan-Apochromat 10x/0.45 M27 objective, and ZEN blue 3.6 software. Fluorescence signal filter cubes with excitation/ emission wavelengths of 370-410 nm/ 430-470 nm (Hoechst 333342) and 450-490 nm/ 500-550 nm (Bodipy 493/503) were utilized. Original images had a scale of 345 nm/pixel across a size of 4096 x 3008 pixels. Images of two fluorescent channels were merged, contrast and brightness were adjusted identically across all pictures and cropped to a size of 2000 x 1500 pixels to enhance visibility using ZEN blue 3.6.

2.2.4 Molecular biology analysis

2.2.4.1 Reverse transcription real time quantitative polymerase chain reaction (RT-qPCR)

Reverse transcription real time quantitative polymerase chain reaction (RT-qPCR) was employed for quantifying mRNA expression levels. Total RNA was extracted using the miRNeasy Mini Kit, followed by cDNA synthesis from up to 1000 ng of RNA utilizing the QuantiTect Reverse Transcription Kit, as per the manufacturer's instructions.

For quantification of mRNA expression, the Quantitect SYBR Green PCR kit and the StepOnePlus Real-Time PCR System were utilized following the manufacturer's protocol. Each sample was assessed in duplicates, and PCR reactions underwent 40 cycles with denaturation at 95 °C for 10 s, annealing at 55-61 °C for 20 s, and elongation at 72 °C for 30 s. The annealing temperature was adjusted based on the primers used (Table 7 and Table 8). To normalize expression data, six reference genes (hypoxanthine guanine phosphoribosyl transferase *(Hprt),* actin beta *(Actb),* beta-2 microglobulin *(B2m),* glyceraldehyde-3-phosphate

dehydrogenase *(Gapdh),* TATA box binding protein *(Tbp),* ubiquitin-conjugating enzyme E2D 2A *(Ube2d2a)*) were measured, and the most stable combination of two reference genes was determined using geNorm (Vandesompele et al., 2002). RT-qPCR reaction efficiency was determined using LinRegPCR 2017 (Ruijter et al., 2009), and expression levels were calculated according to the modified Pfaffle equation as previously described (Hellemans et al., 2007). All used primers are listed in Table 7 and Table 8.

2.2.4.2 RNA sequencing

RNA sequencing was performed in cooperation with the Genomics and Transcriptomics laboratory of the Heinrich-Heine-University Düsseldorf.

RNA was again isolated using the miRNeasy Mini Kit now including a DNase digestion step using the RNase-Free DNase Set. DNase digested total RNA samples used for transcriptome analyses were quantified (Qubit RNA HS Assay) and quality was measured by capillary electrophoresis using the Fragment Analyzer and the 'Total RNA Standard Sensitivity Assay'. All samples in this study showed high quality RNA Quality Numbers (RQN; mean = 10.0). The library preparation was performed according to the manufacturer's protocol using the Illumina Stranded Total RNA Prep, Ligation with Ribo-Zero Plus. Briefly, 700 ng total RNA were used as input for rRNA Depletion, fragmentation, the synthesis of cDNA, adapter ligation, and library amplification. Bead purified libraries were normalized and finally sequenced on the HiSeq 3000/4000 system with a read setup of 1x150 bp. The bcl2fastq tool (v2.20.0.422) was used to convert the bcl files to fastq files as well for adapter trimming and demultiplexing.

Data analyses on fastq files were conducted with CLC Genomics Workbench. The reads of all probes were adapter trimmed (Illumina TruSeq) and quality trimmed (using the default parameters: bases below Q13 were trimmed from the end of the reads, ambiguous nucleotides maximal 2). Mapping was done against the Mus musculus (mm39; GRCm39.105) (January 12, 2022) genome sequence. After grouping samples (six biological replicates each) according to their respective experimental condition, the statistical differential expression was determined using the "Differential Expression for RNA-Seq tool" (version 2.6). The resulting p-values were corrected for multiple testing by FDR. A p-value of ≤ 0.05 was considered significant. Reads Per Kilobase Million (RPKM) threshold for detection was set to 0.5, and at least three samples of each condition had to be above the detection threshold to involve transcripts in further analysis (Koch et al., 2018).

2.2.4.3 Microarray analysis

Microarray analysis was performed previously in the research group of Prof. Ensenauer on subgroups of female mouse offspring aged 6 and 20 weeks. Each animal's tissue sample, weighing 50-100 mg, was homogenized in 1.2 ml of Trizol reagent, and total RNA was extracted following the manufacturer's protocol. The purified RNA underwent integrity and

purity checks using silica membranes (RNeasy Micro Kit). Two different microarray platforms were utilized.

In this thesis, previously acquired and analyzed datasets from 6- and 20-week-old offspring were used. For the expression analysis of abdominal adipose tissue from 6-week-old female offspring, 300 ng of total RNA from 10 randomly selected individuals per group had been amplified using the Illumina TotalPrep RNA Amplification Kit, then hybridized to Mouse Ref-8 v2.0 Expression BeadChips. Data processing employed GenomeStudio software (Version V2010.1, gene expression module version 1.6.0) along with the MouseRef-8_V2_0_R3_11278551_A.bgx annotation file. Background subtraction was applied, and an offset was used to eliminate remaining negative expression values. Statistical analysis and fold change evaluation employed the “Ttest of the limma” package in the Bioconductor suite. Genes with a fold change (FC) > 1.2 and a p-value < 0.5 were considered differentially expressed.

For the microarray analysis of abdominal tissue from 20-week-old female offspring, 100 ng RNA from 5 individuals per group had been used to prepare labeled probes for microarray hybridization on Affymetrix Mouse Gene 1.0 ST Arrays. Affymetrix WT cDNA synthesis and amplification kits, as well as Terminal labeling kits, were used according to the manufacturer's instructions. Statistical analysis in this assay employed the local pooled error method due to the small sample number. Genes with a log2 fold change > 0.6 and a p-value < 0.5 were considered differentially expressed.

2.2.4.4 Western blot analysis

Cells were lysed in RIPA lysis buffer containing protease inhibitor and phosphatase inhibitor by homogenization using a micropistil and incubation for 15 min on ice. Afterwards, they were centrifuged for 15 min at 12 000 xg and 4 °C and the supernatant was transferred to remove cell and lipid debris. This step was repeated once. The protein concentration was measured using the Pierce BCA protein assay kit according to the manufacturer’s instructions.

After adding NuPage LDS Sample Buffer and NuPAGE Reducing Agent, samples were heated for 10 minutes at 70 °C and stored on ice afterwards. Subsequently, samples were separated on either NuPAGE 7% Tris-Acetate gels with Tris-Acetate SDS Running Buffer for FASN and ACACA detection or NuPAGE 4-12% Bis-Tris gels with MES SDS Running Buffer for ALDH1A1, FABP4, ADIPONECTIN, PPARG1, and PPARG2 detection. HiMark Pre-Stained HMW Protein Standard and PageRuler Plus Prestained Protein Ladder were used as protein size standards. Proteins were then transferred onto nitrocellulose membranes at 200 mA for 90 minutes using NuPAGE Transfer Buffer. A 0.5% [w/v] Ponceau S stain was applied to membranes for two minutes and imaged as a loading control (Romero-Calvo et al., 2010). After a 60-minute blocking using a 3% milk solution, membranes were probed with protein-

specific primary antibodies and corresponding secondary antibodies conjugated to horseradish peroxidase both diluted 1:1000 in tris-buffered saline containing 1% Tween (Table 9). Antibody detection was performed using BM Chemiluminescence Blotting Substrate and a ChemiDoc Touch imaging system. Densitometric analysis of images was conducted using Image Lab software 6.0.1, and expression values were normalized to the mean expression of control samples.

2.2.4.5 Mass spectroscopy for proteomic analysis

Mass spectroscopy (MS) proteomic analysis was performed in cooperation with the Proteome Analysis Unit from the Institute for Clinical Biochemistry and Pathobiochemistry of the German Diabetes Center Düsseldorf. Due to that, the following section was mainly written by Dr. Sonja Hartwig from the Proteome Analysis Unit.

For proteomic profiling, MEFs were solubilized in denaturing sodium dodecyl sulfate (SDS) buffer (100 mM Tris-HCl, 4% SDS and 20 mM dithiothreitol (DTT), supplemented with protease and phosphatase inhibitors), by 10 strokes through an insulin syringe (needle 26 gauge) followed by sonication (2 times pulse 0.09sec_10sec (Sonoplus)). After centrifugation at 75.000 xg for 30 min at 4 °C, supernatants were transferred to fresh reaction tubes and proteins were digested with LysC/Trypsin Mix (1:25 w/w) utilizing µS-Trap columns according to manufacturer's recommendation.

For MS analysis, lyophilized peptides were reconstituted in 1% trifluoroacetic acid (TFA) (v/v), and peptide concentrations were measured using Quantitative Colorimetric Peptide Assay (Pierce). Samples (400 ng) were separated as triplicates by liquid chromatography (Ultimate3000) and measured on an Orbitrap Fusion Lumos mass spectrometer coupled to a Nanospray FlexTM ion source and equipped with a FAIMS Pro (High-Field Asymmetric Waveform Ion Mobility Spectrometry) Interface.

Peptides were trapped and desalted on an Acclaim PepMap C18-LC-column (ID: 75 µm, 2 cm length) and subsequently separated via an Aurora C18 column (AUR2-25075C18A, 25 cm x 75 µm C18 1.6µm) using a 2 h three step gradient at a total flow rate of 300 nl/min with buffer A (0.1% formic acid) and buffer B (80% acetonitrile (ACN), 0.1% formic acid). First, peptides were separated for 72 min using a linear buffer gradient from 2-19% buffer B, second for 28 min using a linear buffer gradient from 19-29% buffer B, followed by 20 min using a linear buffer gradient from 29-41% buffer B and lastly, a 1 min linear gradient increasing buffer B to 95%.

MS-data were acquired in DDA (data dependent acquisition) mode utilizing high field asymmetric waveform ion mobility spectrometry (FAIMS) compensation voltage (CV) of -40 V(1.4 s cycle time), -60 V (1 s cycle time) and -80 V (0.6 s cycle time) at 120,000 resolution

and m/z range of 350-1,600. Automatic gain control (AGC) target value and injection time were adjusted automatically. For fragmentation, precursor selection filter was set to charge state between 2 and 7 and dynamic exclusion of 30 s. Fragmentation of precursors was done with an isolation window (m/z) 3.6, higher-energy collisional dissociation energy of 30% at 30,000 resolution with automatic adjustment of AGC target value and injection time.

Mass spectrometry raw files were analyzed with Proteome Discoverer 3.0 software. “SpectrumRC” node was used with FASTA database (reviewed SwissProt, Mus musculus canonical (v2023-06-28)) to recalibrate spectra. For quantification purpose, “Minora feature detector” node was used with standard settings (minimum trace length 5, max. delta RT of isoptope pattern multiplets of 0.2 min, and for feature to ID linking use only high confident PSMs). For identification search was done with “Chimerys” (inferys_2.1_fragmentation) against UniProtKB databases (reviewed SwissProt, Mus musculus with isoforms (v2023-06-28), Bos taurus canonical (v2023-06-28) and an in-house contaminant fasta file). “Enzymatic Digest” was set to trypsin with maximum 2 missed cleavage sites allowed. Carbamidomethylation of cysteine was set as static modification and methionine oxidation was allowed as dynamic modifications. “Percolator” was applied for FDR data validation. Proteins with an abundance ratio p-value > 0.7 that were detected with high confidence (“Protein FDR Confidence” equals “high”) in both sample groups were used to normalize protein abundance across samples. Labelfree quantification was performed on precursor intensity present in at least 20% of the replicates. Protein ratios were calculated pairwise ratio-based and a background based t-test was performed in Proteome Discoverer. Furthermore, p values were corrected for multiple testing using the Benjamin-Hochberg correction for the false discovery rate. Proteins labeled as contaminants by above mentioned databases were filtered out, and only murine proteins of whom abundance calculation was possible in both groups annotated were included. Enrichment analysis was performed using clusterProfiler 4.10.0 in RStudio 2023.12.1 running R 4.3.2 (Wu et al., 2021).

2.2.4.6 Reduced representative bisulfite sequencing

DNA methylation was assessed on a global scale by performing reduced representation bisulfite sequencing (RRBS) in cooperation with Diagenode (Seraing, Belgium).

DNA was isolated using DNeasy Blood and Tissue Kit according to manufacturer’s instructions. Qubit® dsDNA HS Assay Kit was used to measure DNA concentration and the Fragment Analyzer and the DNF-488 High Sensitivity genomic DNA Analysis Kit were used to check DNA quality. Premium RRBS v2 Kit was used to prepare RRBS libraries utilizing 100 ng of genomic DNA. After pooling samples by 10 and final library preparation, samples were cleaned by a 1.45x beads:sample ratio of Agencourt AMPure XP. DNA concentration was

again measured using Qubit® dsDNA HS Assay Kit and DNA profile using DNF-474 NGS fragment kit on a Fragment Analyzer.

Samples were sequenced on an Illumina NovaSeq6000 running NovaSeq Control Software 1.7.5, RTA v3.4.4, and bcl2fastq 2.20 v2.20.0.422 generating 50 bases reads (PE50) in paired-end mode. Samples were demultiplexed by unique dual indexing (UDI) indices (Supplementary Table S1) using demultiplex function of “fumi tool”. FastQC version 0.11.8. was used for quality control of sequencing reads (Andrews, 2010) and adapters were removed by Trim Galore Version 0.4.1 (Krueger, 2010). Alignment to the mm10 genome was performed by bismark v0.20.0 (Krueger & Andrews, 2011). Only CpGs covered in each sample were analyzed further and bisulfite conversion rates and efficiency were checked using spike-in controls. Differential methylation analysis was performed using the R package Methylkit v1.7.0 (Akalin et al., 2012). Low coverage (less than 10x in all samples) and highest coverage (above 99.9th percentile) CpGs were discarded, and data was normalized for read coverage distribution between samples using the Methylkit software package. P-values were corrected to q-values for multiple comparisons using the sliding window model. Differentially methylated CpGs (DMCs) identification thresholds were set to $q < 0.01$ and methylation difference higher 25% compared to mat-CD samples. Annotation was performed by annotatr (Cavalcante & Sartor, 2017) and enrichment analysis using clusterProfiler 4.10.0 in RStudio 2023.12.1 running R 4.3.2 (Wu et al., 2021).

2.2.5 Statistical analysis

If not stated otherwise, statistics were performed in GraphPad Prism Version 7.05 (GraphPad Software, San Diego, CA, USA). Sample size and statistical tests are stated in the respective figure legends. Results are presented as mean ± SEM (standard error of the mean), with statistical significance considered at $p < 0.05$. According to the number of groups and variables, student’s t-test, one-way or two-way ANOVA followed by either Dunnett’s, Sidak’s, or Tukey’s multiple comparison test as recommended by GraphPad Prism 7.05 were used to compare multiple groups. Statistical analysis of RNA sequencing, microarray, MS, and RRBS data are described in detail in the respective sections above (2.2.4.2, 2.2.4.3, 2.2.4.5, and 2.2.4.6).

3 Results

3.1 HCD feeding causes increased body weight and reduced glucose tolerance in NMRI dams

An established mouse model for investigating fetal programming by maternal HCD feeding using NMRI was utilized similar to previous work of my research group (Dahlhoff et al., 2014). The following data was produced by Celina Uhlemeyer and me. HCD feeding starting at 3 weeks of age caused a significantly increased body weight in NMRI mice from week 5 of age onward until the time of mating (Figure 5A, Sidak's multiple comparisons test, $p < 0.039$). In contrast, no differences in non-fasted blood glucose measurements were induced (Figure 5B). An intraperitoneal glucose tolerance test (ipGTT) was performed at 10 weeks of age to test dam's glucose tolerance. It revealed prolonged and increased blood glucose levels after glucose injection (Figure 5C, Sidak's multiple comparisons test, 20-60 min: $p < 0.001$, 80 min $p = 0.006$). Furthermore, the area under the curve (AUC) of the glucose levels during the ipGTT is increased in HCD fed animals (Figure 1D, t-test, $p < 0.001$) accompanied by an increase in plasma insulin levels (Figure 5E, Sidak's multiple comparisons test, 20 min: $p < 0.001$, 120 min: $p = 0.002$). Lastly, litter size did not differ between diets (Figure 5F). Overall, these results display a relatively mild diet induced obesity phenotype with increased body weight and decreased glucose tolerance in outbred NMRI mice after HCD feeding previously described and aimed for in this thesis (Dahlhoff et al., 2014).

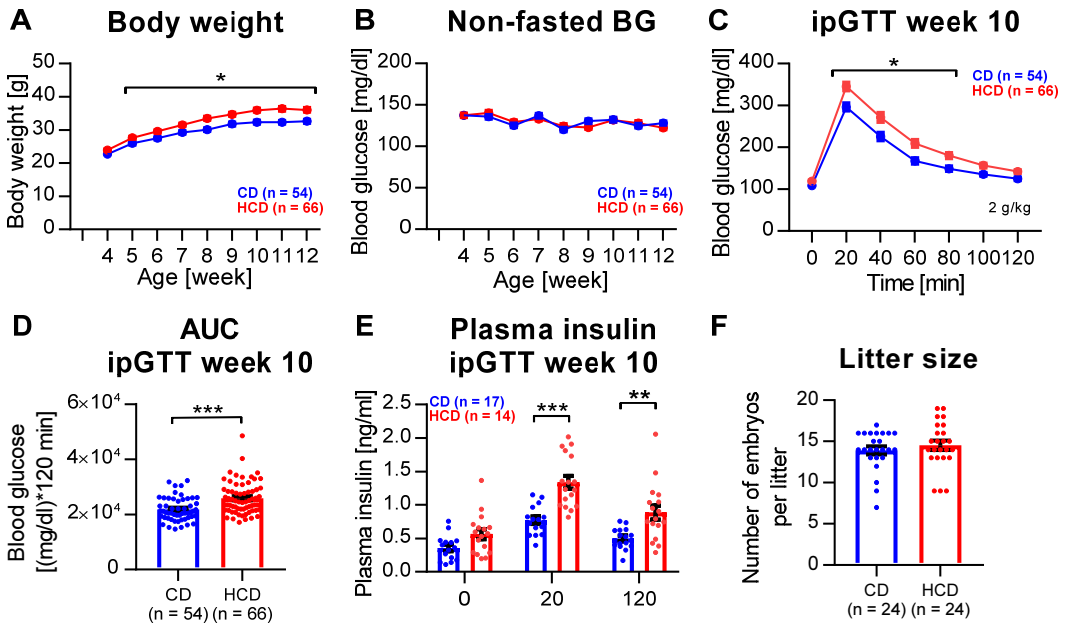

Figure 5: Impact of HCD feeding on NMRI dams.
NMRI dams were fed either a CD or an HCD diet starting at age 3 and mated at age 12 weeks. Body weight (A: n = 54/66 (CD/HCD)) and non-fasted blood glucose (B: n = 54/66 (CD/HCD)) were measured weekly. At age 10 weeks an intraperitoneal glucose tolerance test was performed and blood glucose

was measured every 20 minutes after injecting 2 g/kg glucose intraperitoneally (C: n = 54/66 (CD/HCD)). The area under curve was calculated (D: n = 54/66 (CD/HCD)) and plasma insulin levels were measured (E: n = 17/14 (CD/HCD)). Lastly, litter size was counted (F: n = 24/24 (CD/HCD)). All data are depicted as mean ± SEM. Statistics: 2-way ANOVA + Sidak's multiple comparisons test (A, B, C, E), t-test (D, F). $p < 0.05$ *, $p < 0.01$ **, $p < 0.001$ ***
CD = Control diet; HCD = High caloric diet; NMRI = Naval Medical Research Institute; BG = blood glucose; ipGTT = intraperitoneal glucose tolerance test; AUC = Area under curve

3.2 Maternal diet and offspring sex do not influence *ex vivo* differentiation of MEFs

To investigate the impact of maternal HCD feeding on adipogenic differentiation capacity of offspring preadipocytes, MEFs were isolated, differentiated into adipocytes for two weeks and lipid droplet formation was quantified using Bodipy fluorescence staining on day 12 of differentiation. Isolated MEFs were successfully differentiated into adipocytes indicated by increased formation of lipid droplets compared to undifferentiated control cells (inset) visualized using Bodipy fluorescence staining (Figure 6A) and quantified by total Bodipy fluorescence measurements (Figure 6B, Sidak's multiple comparisons test, mat-CD: $p < 0.001$, mat-HCD, $p < 0.001$). Next, the impact of maternal diet and offspring sex on adipogenic differentiation capacity of MEFs was tested revealing no differences between groups (Figure 6C).

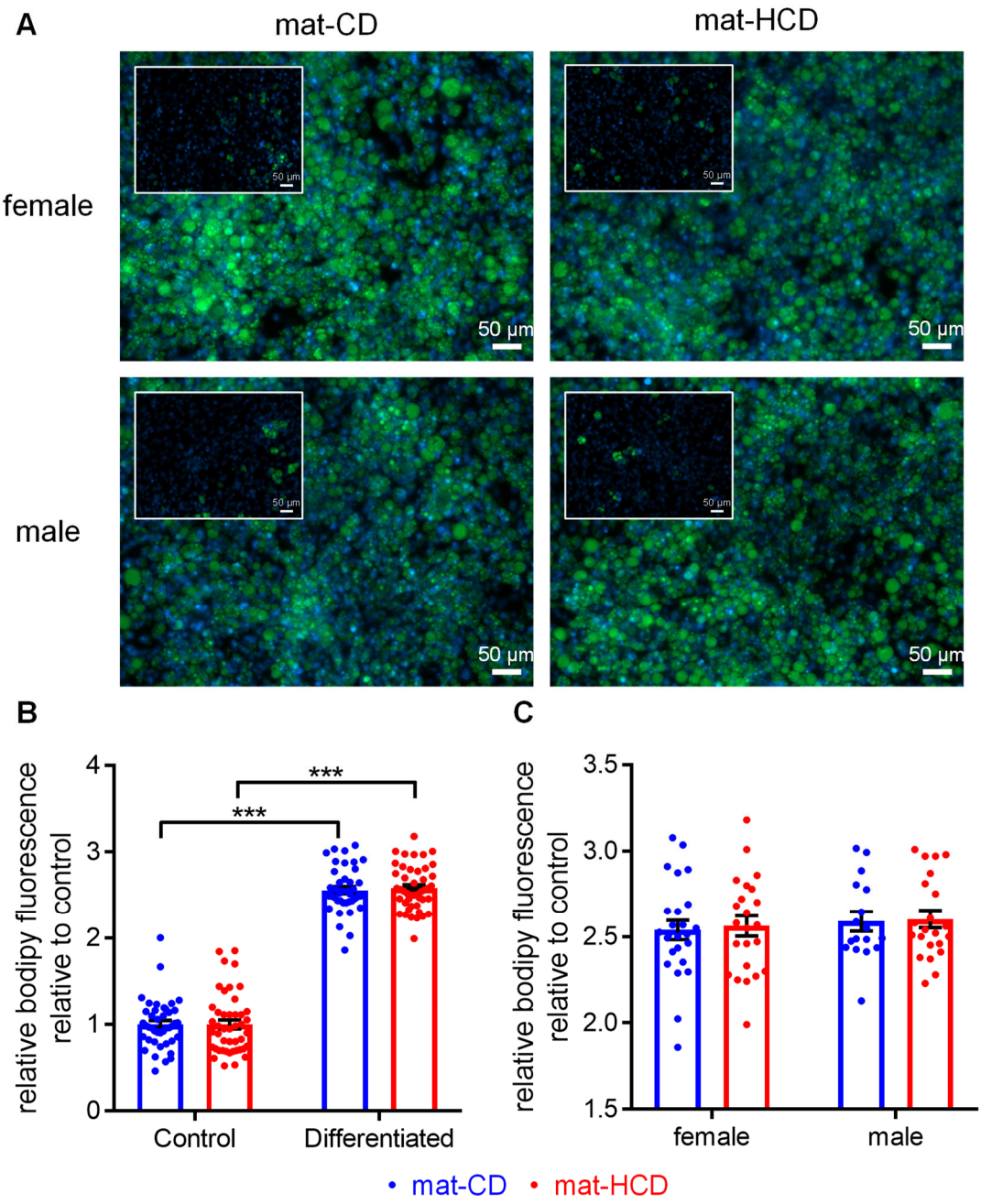

Figure 6: *Ex vivo* differentiation of mouse embryonic fibroblasts into adipocytes.
A: After isolation mouse embryonic fibroblasts (MEFs) were differentiated *ex vivo*. Differentiated and undifferentiated (inset) cells' nuclei (blue, Hoechst 33342) and lipid droplets (green, Bodipy 493/503) were stained. Depicted are representative pictures of MEFs obtained from male and female offspring of both CD and HCD fed dams. B+C: Lipids droplet content was quantified by measuring Bodipy fluorescence (B: n = 42/45 (mat-CD/mat-HCD), C: female: n = 25/23 (mat-CD/mat-HCD); male: n = 17/22 (mat-CD/mat-HCD)). All data are depicted as mean ± SEM. Statistics: 2-way ANOVA + Sidak's multiple comparisons test (B, C). $p < 0.05$ *, $p < 0.01$ **, $p < 0.001$ ***
MEF = mouse embryonic fibroblast; mat-CD = maternal control diet; mat-HCD = maternal high caloric diet;

Microscopic observations revealed that only parts of the heterogenic MEF cell culture accumulate lipid droplets and differentiate into adipocytes. Further flow cytometric analysis revealed that around 20% of total cells harvested using trypsin contained lipid droplets (Figure

7B). In order to investigate adipocyte specific effects it was aimed to increase adipocyte purity in samples generated for later analysis. Testing revealed that collagenase and dispase treatment primarily detached cells containing lipid droplets, thereby increasing adipocyte purity to around 50% (Figure 7B). Next, decreased adipocyte density caused by the low density of lipid droplets was utilized to increase adipocyte purity using density based gradient sorting (Figure 7A). In this way, adipocyte samples with a purity of around 80% were generated for later molecular biological analysis.

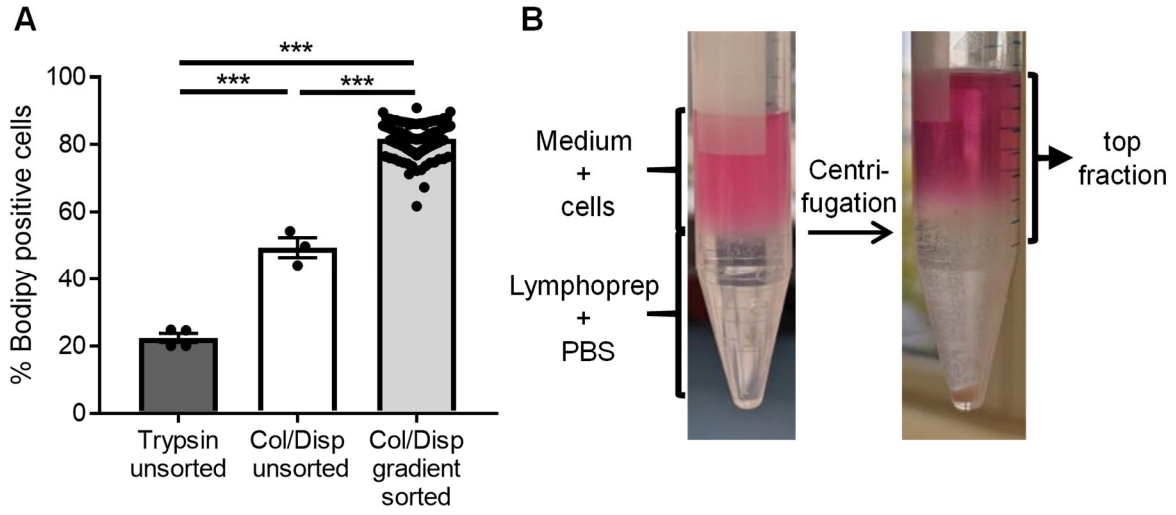

Figure 7: *Ex vivo* differentiation of mouse embryonic fibroblasts.
A: After harvest, adipocytes were enriched using density based gradient sorting. Cell suspension in medium was layered on top of a 50%-Lymphoprep-50%-PBS-mixture. After centrifugation adipocyte containing top fraction was further analyzed. B: Percentage of Bodipy positive cells after different harvesting protocols was quantified using flow cytometry (B: n = 152/3/4 (Col/Disp sorted/ Col/Disp unsorted/ Trypsin unsorted)). All data are depicted as mean ± SEM. Statistics: 1-way ANOVA + Tukey's multiple comparisons test. $p < 0.05$ *, $p < 0.01$ **, $p < 0.001$ ***
Col = Collagenase D; Disp = Dispase II

3.3 Transcriptome of female *ex vivo* differentiated adipocytes is altered by maternal HCD diet

The transcriptome of offspring's adipocyte differentiated from MEFs was analyzed to investigate whether maternal obesity in pregnancy affects gene expression in female offspring. RNA sequencing analysis of both mat-CD and mat-HCD female E13.5 adipocytes was performed in collaboration with the Genomics and Transcriptomics laboratory of the Heinrich-Heine-University Düsseldorf. It revealed the significant downregulation of Aldehyde dehydrogenase family 1, subfamily A1 (*Aldh1a1,* FDR = 0.016) and Aldehyde dehydrogenase family 1, subfamily A7 (*Aldh1a7,* FDR = 0.007) and upregulation of SCAN domain-containing 1 (*Scand1,* FDR = 0.007), and histocompatibility 2, Q region locus 2 (*H2-Q2,* FDR = 0.018) in mat-HCD offspring compared to mat-CD offspring (Table 12 + Table 13, Figure 8A).

Table 12: Top 10 upregulated genes in mat-HCD female E13.5 adipocytes compared to mat-CD samples analyzed by RNA sequencing and sorted by false discovery rate (FDR).

Gene ID	Identifier	Log2(fold change)	Fold change	p-value	FDR
Scand1	ENSMUSG00000046229	0.80	1.75	< 0.001	0.007
H2-Q2	ENSMUSG00000091705	1.21	2.32	< 0.001	0.018
Gm11127	ENSMUSG00000079492	1.17	2.24	< 0.001	0.051
Dusp3	ENSMUSG00000003518	0.55	1.47	< 0.001	0.055
H2-Q6	ENSMUSG00000073409	1.18	2.27	< 0.001	0.055
Lgals3bp	ENSMUSG00000033880	0.58	1.49	< 0.001	0.081
Ly6e	ENSMUSG00000022587	0.59	1.51	< 0.001	0.094
Gvin2	ENSMUSG00000078606	1.06	2.08	< 0.001	0.100
H2-Q7	ENSMUSG00000060550	1.40	2.65	< 0.001	0.125
H2-Q10	ENSMUSG00000067235	1.14	2.21	< 0.001	0.130

Table 13: Top 10 downregulated genes in mat-HCD female E13.5 adipocytes compared to mat-CD samples analyzed by RNA sequencing and sorted by false discovery rate (FDR).

Gene ID	Identifier	Log2(fold change)	Fold change	p-value	FDR
Aldh1a7	ENSMUSG00000024747	-1.13	-2.19	< 0.001	0.007
Aldh1a1	ENSMUSG00000053279	-0.74	-1.67	< 0.001	0.016
Acbd6	ENSMUSG00000033701	-0.50	-1.41	< 0.001	0.051
Ncan	ENSMUSG00000002341	-1.07	-2.10	< 0.001	0.051
Col2a1	ENSMUSG00000022483	-1.54	-2.92	< 0.001	0.213
Glrx3	ENSMUSG00000031068	-0.44	-1.35	0.001	0.295
Anxa8	ENSMUSG00000021950	-0.46	-1.38	0.002	0.483
Camp	ENSMUSG00000038357	-1.35	-2.56	0.003	0.609
H4c9	ENSMUSG00000060639	-0.55	-1.47	0.003	0.621
Lss	ENSMUSG00000033105	-0.39	-1.31	0.006	0.873

Next, RT-qPCR and western blotting were used to validate expression changes identified using RNA sequencing. RT-qPCR analysis backed observed changes in *Aldh1a1* (t-test, p = 0.007) and *Aldh1a7* (t-test, p = 0.004) expression, but revealed a decreased *Scand1* (t-test, p = 0.003) and an unchanged *H2-Q2* expression (Figure 8B). Due to limited antibody availability, protein expression only of ALDH1A! was studied using western blotting, which was unchanged in mat-HCD offspring (t-test, p = 0.112, Figure 8C).

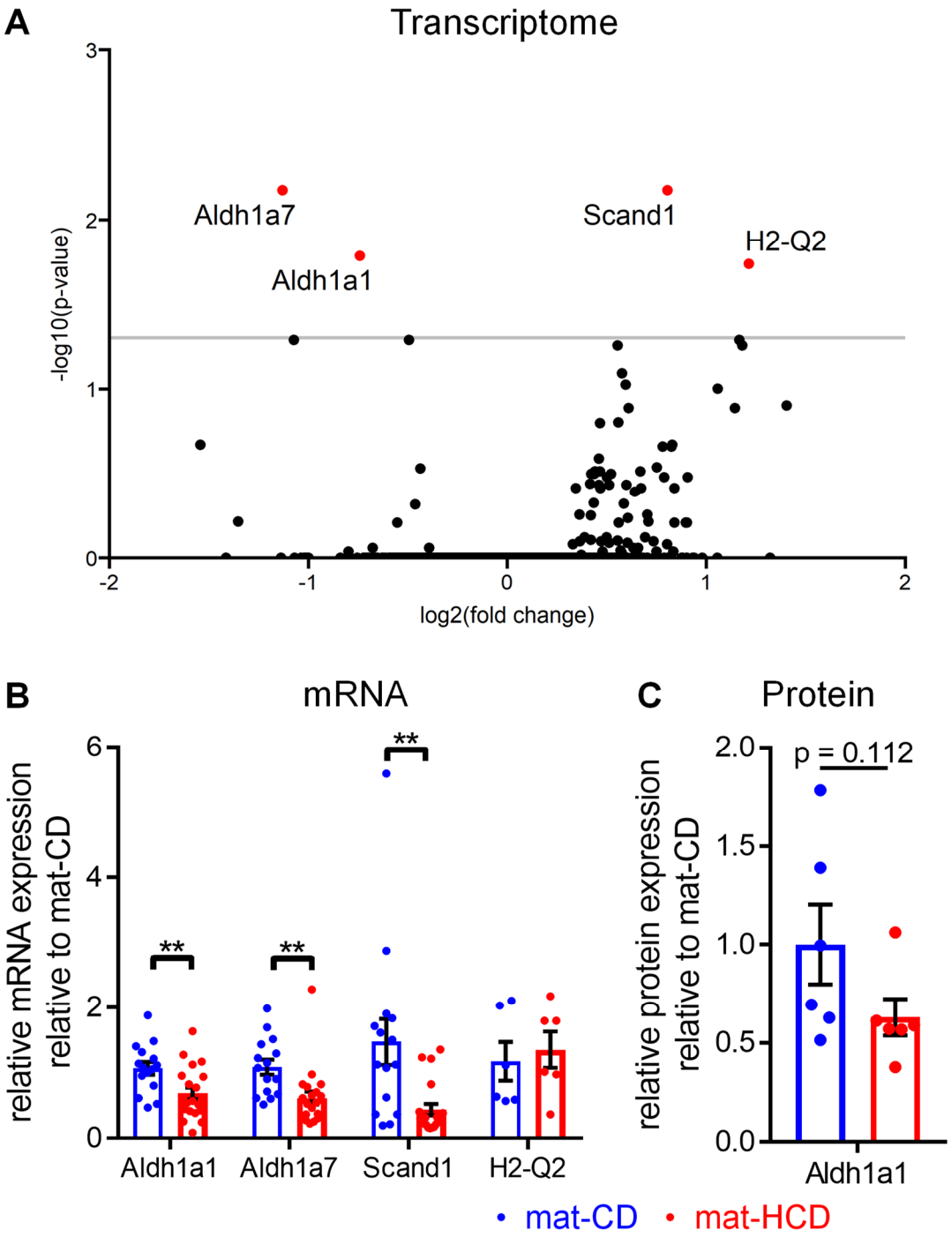

Figure 8: Transcriptomic analysis of female E13.5 adipocytes differentiated from MEFs.
A: Female E13.5 adipocyte transcriptome was analyzed using RNA sequencing (n = 6/6 (mat-CD/ mat-HCD)). B+C: Expression of significantly dysregulated genes was further analyzed using RT-qPCR (B: *Aldh1a1*, *Aldh1a7*, *Scand1* n = 15/20 (mat-CD/ matHCD), *H2-Q2* n = 6/6 (mat-CD/ matHCD)) and western blotting (C: n = 6/6 (mat-CD/matHCD)). All data are depicted as mean ± SEM. Statistics: t-test (B-C). $p < 0.05$ *, $p < 0.01$ **, $p < 0.001$ ***
MEF = Mouse embryonic fibroblast; mat-CD = maternal control diet; mat-HCD = maternal high caloric diet; *Aldh1a1* = Aldehyde dehydrogenase family 1, subfamily A1; *Aldh1a7* = Aldehyde dehydrogenase family 1, subfamily A7; *Scand1* = SCAN domain-containing 1; *H2-Q2* = histocompatibility 2, Q region locus 2

To test whether dysregulation of these genes continues into adulthood visceral adipose tissue samples from adult mat-CD and mat-HCD exposed offspring previously isolated and analyzed using microarray analysis by my research group was used. By checking microarray analysis data for *Aldh1a1*, *Aldh1a7*, and *Scand1* expression levels revealed significant downregulation of *Aldh1a7* expression by mat-HCD feeding in both 6- as well as 20-week-old offspring (Figure 9A+B, 6 weeks: raw-p = 0.048, 20 weeks: FDR = 0.027; unpublished data) as well as downregulation of *Aldh1a1* in 20-week-old offspring while it was not detected in 6-week-old offspring (Figure 9A+B, 20 weeks: FDR = 0.022, unpublished data). Microarray analysis was not able to detect any *Scand1* expression. Using RT-qPCR to validate these findings did not reveal statistically significant differences in *Aldh1a1* and *Aldh1a7* expression in 6- and 16-week-old offspring (Figure 9C+D). Again, it was not possible to detect any *Scand1* expression in these samples.

Overall, these data reveal the dysregulation of *Aldh1a1, Aldh1a7,* and *Scand1* by maternal HCD feeding in female offspring embryonic adipocytes and suggest a persistent later life downregulation of *Aldh1a1* and *Aldh1a7* in visceral adipose tissue of adult female mat-HCD offspring.

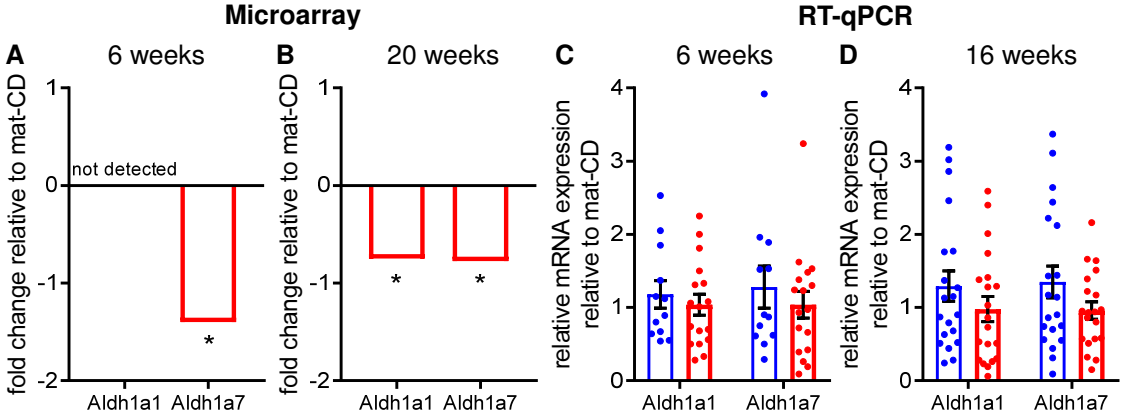

Figure 9: Analysis of *Aldh1a1* and *Aldh1a7* mRNA in adult female offspring visceral adipose tissue.
Aldh1a1 and *Aldh1a7* expression was studied using microarray analysis in 6- (A: n = 10/10 (mat-CD/ mat-HCD)) and 20-weeks-old female offspring (B, n = 5/5 (mat-CD/ mat-HCD)) and RT-qPCR in 6 weeks (C, n = 12/17 (mat-CD/ mat-HCD)) and 16 weeks (D, n = 20/20 (mat-CD/ mat-HCD)) old offspring. All data are depicted as mean ± SEM. Statistics: t-test (A, C, D), local pooled error test (B) $p < 0.05$ *, $p < 0.01$ **, $p < 0.001$ ***
mat-CD = maternal control diet; mat-HCD = maternal high caloric diet; *Aldh1a1* = Aldehyde dehydrogenase family 1, subfamily A1; *Aldh1a7* = Aldehyde dehydrogenase family 1, subfamily A7

3.4 Adipogenic differentiation of 3T3-L1 cells using PPARG agonist rosiglitazone

The murine 3T3-L1 preadipocyte cell line is commonly used to investigate adipogenesis (Dufau et al., 2021). Recently, an optimized differentiation protocol including PPARG agonist rosiglitazone was presented, but adipogenic differentiation was only assessed by analyzing

lipid droplet formation (Zebisch et al., 2012). This new protocol was introduced in my laboratory and its suitability for my research was assessed morphologically by fluorescence staining and regarding mRNA and protein expression of genes involved in adipogenic differentiation, DNL, fatty acid storage and transport, as well as adipokine and cytokine signaling.

3T3-L1 preadipocytes were adipogenically differentiated for 15 days with sample points on days 0, 2, 4, 7, 11, and 15 of differentiation. Morphological analysis using fluorescence Bodipy (lipid droplets, green) and Hoechst (nuclei, blue) staining and subsequent fluorescence microscopy revealed increasing lipid droplet formation, especially between days 4 and 7 of differentiation (Figure 10A). This was confirmed by subsequent lipid droplet quantification using Bodipy fluorescence measurements (Figure 10B: Dunnett's multiple comparisons test in comparison to day 0, day 4 $p = 0.001$, day 7-15 $p < 0.001$). Furthermore, cell lipid droplet content plateaued on day 11 of differentiation and remained at this increased level afterwards (Figure 10B).

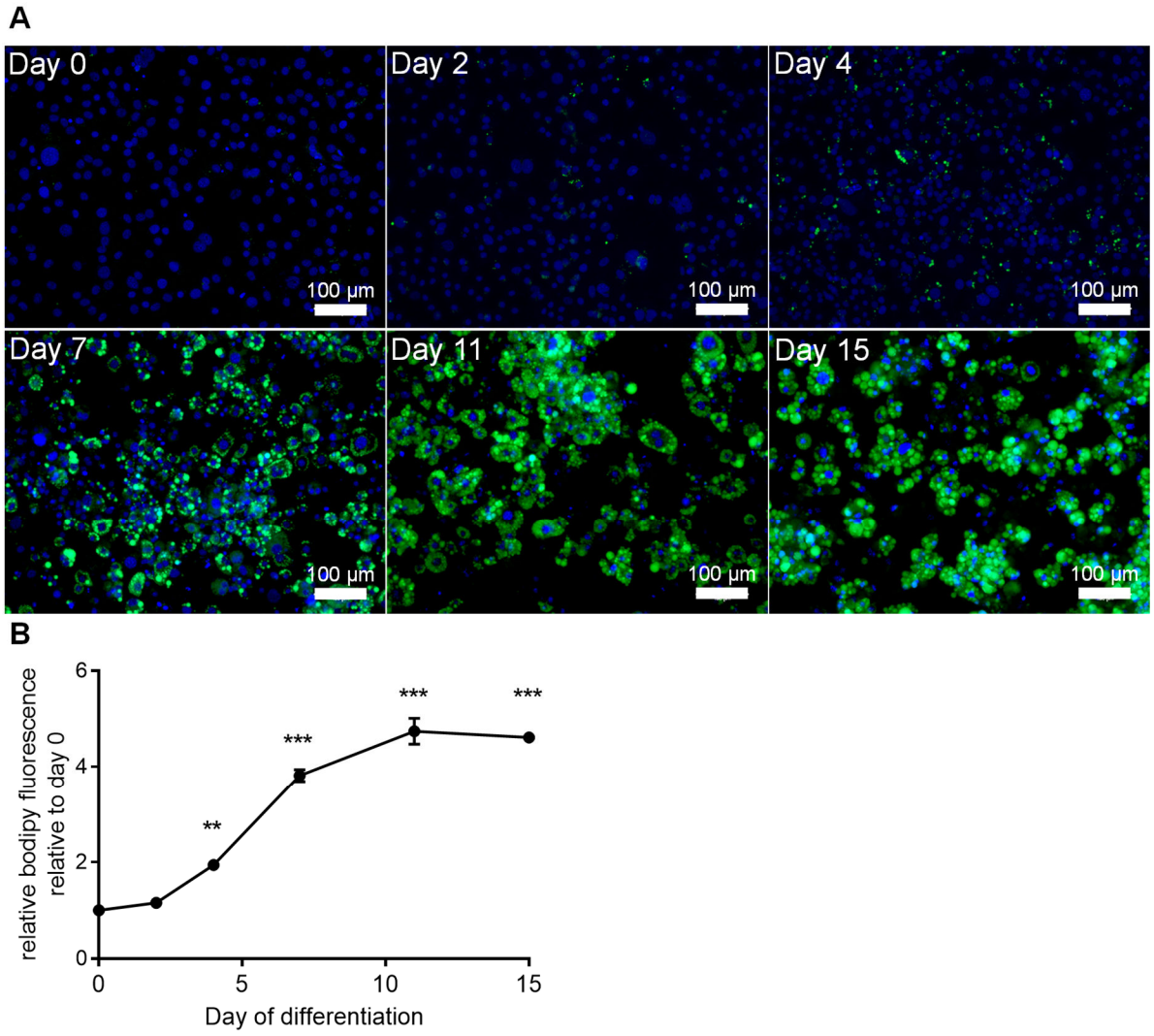

Figure 10: Morphological analysis of 3T3-L1 cells during adipogenic differentiation induced using PPARG agonist rosiglitazone.

3T3-L1 cell adipogenic differentiation was induced using insulin, IBMX, dexamethasone, and Pparg agonist rosiglitazone. A: At different days of differentiation cells were stained using Hoechst 33342 (nuclei, blue) and Bodipy 493/503 (lipid droplets, green) and imaged using fluorescence microscopy. B: Lipid droplet formation was quantified using Bodipy fluorescence quantification. All data are depicted as mean ± SEM and n = 3 for all data. Statistics: 1-way ANOVA + Dunnett's multiple comparisons test in comparison to day 0 (B). $p < 0.05$ *, $p < 0.01$ **, $p < 0.001$ ***

To further evaluate this differentiation protocol and its suitability for my research expression of different commonly investigated genes involved in adipogenic differentiation, DNL, fatty acid storage and transport, as well as adipokine and cytokine signaling during adipogenesis was assessed.

Pparg2 mRNA expression strongly increased during differentiation and remained on an elevated level from day 4 of differentiation (Figure 11A; Dunnett's multiple comparison test in comparison to day 0, only significant results stated, day 7-15 $p \leq 0.014$). PPARG2 protein expression mostly mimicked its mRNA expression profile but decreased from day 11 to day 15 of differentiation (day 7+11 $p \leq 0.009$). *Pparg1* mRNA expression increased up to day 4 and decreased again afterwards (Figure 11A; day 4 $p = 0.023$). PPARG1 protein expression on the other hand sharply increased up to day 4 of differentiation and decreased again afterwards revealing larger changes in expression on the protein compared to the mRNA level (Day 2-11 $p \leq 0.033$). *Cebpa* mRNA expression increased up to day 4, and decreased afterwards (day 4 $p = 0.003$).

Examining mRNA expression of *Acaca, Fasn, Nr1h3,* and *Srebf1c,* which are all involved in DNL in adipocytes, revealed increased expression of *Acaca* and *Fasn* during adipogenic differentiation but no changes in *Nr1h3* and *Srebf1c* expression (Figure 11B). Both *Acaca* and *Fasn* expression increased up to day 7 of differentiation and remained elevated afterwards (*Acaca*: day 7-15 $p \leq 0.016$; *Fasn:* day 4-15 $p \leq 0.003$). Their protein expression levels followed a similar pattern. However, ACACA protein expression levels decreased after day 7 of differentiation (ACACA: day 4-15 $p \leq 0.022$; FASN: day 7-15 $p \leq 0.012$).

Fatty acid transport and storage within adipocytes is a key function of adipocytes involving genes like *Cd36, Cidea, Fabp4,* and *Pgc-1a,* whose expression was examined next. Both *Cd36* and *Fabp4* mRNA expression strongly increased up to day 4 of differentiation and remained constantly increased afterwards (Figure 11C; *Cd36*: day 4+11+15 $p \leq 0.021$; *Fabp4*: day 4-15 $p \leq 0.046$). FABP4 protein expression mirrored this pattern being nearly undetectable until day 2 and strongly expressed afterwards (day 4-15 $p \leq 0.001$). *Cidea* expression peaked on day 7 and decreased afterwards (day 7 $p = 0.002$). *Pgc-1a* expression remained unchanged during adipogenic differentiation.

Another important adipocyte function involves adipokine and cytokine signaling to regulate metabolism. ADIPONECTIN protein expression strongly increased during differentiation but

there were no changes in mRNA expression (*Adipoq*: Figure 11D; ADIPONECTIN: Day 7-15 $p \leq 0.037$). *Lep* mRNA expression was undetectable in undifferentiated 3T3-L1 cells and remained detectable but unchanged starting on day 2 of differentiation until the end of differentiation. Similarly, *Il6* mRNA expression remained unchanged during adipogenesis. On the other hand, *Mcp-1* mRNA expression is decreased during days 2 to 11 of differentiation compared to undifferentiated cells (day 2-11 $p \leq 0.046$).

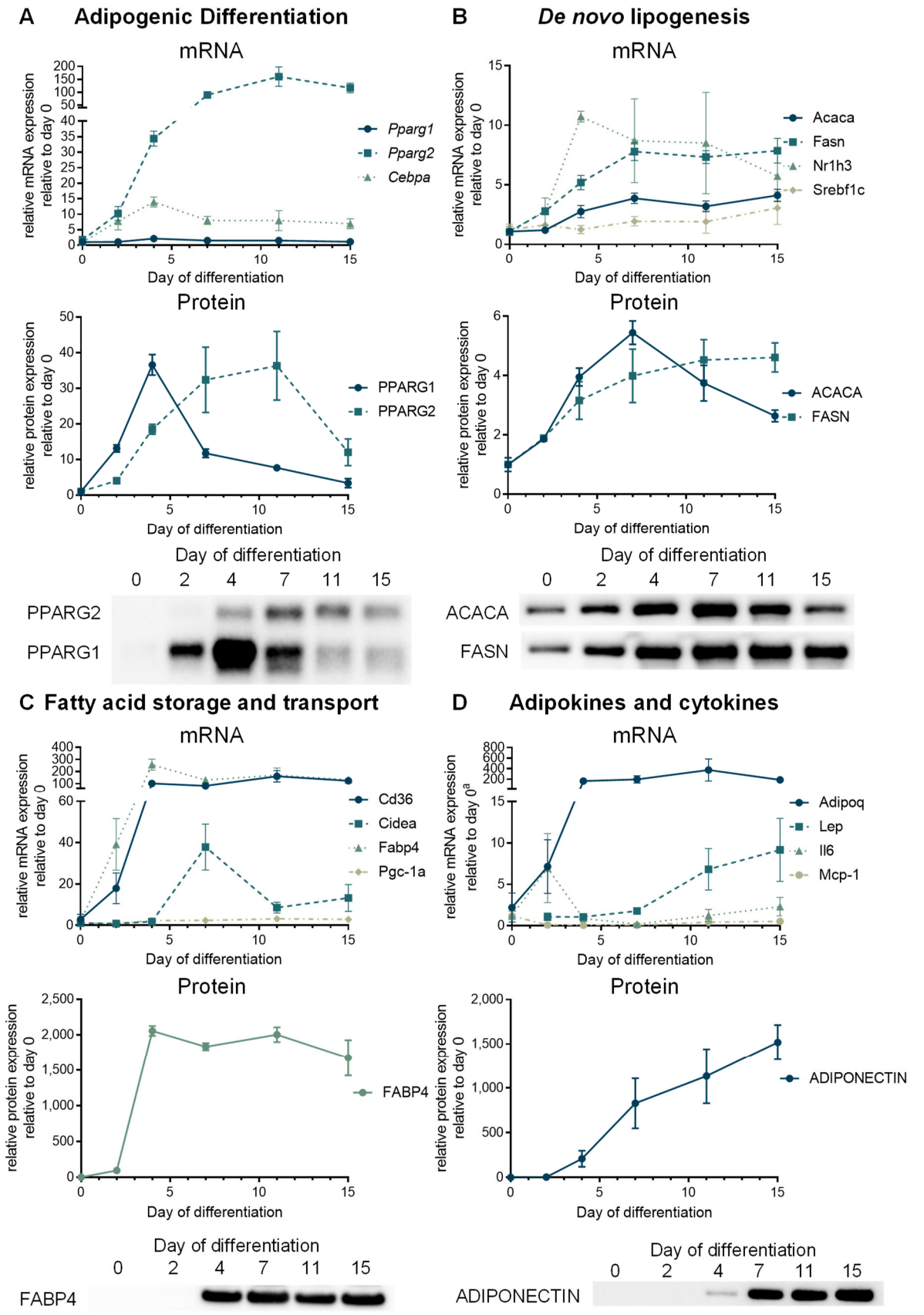

Figure 11: Analysis of mRNA and protein expression of genes related to adipocyte differentiation and function during adipogenic differentiation of 3T3-L1 cells induced using PPARG agonist rosiglitazone.

3T3-L1 cell adipogenic differentiation was induced using insulin, IBMX, dexamethasone, and Pparg agonist rosiglitazone. At different days of differentiation mRNA and protein expression of genes involved

in adipogenic differentiation (C), de novo lipogenesis (D), fatty acid storage and transport (E), and adipokines and cytokines were quantified using RT-qPCR and western blotting respectively. Significant differences relative to expression levels of day 0 are not indicated to avoid overloading plots. All data are depicted as mean ± SEM and n = 3 for all data.
[a]*Lep* expression was not detectable on day 0 of differentiation and therefore day 2 of differentiation was used as a reference point instead of day 0.
IBMX = 3-isobutyl-1-methylxanthine; *Pparg1* = Peroxisome proliferator-activated receptor gamma 1; *Pparg2* = Peroxisome proliferator-activated receptor gamma 2; *Cebpa* = CCAAT/enhancer-binding protein alpha; *Acaca* = Acetyl-CoA carboxylase 1; *Fasn* = Fatty acid synthase; *Nr1h3* = Nuclear receptor subfamily 1, group H, member 3; *Srebf1c* = Sterol regulatory element binding transcription factor 1c; *Cidea* = Cell death-inducing DNA fragmentation factor, alpha subunit-like effector A; *Cd36* = Cluster of differentiation 36; *Fabp4* = Fatty acid binding protein 4; *Pgc-1a* = Peroxisome proliferative activated receptor, gamma, coactivator 1 alpha; *Lep* = Leptin; *Adipoq* = Adiponectin, C1Q and collagen domain containing; *Il6* = Interleukin 6; *Mcp-1* = Monocyte Chemoattractant Protein-1

As lipid droplet formation plateaued starting on day 11 of differentiation it was decided to use this as the time point of completed adipocyte differentiation and tested which genes can be used as markers for successful adipocyte differentiation using rosiglitazone. Expression of *Pparg1* (Dunnett's multiple comparison test in comparison to day 0, protein, $p = 0.033$), *Pparg2* (mRNA $p < 0.001$, protein $p = 0.004$), *Acaca* (mRNA $p = 0.016$, protein, $p < 0.001$), *Fasn* (mRNA $p < 0.001$, protein $p = 0.004$), *CD36* (mRNA $p < 0.001$), *Fabp4* (mRNA $p = 0.009$, protein $p < 0.001$), and *Adipoq* (protein $p = 0.005$) were significantly increased after differentiation on day 11 compared to undifferentiated cells. Therefore, they were considered suitable to be used as markers for successful adipogenesis in 3T3-L1 cells differentiated using rosiglitazone.

Taken together, an optimized 3T3-L1 differentiation protocol including rosiglitazone was suitable to investigate genes involved in adipogenesis, and markers for successful adipocyte differentiation were defined.

3.5 *Aldh1a7* but not *Aldh1a1* knockdown impairs early stages of adipogenesis

Having established the new protocol for adipogenically differentiating 3T3-L1 cells, the role of *Aldh1a1* and *Aldh1a7* during murine adipogenesis was investigated next. First, the time course of their mRNA expression during adipogenic differentiation of 3T3-L1 cells was examined revealing that *Aldh1a7* mRNA expression strongly increased up to day 4 and remained significantly elevated afterwards (Figure 12; Dunnett's multiple comparisons test in comparison to day 0, day 4-11 $p \leq 0.018$). However, *Aldh1a1* mRNA expression did not increase during differentiation, implying a larger role of *Aldh1a7* in adipogenesis compared to *Aldh1a1*.

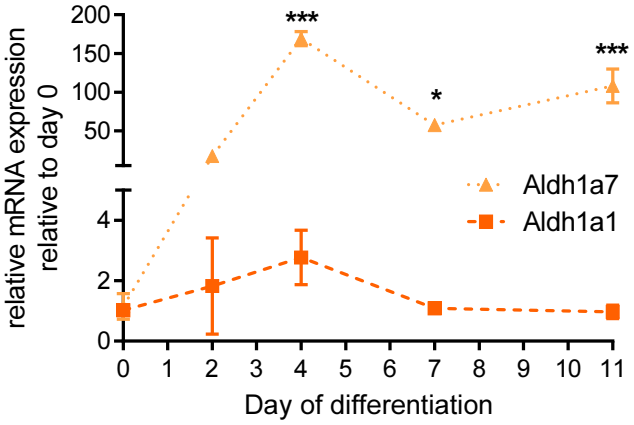

Figure 12: *Aldh1a1* and *Aldh1a7* mRNA expression during adipogenic differentiation of 3T3-L1 cells.
Aldh1a1 and *Aldh1a7* mRNA expression was quantified at different time points of adipogenic differentiation using RT-qPCR. All data are depicted as mean ± SEM and n = 3 for all data. Statistics: 1-way ANOVA + Dunnett's multiple comparisons test in comparison to day 0. $p < 0.05$ *, $p < 0.01$ **, $p < 0.001$ ***
Aldh1a1 = Aldehyde dehydrogenase family 1, subfamily A1; *Aldh1a7* = Aldehyde dehydrogenase family 1, subfamily A7;

Next, isoform-specific siRNA knockdown was used to further investigate *Aldh1a1's* and *Aldh1a7's* involvement in adipogenesis. Lipofectamine mediated siRNA knockdown was applied one day prior to differentiation (day -1 of differentiation) for 24 hours. It successfully decreased *Aldh1a1* (Dunnett's multiple comparisons test in comparison to control, $p = 0.004$) and *Aldh1a7* expression ($p < 0.001$) specifically down to 14% and 16%, respectively, on day 0 of differentiation (Figure 13).

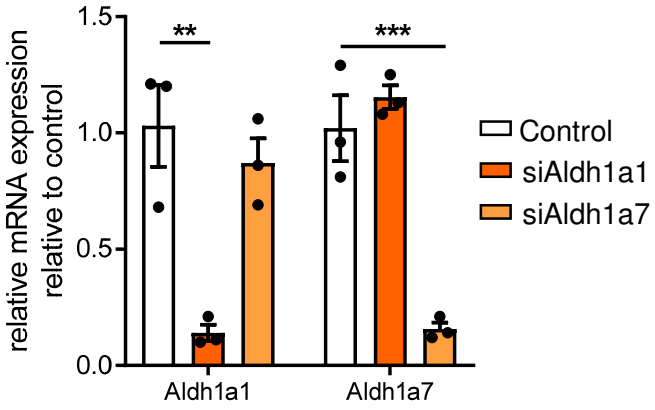

Figure 13: Quantification of knockdown efficiency by gene specific *Aldh1a1* and *Aldh1a7* siRNA guided knockdown.
Gene specific *Aldh1a1* and *Aldh1a7* siRNA induced knockdown was performed one day prior to differentiation start and knockdown efficiency was measured on day 0 of differentiation using RT-qPCR. All data is depicted as mean ± SEM and n = 3 for all data. Statistics: 1-way ANOVA + Dunnett's multiple comparisons test in comparison to control. $p < 0.05$ *, $p < 0.01$ **, $p < 0.001$ ***
Aldh1a1 = Aldehyde dehydrogenase family 1, subfamily A1; *Aldh1a7* = Aldehyde dehydrogenase family 1, subfamily A7; siAldh1a1 = siRNA targeting *Aldh1a1*; siAldh1a7 = siRNA targeting *Aldh1a7*

Using this technique, the impact of *Aldh1a1* and *Aldh1a7* specific knockdown on early stages of adipogenic differentiation of 3T3-L1 cells was investigated. Adipogenic differentiation was induced one day after knockdown and morphological assessment of differentiation on day 4 revealed a significant reduction in lipid droplet formation after *Aldh1a7* knockdown (Figure 14A+B; Dunnett's multiple comparisons test in comparison to control, $p < 0.001$) but not after *Aldh1a1* knockdown ($p = 0.128$). To test whether this inhibitory effect on adipogenesis also affects mRNA and protein expression of genes linked to adipocyte differentiation and function, RT-qPCR and western blotting were utilized. Expression analysis revealed that mRNA and/ or protein expression of *Pparg2* (Dunnett's multiple comparisons test in comparison to control, mRNA $p = 0.002$), *Cebpa* (mRNA $p = 0.012$), *Fabp4* (mRNA $p = 0.005$, protein $p < 0.001$), *Fasn* (mRNA $p = 0.006$), *Adipoq* (mRNA $p = 0.048$, protein $p = 0.009$), and *Pgc-1a* (mRNA $p = 0.027$) was significantly decreased after knocking down *Aldh1a7* but remain unchanged in *Aldh1a1* knockdown cells (Figure 14C+D).

Concluding, this data revealed an inhibitory effect of *Aldh1a7* but not *Aldh1a1* knockdown on early stages of adipogenic differentiation both on lipid droplet phenotype and the molecular level. Hence, whether this effect perpetuates into later stages of adipogenic differentiation was investigated subsequently.

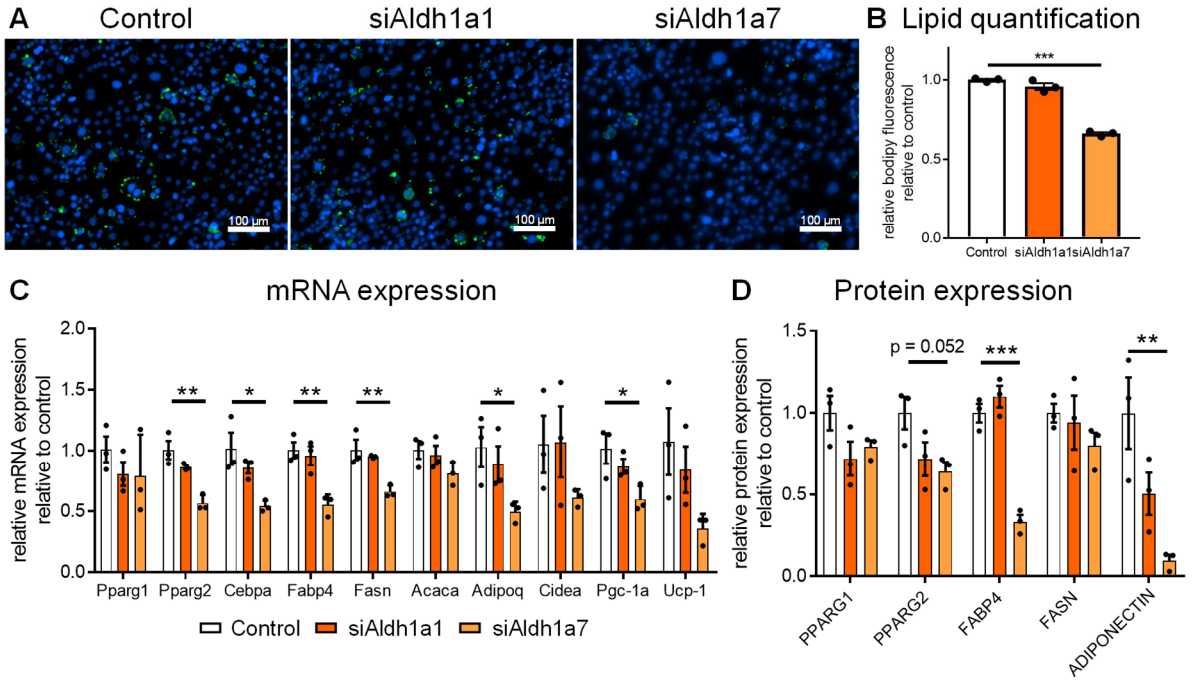

Figure 14: Impact of *Aldh1a1* and *Aldh1a7* knockdown on early stages of adipogenesis of 3T3-L1 cells.
Gene specific *Aldh1a1* and *Aldh1a7* siRNA guided knockdowns were induced one day prior to differentiation start (day -1 of differentiation). A+B: On day 4 of differentiation lipid droplet formation was assessed by staining (A; lipid droplets: green, Bodipy 493/503; nuclei: blue, Hoechst 33342) and Bodipy fluorescence quantification (B). mRNA (C) and protein expression (D) of genes involved in adipogenesis were quantified using RT-qPCR and western blotting respectively. All data are depicted as mean ± SEM and n = 3 for all data. Statistics: 1-way ANOVA + Dunnett's multiple comparisons test in comparison to control (B-D). $p < 0.05$ *, $p < 0.01$ **, $p < 0.001$ ***

Aldh1a1 = Aldehyde dehydrogenase family 1, subfamily A1; *Aldh1a7* = Aldehyde dehydrogenase family 1, subfamily A7; *Pparg1* = Peroxisome proliferator-activated receptor gamma 1; *Pparg2* = Peroxisome proliferator-activated receptor gamma 2; *Cebpa* = CCAAT/enhancer-binding protein alpha; *Fabp4* = Fatty acid binding protein 4; *Fasn* = Fatty acid synthase; *Acaca* = Acetyl-CoA carboxylase 1; *Adipoq* = Adiponectin, C1Q and collagen domain containing; *Cidea* = Cell death-inducing DNA fragmentation factor, alpha subunit-like effector A; *Pgc-1a* = Peroxisome proliferative activated receptor, gamma, coactivator 1 alpha; *Ucp-1* = Uncoupling protein 1; siAldh1a1 = siRNA targeting *Aldh1a1*; siAldh1a7 = siRNA targeting *Aldh1a7*

3.6 *Aldh1a1* and *Aldh1a7* knockdown alter brown adipocyte marker expression at late stages of adipogenesis

Again, isoform specific knockdown was performed one day prior to differentiation (day -1 of differentiation) and 3T3-L1 cells were adipogenically differentiated afterwards. Investigating cells at the end of differentiation (day 11) revealed no significant difference in lipid droplet formation between the groups (Figure 15A+B). Even though a trend for a slightly reduced lipid droplet formation was observed after *Aldh1a7* knockdown (Dunnett's multiple comparisons test in comparison to control, p = 0.064). Expression analysis revealed downregulated mRNA expression of brown adipocyte markers *Cidea* (siAldh1a1: p = 0.025, siAldh1a7: p = 0.003) and *Pgc-1a* (siAldh1a1: p = 0.031, siAldh1a7: p = 0.026) after either *Aldh1a1* or *Aldh1a7* knockdown (Figure 15C).

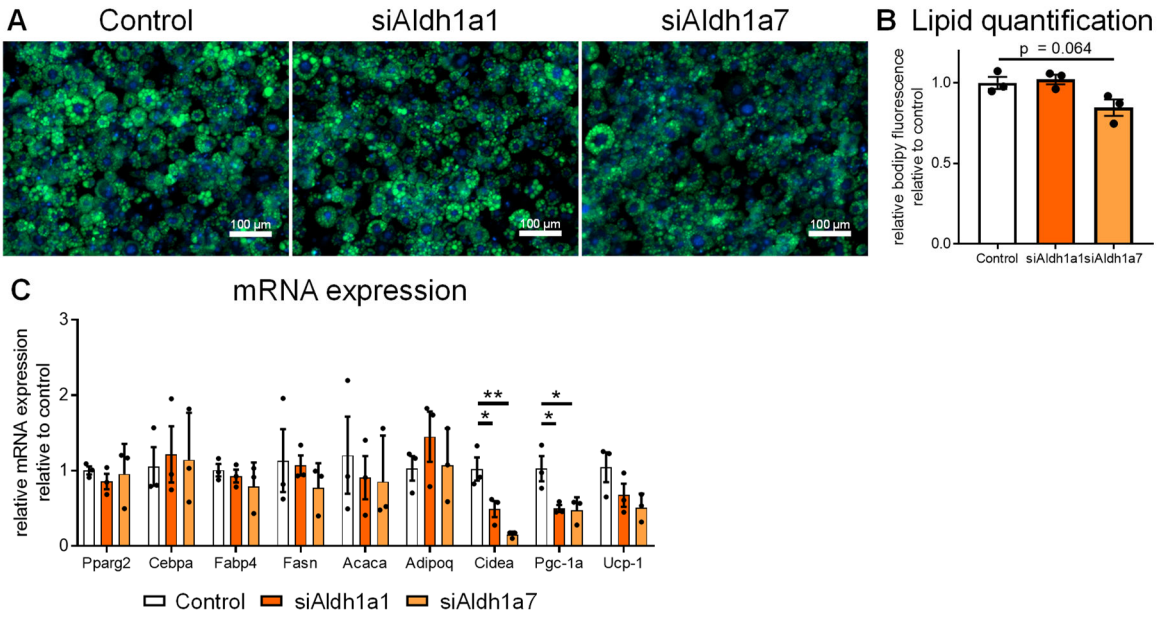

Figure 15: Impact of *Aldh1a1* and *Aldh1a7* knockdown on late stages of adipogenesis of 3T3-L1 cells.
Gene specific *Aldh1a1* and *Aldh1a7* siRNA guided knockdowns were induced one day prior to differentiation start. A+B: On day 11 of differentiation lipid droplet formation was assessed by staining (A; lipid droplets: green, Bodipy 493/503; nuclei: blue, Hoechst 33342) and Bodipy fluorescence quantification (B). C: mRNA expression of genes involved in adipogenesis was quantified using RT-qPCR. All data are depicted as mean ± SEM and n = 3 for all data. Statistics: 1-way ANOVA + Dunnett's multiple comparisons test in comparison to control (B+C). p < 0.05 *, p < 0.01 **, p < 0.001 *** *Aldh1a1* = Aldehyde dehydrogenase family 1, subfamily A1; *Aldh1a7* = Aldehyde dehydrogenase family 1, subfamily A7; *Pparg2* = Peroxisome proliferator-activated receptor gamma 2; *Cebpa* = CCAAT/enhancer-binding protein alpha; *Fabp4* = Fatty acid binding protein 4; *Fasn* = Fatty acid

synthase; *Acaca* = Acetyl-CoA carboxylase 1; *Adipoq* = Adiponectin, C1Q and collagen domain containing; *Cidea* = Cell death-inducing DNA fragmentation factor, alpha subunit-like effector A; *Pgc-1a* = Peroxisome proliferative activated receptor, gamma, coactivator 1 alpha; *Ucp-1* = Uncoupling protein 1; siAldh1a1 = siRNA targeting *Aldh1a1*; siAldh1a7 = siRNA targeting *Aldh1a7*

These results suggest effects of a pre-differentiation *Aldh1a1* or *Aldh1a7* knockdown only on the expression of brown adipocyte markers *Pgc-1a* and *Cidea*, but not on lipid droplet formation at the end of differentiation. Overall, this data unveil a key role of *Aldh1a7* but not *Aldh1a1* in early but not later stages of murine adipogenesis. Whether *Scand1,* which was also dysregulated in mat-HCD female E13.5 adipocytes, is also involved in the regulation of adipogenesis remained open for investigation.

3.7 *Scand1* knockdown does not impact adipogenesis

The role of *Scand1* in adipogenesis was examined next starting by quantifying its mRNA expression during adipogenic differentiation. A significantly reduced *Scand1* mRNA expression on days 2 to 11 of differentiation was observed (Figure 16; Dunnett's multiple comparison test in comparison to day 0, day 2-11 $p \leq 0.009$) implying an involvement in adipogenesis.

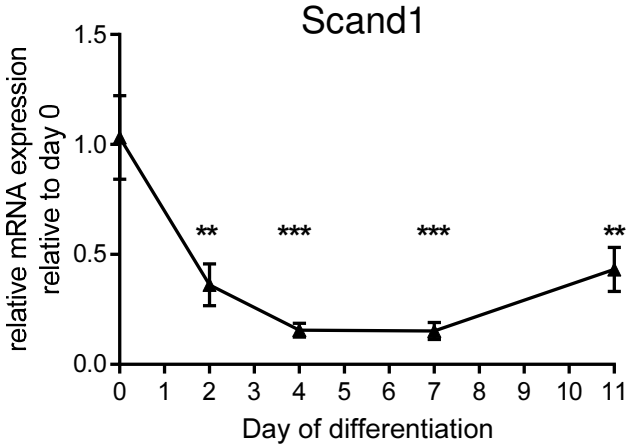

Figure 16: *Scand1* mRNA expression during adipogenic differentiation of 3T3-L1 cells
Scand1 mRNA expression was quantified at different time points of adipogenic differentiation using RT-qPCR. All data are depicted as mean ± SEM and n = 3 for all data. Statistics: 1-way ANOVA + Dunnett's multiple comparisons test in comparison to day 0. $p < 0.05$ *, $p < 0.01$ **, $p < 0.001$ ***
Scand1 = SCAN domain-containing 1

Again, Lipofectamine mediated siRNA knockdown was applied one day prior to differentiation (day -1 of differentiation) for 24 hours, and it successfully reduced *Scand1* expression to 16% on day 0 of differentiation (Figure 17; t-test, $p = 0.020$).

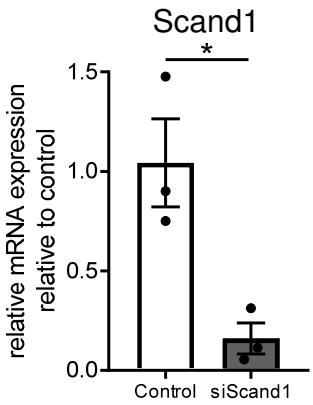

Figure 17: Quantification of knockdown efficiency by gene specific *Scand1* siRNA guided knockdown.
Gene specific Scand1 siRNA knockdown was induced one day prior to differentiation start and knockdown efficiency was measured on day 0 of differentiation using RT-qPCR. All data are depicted as mean ± SEM and n = 3 for all data. Statistics: t-test. $p < 0.05$ *, $p < 0.01$ **, $p < 0.001$ ***
Scand1 = SCAN domain-containing 1; siScand1 = siRNA targeting *Scand1*

First, the impact of *Scand1* knockdown on early stages of differentiation was examined. By quantifying lipid droplet formation on day 4 of differentiation, a slight but significant reduction in lipid droplet formation was observed after *Scand1* knockdown (Figure 18A+B; t-test, p = 0.019). Additionally, mRNA expression of *Cebpa* (t-test, p = 0.049) and *Ucp-1* (p = 0.043) was slightly reduced in siScand1 treated cells (Figure 18C).

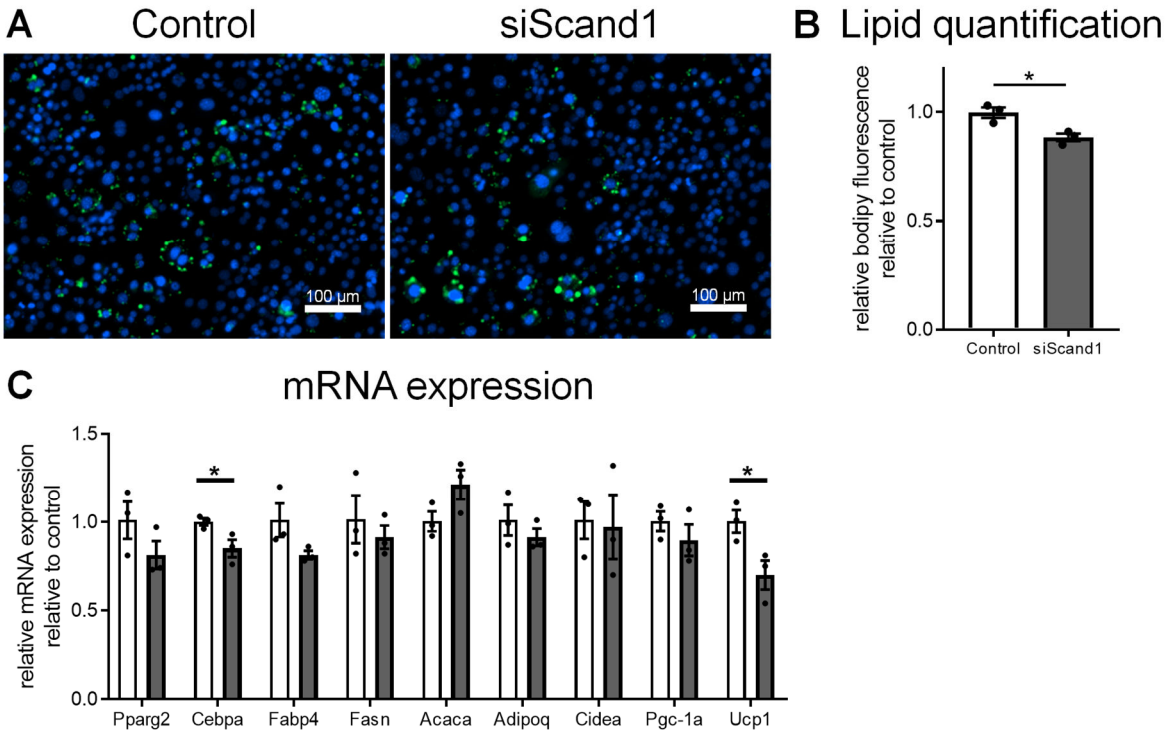

Figure 18: Impact of *Scand1* knockdown on early stages of adipogenesis of 3T3-L1 cells.
Gene specific Scand1 siRNA knockdown was induced one day prior to differentiation start. A+B: On day 4 of differentiation lipid droplet formation was assessed by staining (A; lipid droplets: green, Bodipy 493/503; nuclei: blue, Hoechst 33342) and Bodipy fluorescence quantification (B). C: mRNA expression

of genes involved in adipogenesis was quantified using RT-qPCR. All data are depicted as mean ± SEM and n = 3 for all data. Statistics: t-test (C-B). p < 0.05 *, p < 0.01 **, p < 0.001 ***
Scand1 = SCAN domain-containing 1; Pparg2 = Peroxisome proliferator-activated receptor gamma 2; Cebpa = CCAAT/enhancer-binding protein alpha; Fabp4 = Fatty acid binding protein 4; Fasn = Fatty acid synthase; Acaca = Acetyl-CoA carboxylase 1; Adipoq = Adiponectin, C1Q and collagen domain containing; Cidea = Cell death-inducing DNA fragmentation factor, alpha subunit-like effector A; Pgc-1a = Peroxisome proliferative activated receptor, gamma, coactivator 1 alpha; Ucp-1 = Uncoupling protein 1; siScand1 = siRNA targeting *Scand1*

Next, the influence of a pre-differentiation *Scand1* knockdown on late stages of adipogenesis was investigated. No changes were seen for both lipid droplet formation (Figure 19A+B) as well as mRNA expression of genes related to adipocyte development and function (Figure 19C).

In conclusion, the course of its reduced expression during adipogenesis suggests that *Scand1* is involved or at least regulated during adipogenesis. However, siRNA knockdown influenced adipogenesis barely at early stages and not at all in late stages.

Overall, data provide evidence of an involvement of *Aldh1a1, Aldh1a7,* and *Scand1,* that were dysregulated by maternal HCD feeding before and during pregnancy in murine adipogenesis raising the question of whether these results can be translated into human adipogenesis.

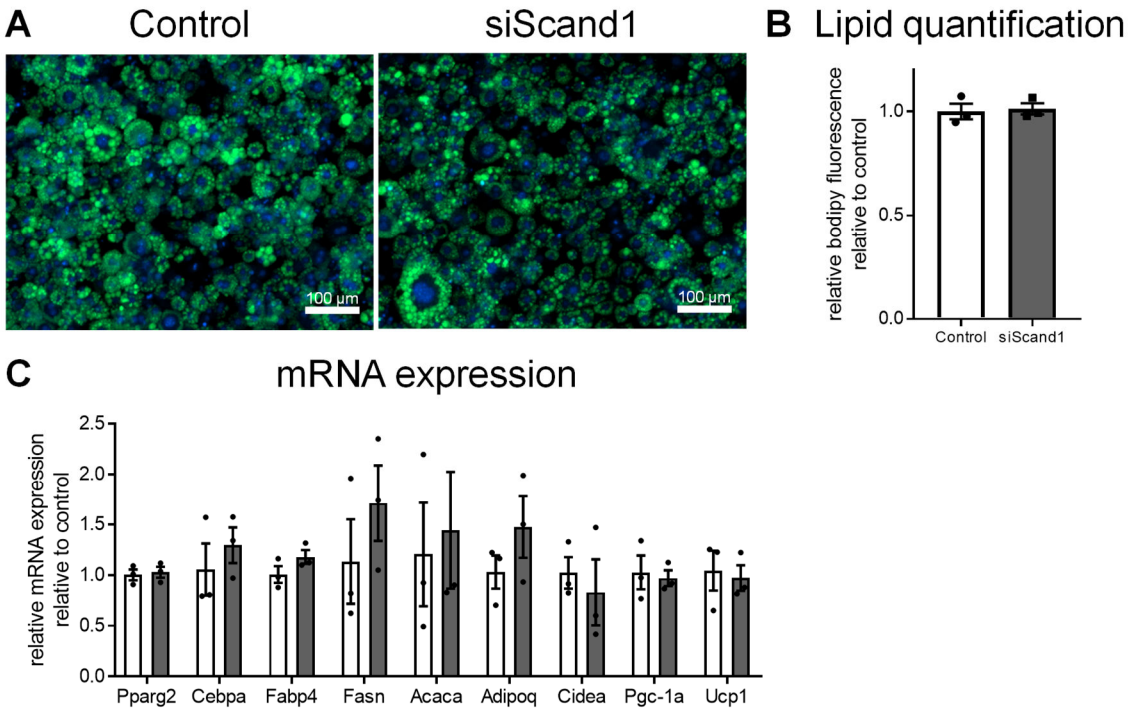

Figure 19: Impact of *Scand1* knockdown on late stages of adipogenesis of 3T3-L1 cells.
Gene specific Scand1 siRNA knockdown was induced one day prior to differentiation start. A+B: On day 11 of differentiation lipid droplet formation was assessed by staining (A; lipid droplets: green, Bodipy 493/503; nuclei: blue, Hoechst 33342) and Bodipy fluorescence quantification (B). C: mRNA expression of genes involved in adipogenesis was quantified using RT-qPCR. All data are depicted as mean ± SEM and n = 3 for all data. Statistics: t-test (C-B). p < 0.05 *, p < 0.01 **, p < 0.001 ***
Scand1 = SCAN domain-containing 1; *Pparg2* = Peroxisome proliferator-activated receptor gamma 2; *Cebpa* = CCAAT/enhancer-binding protein alpha; *Fabp4* = Fatty acid binding protein 4; *Fasn* = Fatty acid synthase; *Acaca* = Acetyl-CoA carboxylase 1; *Adipoq* = Adiponectin, C1Q and collagen domain containing; *Cidea* = Cell death-inducing DNA fragmentation factor, alpha subunit-like effector A; *Pgc-1a*

= Peroxisome proliferative activated receptor, gamma, coactivator 1 alpha; *Ucp-1* = Uncoupling protein 1; siScand1 = siRNA targeting *Scand1*

3.8 *Aldh1a* isoforms and *Scand1* mRNA expression are altered during human adipogenesis

SGBS cells, which were kindly provided by Prof. Wabitsch, University of Ulm, are a human preadipocyte cell line that can be differentiated into adipocytes *in vitro* and is therefore used for studying human adipogenesis. As it was the first time this cell line was used in my working group, *in vitro* differentiation was evaluated. Fluorescent staining of lipid droplet formation using microscopy and plate reader quantification revealed an increasing lipid droplet formation starting at day 4 of differentiation reaching a plateau on day 14 of differentiation (Figure 20A+B; Dunnett's multiple comparison test in comparison to day 0, day 7-21 $p \leq 0.001$).

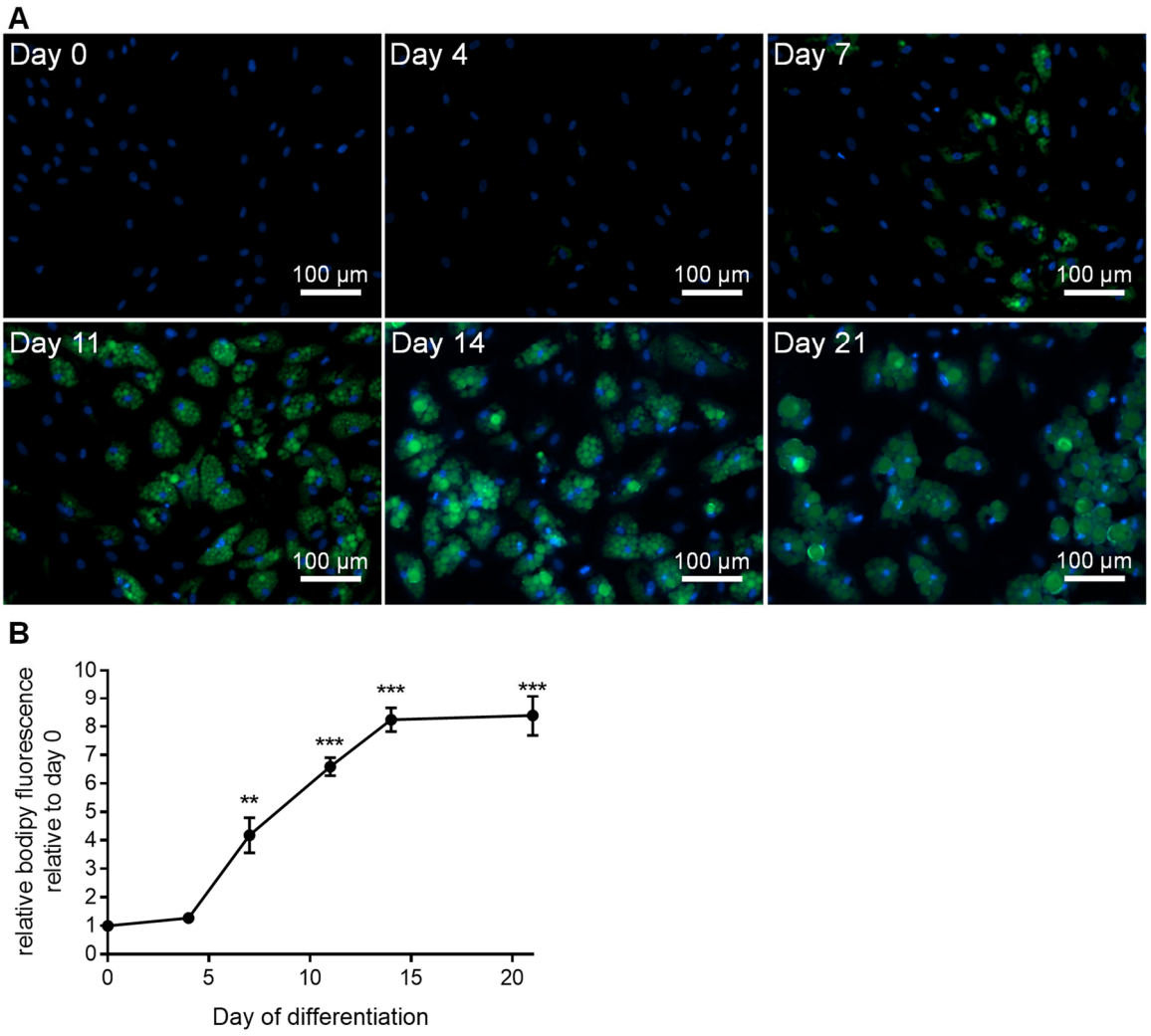

Figure 20: Morphological analysis of SGBS cells during adipogenic differentiation.
Adipogenic differentiation of SGBS cells was induced using transferrin, insulin, cortisol, triiodothyronine, IBMX, dexamethasone, and rosiglitazone. At different days of differentiation, cells were stained using Hoechst 33342 (nuclei, blue) and Bodipy 493/503 (lipid droplets, green), and lipid droplet formation was quantified using Bodipy fluorescence quantification (A). All data are depicted as mean ± SEM and n = 3 for all data. Statistics: 1-way ANOVA + Dunnett's multiple comparisons test (B) $p < 0.05$ *, $p < 0.01$ **, $p < 0.001$ ***
SGBS = Simpson-Golabi-Behmel syndrome; IBMX = 3-isobutyl-1-methylxanthine

Transcriptional analysis using RT-qPCR was performed next to further assess differentiation success. It revealed an increasing expression of all tested adipogenesis markers *PPARG1, PPARG2, CEBPA, FABP4,* and *FASN* (Figure 21A+B; Dunnett's multiple comparison test in comparison to day 0, *PPARG1*: Day 4-21 $p \leq 0.006$; *PPARG2*: Day 11-21 $p \leq 0.012$; *CEBPA*: day 4-21 $p \leq 0.014$; *FABP4*: Day 4-21 $p \leq 0.005$; *FASN*: Day 11-21 $p \leq 0.004$). *PPARG2* expression was undetectable in undifferentiated cells but increased to a detectable concentration on day 4 of differentiation, which was used as a reference for quantification and statistical testing. I determined cells to be completely differentiated at day 14 of differentiation as lipid droplet formation plateaued and adipogenesis marker expression was significantly increased compared to undifferentiated cells (Figure 21; Dunnett's multiple comparison test in comparison to day 0, *PPARG1* $p < 0.001$, *PPARG2* $p = 0.002$, *CEBPA* $p < 0.001$, *FABP4* $p < 0.001$, *FASN* $p = 0.001$).

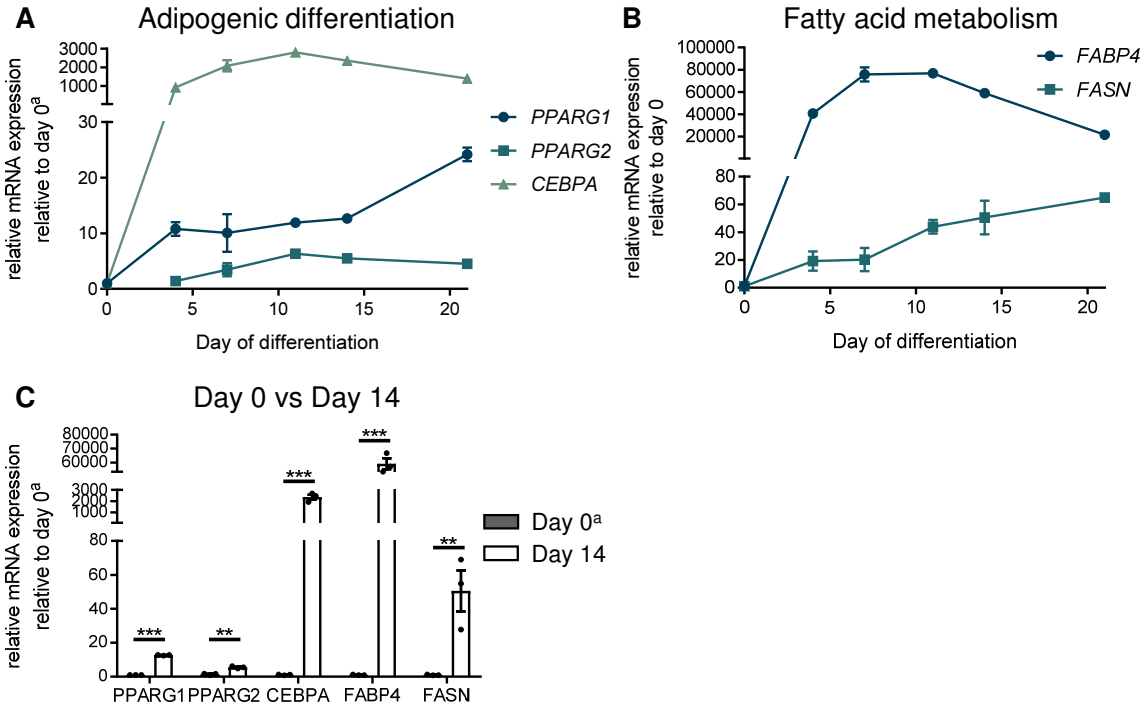

Figure 21: Analysis of mRNA expression of genes related to adipocyte differentiation and function during adipogenic differentiation of SGBS cells.
Adipogenic differentiation of SGBS cells was induced using transferrin, insulin, cortisol, triiodothyronine, IBMX, dexamethasone, and rosiglitazone. At different days of differentiation mRNA expression of genes involved in adipogenic differentiation (A) or fatty acid metabolism (B) was quantified using RT-qPCR. In A and B significant differences relative to expression levels of day 0 are not indicated to avoid overloading plots. Furthermore, gene expression before (day 0) and after adipogenic differentiation (day 14) were compared to verify successful differentiation (C). All data are depicted as mean ± SEM and n = 3 for all data. Statistics: 1-way ANOVA + Dunnett's multiple comparisons test in comparison to day 0 (A+B), t-test (C). $p < 0.05$ *, $p < 0.01$ **, $p < 0.001$ ***
[a]*Pparg2* expression was not detectable on day 0 of differentiation, and therefore day 4 of differentiation was used as a reference point instead of day 0.
SGBS = Simpson-Golabi-Behmel syndrome; IBMX = 3-isobutyl-1-methylxanthine; *PPARG1* = Peroxisome proliferator-activated receptor gamma 1; *PPARG2* = Peroxisome proliferator-activated receptor gamma 2; *CEBPA* = CCAAT/enhancer-binding protein alpha; *FASN* = Fatty acid synthase; *FABP4* = Fatty acid binding protein 4

After successfully establishing the SGBS cell line model in our working group the mRNA expression of the human *ALDH1A* isoforms *ALDH1A1-3* and *SCAND1* during human adipogenesis was quantified. *ALDH1A1* expression remained unchanged until day 14 of differentiation and increased afterwards (Figure 22A; Dunnett's multiple comparison test in comparison to day 0, $p < 0.001$). *ALDH1A3* mRNA expression peaked on day 4 of differentiation ($p < 0.001$) and stayed on starting levels at all other time points. *ALDH1A2* mRNA expression did not change during differentiation. Lastly, *Scand1* mRNA expression increased starting on day 4 and was significantly increased on days 4, 11, 15, and 21 of differentiation (Figure 22B; Day 4-21 $p \leq 0.005$). Concluding, these results indicate an involvement of *ALDH1A1, ALDH1A3,* and *SCAND1* in human adipogenesis.

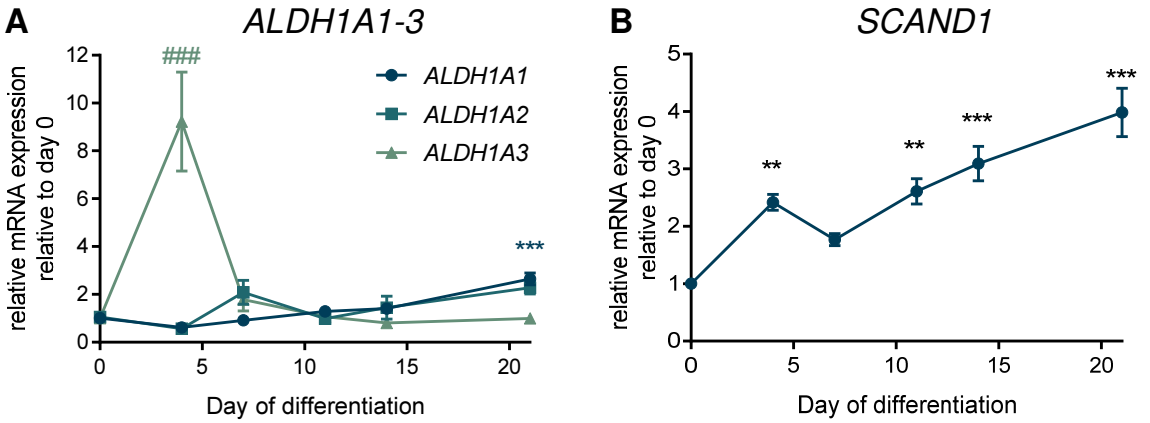

Figure 22: mRNA Expression analysis of *ALDH1A1-3* and *SCAND1* during human adipogenesis. SGBS cell adipogenic differentiation was induced using transferrin, insulin, cortisol, triiodothyronine, IBMX, dexamethasone, and rosiglitazone. At different days of differentiation mRNA expression of *ALDH1-3* (A) and *SCAND1* (B) during human adipogenesis was quantified using RT-qPCR. All data are depicted as mean ± SEM and n = 3 for all data. Statistics: 1-way ANOVA + Dunnett's multiple comparisons test in comparison to day 0. $p < 0.05$ *, $p < 0.01$ **, $p < 0.001$ ***
SGBS = Simpson-Golabi-Behmel syndrome; IBMX = 3-isobutyl-1-methylxanthine; *ALDH1A1* = Aldehyde dehydrogenase family 1, subfamily A1; *ALDH1A2* = Aldehyde dehydrogenase family 1, subfamily A2; *ALDH1A3* = Aldehyde dehydrogenase family 1, subfamily A3; *SCAND1* = SCAN domain-containing 1

3.9 Maternal HCD feeding alters the proteome of female offspring E13.5 adipocytes

RNA sequencing revealed changes in the transcriptome of female offspring E13.5 adipocytes of HCD fed dams, and follow-up analysis of genes changed in expression revealed an involvement in adipogenesis. Hence, the question of whether maternal HCD feeding also changes the proteome of female offspring E13.5 adipocytes was investigated next.

Female offspring E13.5 adipocytes from both mat-CD and mat-HCD offspring were analyzed regarding proteomic changes using mass spectrometry in cooperation with the Proteome Analysis Unit from the Institute for Clinical Biochemistry and Pathobiochemistry of the German Diabetes Center Düsseldorf. Proteomic analysis revealed upregulation of 125 and

downregulation of 99 proteins in mat-HCD compared to mat-CD embryonic offspring (Figure 23A). Top 10 down- and upregulated proteins sorted by adjusted p-value are depicted in Table 14 and Table 15.

Table 14: Top 10 upregulated proteins in mat-HCD female offspring E13.5 adipocytes compared to mat-CD samples analyzed by mass spectrometry sorted by adjusted p-value. (Adj. = adjusted)

Accession ID	Protein name	Gene symbol	Adj. p-value	Abundance ratio
Q9Z331	Keratin, type II cytoskeletal 6B	Krt6b	3.69×10^{-16}	6.805
Q61781	Keratin, type I cytoskeletal 14	Krt14	3.69×10^{-16}	5.247
P49182	Heparin cofactor 2	Serpind1	3.69×10^{-16}	2.994
Q5FW60	Major urinary protein 20	Mup20	3.69×10^{-16}	2.264
B5X0G2	Major urinary protein 17	Mup17	3.69×10^{-16}	1.685
Q61703	Inter-alpha-trypsin inhibitor heavy chain H2	Itih2	3.69×10^{-16}	1.646
Q08879	Fibulin-1	Fbln1	3.69×10^{-16}	1.626
Q07797	Galectin-3-binding protein	Lgals3bp	3.69×10^{-16}	1.579
P11588	Major urinary protein 1	Mup1	3.69×10^{-16}	1.436
Q04690	Neurofibromin	Nf1	3.69×10^{-16}	1.606

Table 15: Top 10 downregulated proteins in mat-HCD female offspring E13.5 adipocytes compared to mat-CD samples analyzed by mass spectrometry sorted by adjusted p-value. (Adj. = adjusted)

Accession ID	Protein name	Gene symbol	Adj. p-value	Abundance ratio
P50114	Protein S100-B	S100b	3.69×10^{-16}	0.387
Q99P72-1	Isoform C of Reticulon-4	Rtn4	3.69×10^{-16}	0.484
P04247	Myoglobin	Mb	3.69×10^{-16}	0.505
P12242	Mitochondrial brown fat uncoupling protein 1	Ucp1	3.69×10^{-16}	0.53
Q9D061	Acyl-CoA-binding domain-containing protein 6	Acbd6	3.69×10^{-16}	0.573
Q9Z2V4	Phosphoenolpyruvate carboxykinase, cytosolic [GTP]	Pck1	3.69×10^{-16}	0.689
Q8BH61	Coagulation factor XIII A chain	F13a1	3.69×10^{-16}	0.69
E9Q4Z2	Acetyl-CoA carboxylase 2	Acacb	3.69×10^{-16}	0.694
Q9CPU0	Lactoylglutathione lyase	Glo1	2.38×10^{-14}	0.704
Q8QZR5	Alanine aminotransferase 1z	Gpt	7.97×10^{-13}	0.723

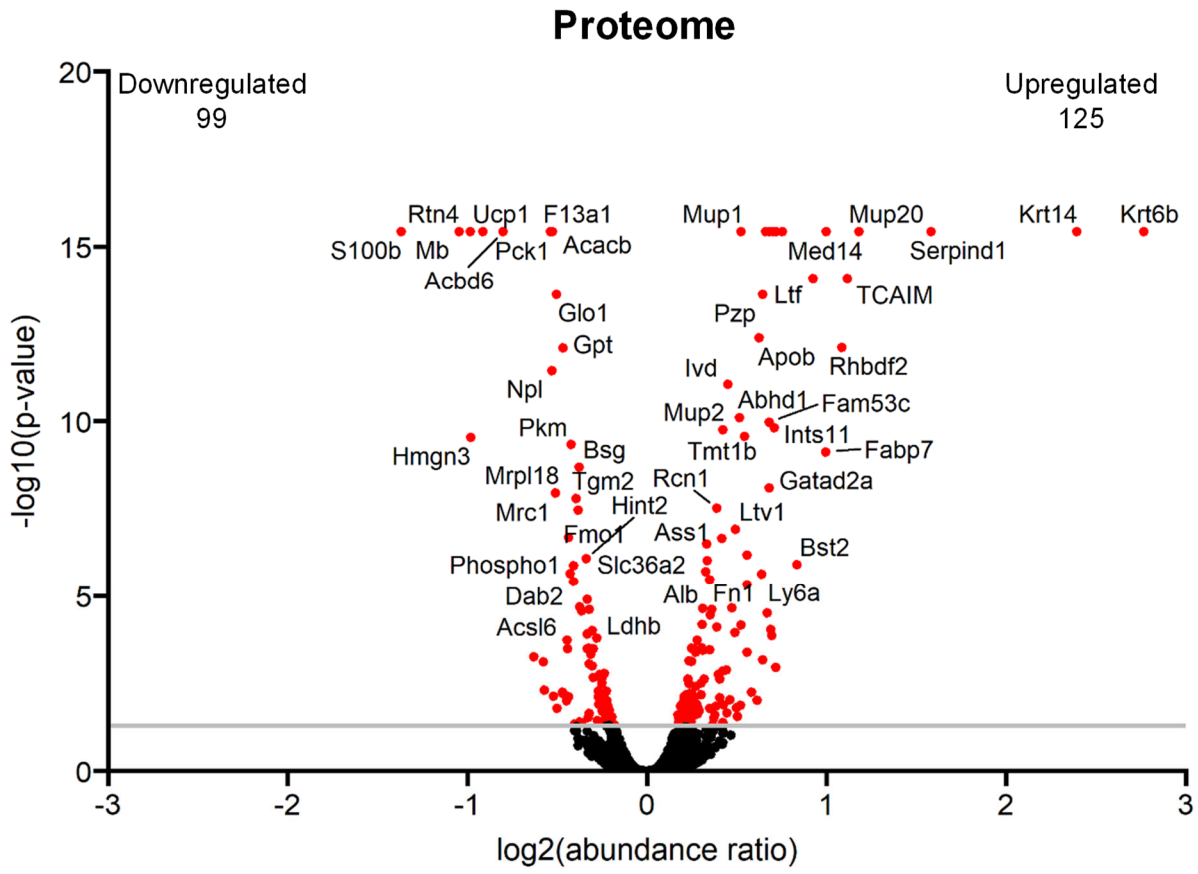

Figure 23: Proteomic analysis of female offspring E13.5 mat-HCD adipocytes compared to mat-CD adipocytes.
Proteome of female E13.5 adipocytes of mat-HCD and mat-CD offspring was analyzed using mass spectrometry, and abundance ratio mat-HCD/ mat-CD was calculated (n = 6). Indicated are gene symbols. Statistics: t-test + false discovery rate.

To assess which biological processes were altered by maternal HCD feeding before and during pregnancy gene ontology (GO) enrichment analysis was performed to examine which biological processes are overrepresented among altered proteins. Analysis of downregulated proteins revealed “fatty acid metabolic process” (GO:0006631; over representation analysis (ORA), $p < 0.001$) and “regulation of lipid metabolic process” (GO:0019216; ORA, $p < 0.001$) among the most significantly enriched GO terms (Figure 24B). Downregulated proteins associated with these GO are listed in Table 16 and Table 17, respectively.

Table 16: Proteins downregulated in mat-HCD female offspring E13.5 adipocytes associated with the biological process GO-Term “fatty acid metabolic process” (GO:0006631). Statistics: t-test + false discovery rate. (Adj. = adjusted)

Accession ID	Protein name	Gene symbol	Adj. p-value	Abundance ratio
Q8VCH0	3-ketoacyl-CoA thiolase B, peroxisomal	Acaa1b	4.65×10^{-04}	0.804
E9Q4Z2	Acetyl-CoA carboxylase 2	Acacb	3.69×10^{-16}	0.694
Q91V92	ATP-citrate synthase	Acly	2.94×10^{-02}	0.865
Q9CZW4	Fatty acid CoA ligase Acsl3	Acsl3	6.09×10^{-03}	0.722

Q91WC3	Long-chain-fatty-acid--CoA ligase 6	Acsl6	2.05 x10^{-05}	0.771
Q8VCT4	Carboxylesterase 1D	Ces1d	2.93 x10^{-02}	0.865
Q924X2	Carnitine O-palmitoyltransferase 1, muscle isoform	Cpt1b	9.83 x10^{-03}	0.732
P31786	Acyl-CoA-binding protein	Dbi	3.12 x10^{-02}	0.866
P34914	Bifunctional epoxide hydrolase 2	Ephx2	3.04 x10^{-03}	0.839
Q05816	Fatty acid-binding protein 5	Fabp5	1.75 x10^{-03}	0.833
Q9JJE7	Fatty acid desaturase 3	Fads3	2.26 x10^{-02}	0.8
P19096	Fatty acid synthase	Fasn	3.30 x10^{-02}	0.867
P50285	Flavin-containing monooxygenase 1	Fmo1	3.39 x10^{-08}	0.766
Q64516	Glycerol kinase	Gk	7.65 x10^{-03}	0.829
Q9Z2V4	Phosphoenolpyruvate carboxykinase, cytosolic [GTP]	Pck1	3.69 x10^{-16}	0.689
Q8BFP9	[Pyruvate dehydrogenase (acetyl-transferring)] kinase isozyme 1, mitochondrial	Pdk1	2.73 x10^{-02}	0.856
Q91WW7	1-acylglycerol-3-phosphate O-acyltransferase Pnpla3	Pnpla3	8.69 x10^{-04}	0.8
P13516	Acyl-CoA desaturase 1	Scd1	9.81 x10^{-05}	0.809

Table 17: Proteins downregulated in mat-HCD female offspring E13.5 adipocytes associated with the biological process GO-Term “regulation of lipid metabolic process” (GO:0019216). Statistics: t-test + false discovery rate. (Adj. = adjusted)

Accession ID	Protein name	Gene symbol	Adj. p-value	Abundance ratio
E9Q4Z2	Acetyl-CoA carboxylase 2	Acacb	3.69 x10^{-16}	0.694
Q9CZW4	Fatty acid CoA ligase Acsl3	Acsl3	6.09 x10^{-03}	0.722
Q8VCT4	Carboxylesterase 1D	Ces1d	2.93 x10^{-02}	0.865
P61022	Calcineurin B homologous protein 1	Chp1	1.65 x10^{-03}	0.847
P98078	Disabled homolog 2	Dab2	3.74 x10^{-06}	0.753
P31786	Acyl-CoA-binding protein	Dbi	3.12 x10^{-02}	0.866
P34914	Bifunctional epoxide hydrolase 2	Ephx2	3.04 x10^{-03}	0.839
Q05816	Fatty acid-binding protein 5	Fabp5	1.75 x10^{-03}	0.833
Q9CR13	Protein FMC1 homolog	Fmc1	4.37 x10^{-02}	0.852
P50285	Flavin-containing monooxygenase 1	Fmo1	3.39 x10^{-08}	0.766
Q64516	Glycerol kinase	Gk	7.65 x10^{-03}	0.829
Q9Z2V4	Phosphoenolpyruvate carboxykinase, cytosolic [GTP]	Pck1	3.69 x10^{-16}	0.689
Q8BFP9	[Pyruvate dehydrogenase (acetyl-transferring)] kinase isozyme 1, mitochondrial	Pdk1	2.73 x10^{-02}	0.856
Q8BJ56	Patatin-like phospholipase domain-containing protein 2	Pnpla2	1.91 x10^{-02}	0.86

Similar analysis of upregulated proteins identified “fatty acid metabolic process” (GO:0006631; ORA, $p < 0.001$) among the top ten enriched biological processes (Figure 24B) with 14 proteins linked to it being upregulated by exposure of fetuses to mat-HCD vs mat-CD (Table 18).

Table 18: Proteins upregulated in mat-HCD female offspring E13.5 adipocytes associated with the biological process GO-Term “fatty acid metabolic process” (GO:0006631). Statistics: t-test + false discovery rate. (Adj. = adjusted)

Accession ID	Protein name	Gene symbol	Adj. p-value	Abundance ratio
Q61285	ATP-binding cassette sub-family D member 2	Abcd2	2.48×10^{-02}	1.173
Q9QZC8	Protein ABHD1	Abhd1	7.73×10^{-11}	1.427
Q3UNX5	Acyl-coenzyme A synthetase ACSM3, mitochondrial	Acsm3	4.75×10^{-02}	1.288
Q64437	All-trans-retinol dehydrogenase [NAD(+)] ADH7	Adh7	4.14×10^{-04}	1.205
Q8K009	Mitochondrial 10-formyltetrahydrofolate dehydrogenase	Aldh1l2	3.15×10^{-07}	1.258
P47740	Aldehyde dehydrogenase family 3 member A2	Aldh3a2	8.10×10^{-03}	1.181
P01027	Complement C3	C3	8.92×10^{-03}	1.153
P33267	Cytochrome P450 2F2	Cyp2f2	2.39×10^{-03}	1.172
Q9Z2A9	Glutathione hydrolase 5 proenzyme	Ggt5	2.75×10^{-02}	1.418
P19157	Glutathione S-transferase P 1	Gstp1	2.55×10^{-03}	1.171
Q9JHI5	Isovaleryl-CoA dehydrogenase, mitochondrial	Ivd	8.80×10^{-12}	1.365
Q99104	Unconventional myosin-Va	Myo5a	1.57×10^{-02}	1.156
Q9D7V9	N-acylethanolamine-hydrolyzing acid amidase	Naaa	1.30×10^{-02}	1.341
Q80W22	Threonine synthase-like 2	Thnsl2	2.20×10^{-02}	1.204

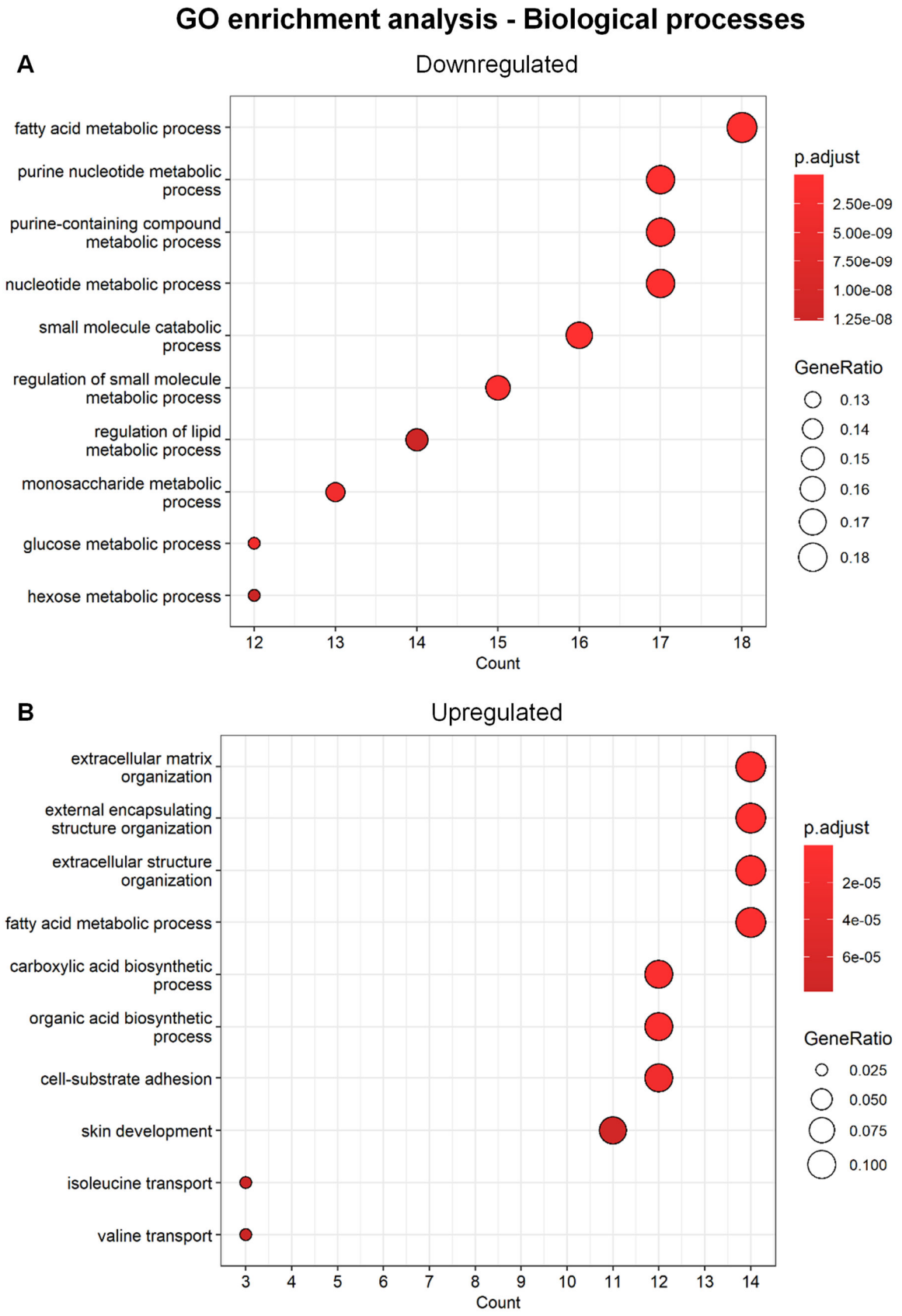

Figure 24: GO enrichment analysis of down- and upregulated proteins in female E13.5 mat-HCD adipocytes compared to mat-CD adipocytes
Proteome of female E13.5 adipocytes was analyzed using mass spectrometry. Biological processes GO enrichment analysis was performed for downregulated (A) and upregulated (B) proteins using clusterProfiler 4.10.0 (Wu et al., 2021). Statistics: Over representation analysis.
GO = Gene ontology

Overall, proteomic analysis revealed dysregulation of proteins involved in processes associated with adipocyte function and development in female offspring E13.5 adipocytes exposed to maternal HCD feeding.

3.10 Impact of mat-HCD on the methylome of female offspring E13.5 adipocytes

As an impact of maternal HCD feeding on female offspring adipocytes' transcriptome and proteome was identified, it remained to investigate whether it also induces epigenetic changes in female offspring E13.5 adipocytes. To assess this question, global DNA methylation was investigated by reduced representation bisulfite sequencing (RRBS) in cooperation with Diagenode.

Global methylomic analysis discovered 354 differentially methylated CpG sites in mat-HCD vs mat-CD adipocytes, 110 being hypomethylated and 244 hypermethylated (Figure 25). The 10 most hyper- and hypomethylated CpG sites sorted by q-value are listed in Table 19 and Table 20, respectively.

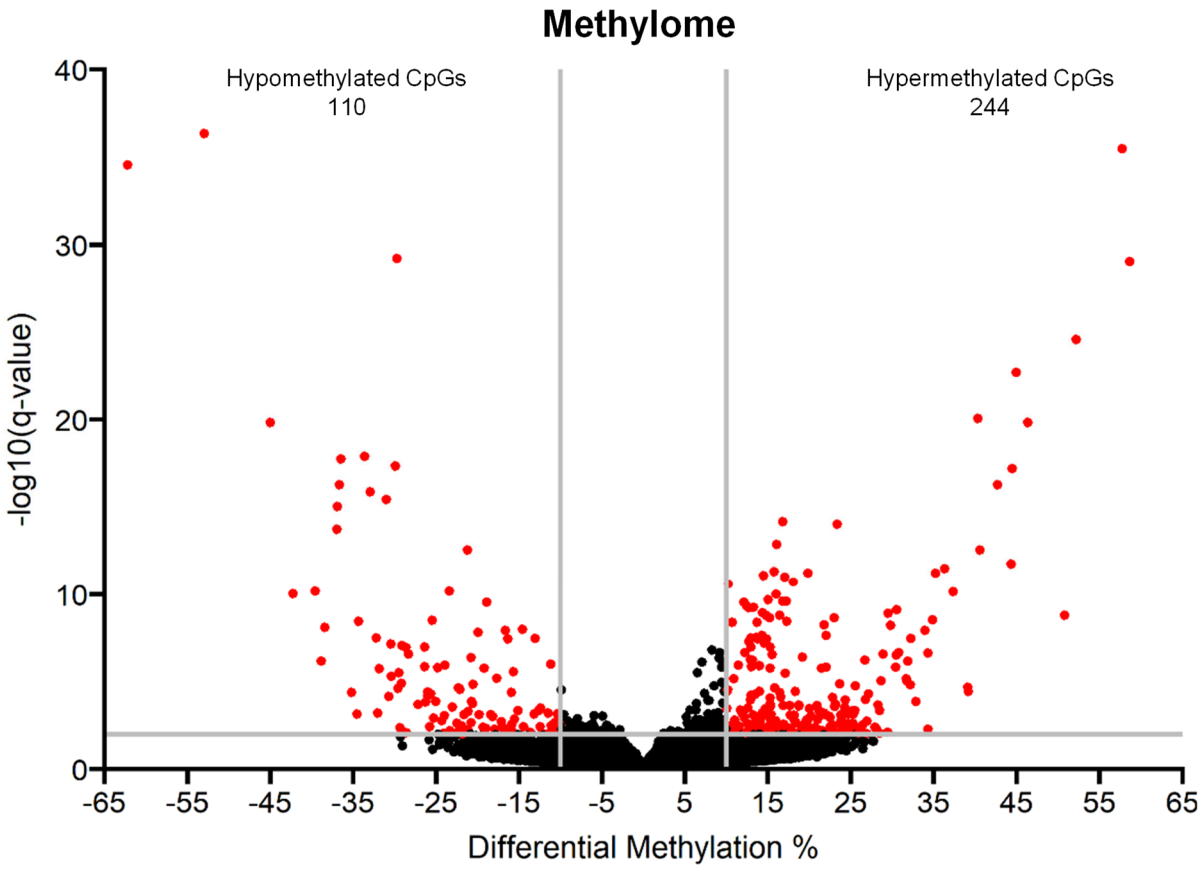

Figure 25: Methylomic analysis of female offspring E13.5 mat-HCD adipocytes compared to mat-CD adipocytes.
Reduced representation bisulfite sequencing was performed to analyze methylome of female offspring E13.5 mat-HCD adipocytes in comparison to mat-CD adipocytes. Differential methylation of CpG sites was determined (n = 5). Statistics: pairwise comparison + sliding window model (SLIM) correction. GO = Gene ontology

Table 19: Top 10 hypermethylated CpG sites with associated genes in mat-HCD female offspring E13.5 adipocytes compared to mat-CD adipocytes analyzed by reduced representative bisulfite sequencing sorted by q-value. Statistics: pairwise comparison + sliding window model (SLIM) correction. (As. = Associated, NA = not available)

Chromosome	Start	End	Strand	q-value	Differential methylation [%]	As. gene Symbol	As. gene ID
9	42083366	42083366	+	3.21×10^{-36}	57.73	Sorl1	20660
9	35400055	35400055	-	8.87×10^{-30}	58.67	NA	NA
15	20666732	20666732	+	2.73×10^{-25}	52.20	Acot10	64833
12	107695861	107695861	-	2.07×10^{-23}	44.97	NA	NA
12	107695860	107695860	+	8.60×10^{-21}	40.34	NA	NA
18	76073692	76073692	-	1.41×10^{-20}	46.38	Zbtb7c	207259
2	118224137	118224137	+	6.02×10^{-18}	44.45	Fsip1	71313
18	76073637	76073637	-	5.08×10^{-17}	42.70	Zbtb7c	207259
7	126759676	126759676	-	6.60×10^{-15}	16.82	Mapk3	26417
6	147099508	147099508	+	9.11×10^{-15}	23.39	Klhl42	232539

Table 20: Top 10 hypomethylated CpG sites with associated genes in mat-HCD female offspring E13.5 adipocytes compared to mat-CD adipocytes analyzed by reduced representative bisulfite sequencing sorted by q-value. Statistics: pairwise comparison + sliding window model (SLIM) correction. (As. = Associated, NA = not available)

Chromosome	Start	End	Strand	q-value	Differential methylation [%]	As. gene Symbol	As. gene ID
15	3267964	3267964	+	4.39×10^{-37}	-52.95	Selenop	20363
12	113190240	113190240	+	2.66×10^{-35}	-62.19	NA	NA
3	44507246	44507246	+	6.02×10^{-30}	-29.74	NA	NA
15	3267965	3267965	-	1.48×10^{-20}	-45.03	Selenop	20363
7	15804375	15804375	-	1.25×10^{-18}	-33.62	NA	NA
7	15804338	15804338	-	1.75×10^{-18}	-36.50	NA	NA
8	125260638	125260638	-	4.43×10^{-18}	-29.93	Disc1	244667
15	94855796	94855796	-	5.03×10^{-17}	-36.70	Tmem117	320709
7	45084306	45084306	-	1.34×10^{-16}	-32.96	Rcn3	52377
8	15016309	15016309	+	3.61×10^{-16}	-31.01	NA	NA

In total, there are 182 genes associated with these differential methylated CpG sites. GO enrichment analysis was performed to examine which biological processes are affected by differential methylation. Biological processes “fat cell differentiation” (GO:0045444; ORA, $p < 0.001$) and “regulation of fat cell differentiation” (GO:0045598; ORA, $p = 0.002$) are significantly enriched in this gene set (Figure 26). Genes associated with these GO-terms are listed in Table 21. Contactin associated protein-like 2 (*Cntnap2)*, Bardet-Biedl syndrome 2 (*Bbs2),* and cAMP responsive element binding protein 5 (*Creb5)* are only associated with “fat cell differentiation”.

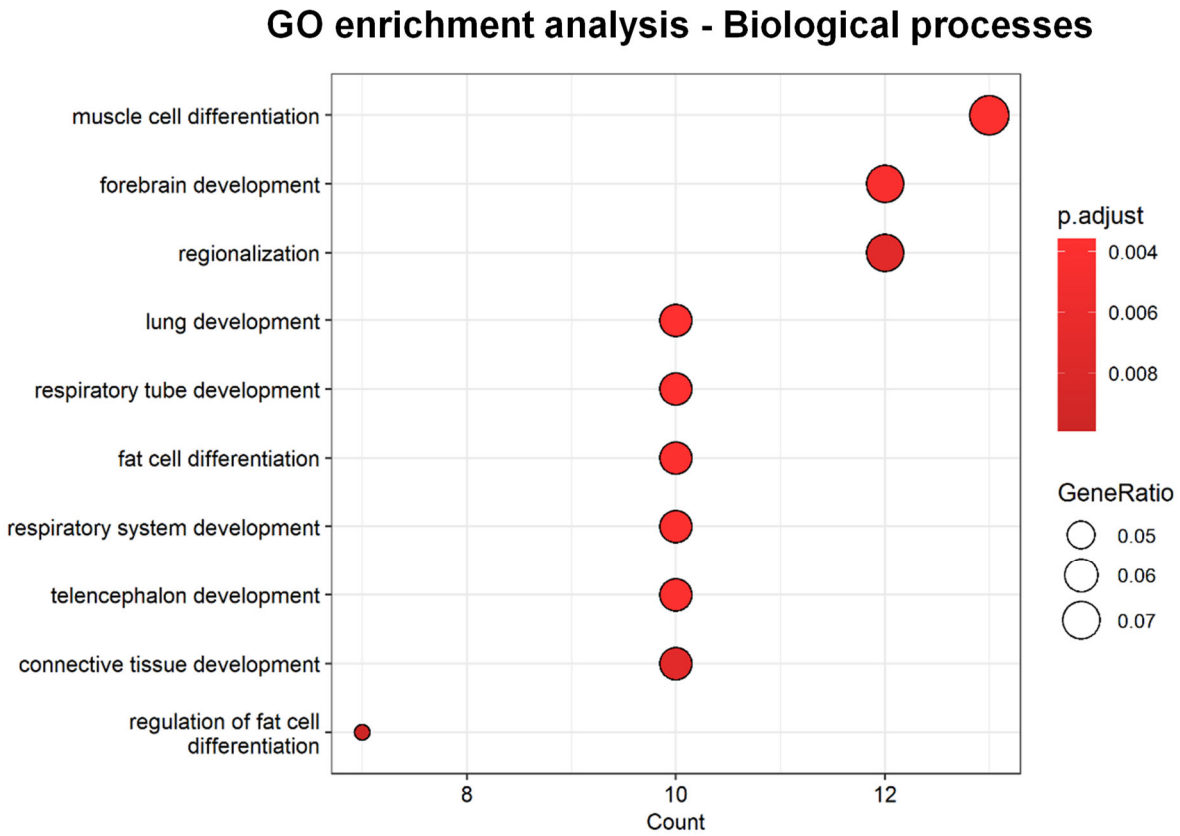

Figure 26: GO enrichment analysis of genes associated with differentially methylated CpG sites in female offspring E13.5 mat-HCD adipocytes compared to mat-CD adipocytes
Reduced representation bisulfite sequencing was performed to analyze methylome of female E13.5 mat-HCD adipocytes in comparison to mat-CD adipocytes. To assess which biological processes were impacted by differential methylation, biological processes GO term enrichment analysis was performed for all genes associated with differentially methylated CpG sites using clusterProfiler 4.10.0 (Wu et al., 2021). Statistics: Over representation analysis.
GO = Gene ontology

Table 21: Differentially methylated CpG sites and respective genes associated with biological processes "fat cell differentiation" (GO:0045444) and "regulation of fat cell differentiation" (GO:0045598). *Cntnap2, Bbs2,* and *Creb5* are only associated with "fat cell differentiation". Statistics: pairwise comparison + sliding window model (SLIM) correction. (As. = Associated)

Chromosome	Start	End	Strand	q-value	Differential methylation [%]	As. gene Symbol	As. gene ID
chr8	94086123	94086123	+	4.21 x10^{-03}	-29.37	Bbs2	67378
chr2	133553167	133553167	-	5.37 x10^{-05}	13.45	Bmp2	12156
chr6	47122260	47122260	-	1.20 x10^{-08}	-16.67	Cntnap2	66797
chr6	53286562	53286562	-	1.14 x10^{-03}	22.50	Creb5	231991
chr2	125500293	125500293	+	4.92 x10^{-06}	-30.39	Fbn1	14118
chr8	91531274	91531274	+	6.77 x10^{-07}	31.90	Fto	26383
chr5	125030819	125030819	-	1.89 x10^{-03}	-17.13	Ncor2	20602
chr9	69291388	69291388	+	7.54 x10^{-03}	22.72	Rora	19883
chr11	16260769	16260769	+	4.09 x10^{-03}	16.80	Vstm2a	211739
chr18	76073637	76073637	-	5.08 x10^{-17}	42.70	Zbtb7c	207259
chr18	76073691	76073691	+	5.74 x10^{-12}	35.20	Zbtb7c	207259
chr18	76073692	76073692	-	1.41 x10^{-20}	46.38	Zbtb7c	207259

Overall, this analysis revealed that maternal HCD feeding changes the DNA methylome of female offspring E13.5 adipocytes revealing an epigenetic impact of maternal diet on the fetus. Furthermore, altered fetal adipocyte DNA methylation is linked to genes involved in fat cell differentiation and regulation.

4 Discussion

In the context of the rising obesity prevalence worldwide, it is important to understand how maternal obesity impacts offspring's health trajectory on a molecular level to develop tailored preventive strategies. Hence, this thesis aimed to investigate the impact of maternal obesity in pregnancy on the function and development of fetal offspring's (pre-)adipocytes using *ex vivo* differentiated E13.5 MEFs. A maternal obesogenic intrauterine environment caused alterations in offspring adipocyte's transcriptome, proteome, and DNA methylome in pathways associated with impaired commitment to the adipogenic lineage and changed lipid metabolism. Furthermore, ALDH1A7 was identified as a regulator active in the early stages of adipogenic differentiation. Firstly, these results identified promising candidate pathways altered by maternal HCD feeding for future investigations aiming at understanding fetal programming processes. Secondly, ALDH1A7 was identified as a new regulator of adipogenesis aiding in the development of needed preventive strategies to mitigate obesity in children exposed to an obesogenic intrauterine environment.

4.1 Impact of maternal obesity on embryonic *ex vivo* differentiated adipocytes

4.1.1 Differentiation capacity of offspring adipocytes remains unaffected by maternal diet and offspring sex

MEFs from embryonic offspring at age E13.5 were adipogenically differentiated *ex vivo* to investigate the impact of maternal HCD feeding on the adipogenic capacity of offspring preadipocytes. MEFs isolated and differentiated in this thesis displayed similar adipogenic differentiation capacities between maternal diets and offspring sex. However, previous studies reported a reduced adipogenic differentiation capacity in E14.5 MEFs derived from offspring of overweight C57BL/6J dams (Yang et al., 2013). My experimental setup differs both in the mouse strain used as well as in the timing of MEF isolation, possibly explaining the observed differences. NMRI mice display a less adverse phenotype after HCD feeding in regard to body weight gain compared to C57BL/6J mice, which translates into respective offsprings' phenotypes (Dahlhoff et al., 2014; Kelly et al., 2022). Additionally, it was hypothesized that the time of MEF isolation impacts adipogenic capacity as preadipocyte development is highly dynamic during embryogenesis (Jiang et al., 2014). Furthermore, different results may explained by poor differentiation efficiency into adipocytes of MEFs especially obtained from control dams judged by depicted images of differentiated cells compared to results obtained in this thesis (Yang et al., 2013).

Flow cytometry revealed that only around 20% of cells in differentiated MEF cell cultures contain lipid droplets and can therefore be identified as adult adipocytes. This complicates the investigation of adipocyte specific effects of maternal obesity using *ex vivo* adipogenically differentiated MEFs. Although the percentage of lipid droplet-containing cells was not

quantified depicted images of differentiated cells stained for lipid droplets indicate similar or smaller percentages of lipid-containing cells in differentiated MEF cultures previously described (Yang et al., 2013). Density based gradient sorting was utilized to increase adipocyte purity in samples to around 80% based on their reduced density caused by intracellular lipid droplets enabling adipocyte-specific analysis. Similar approaches have been used to enrich adult adipocytes in differentiated 3T3-L1 cells (Kajimoto et al., 2012) but have previously not been described to be used in differentiated MEF cell cultures.

4.1.2 Maternal obesity impacts offspring adipocytes on multi-omics level

After investigating the adipogenic capacity of offspring preadipocytes the focus of my thesis was on the female offspring adipocytes since previous studies of my research group observed reduced body fat percentage and adipocyte size in adult female mat-HCD offspring (Dahlhoff et al., 2014). It was aimed to identify potential target genes and pathways crucial for fetal programming of offspring adipocytes by maternal HCD feeding. Multi-omics analysis revealed only small changes in the transcriptome but bigger alterations in the proteome and methylome of offspring adipocytes induced by maternal HCD feeding.

RNA sequencing analysis revealed four differentially expressed genes (DEGs; namely *Aldh1a1, Aldh1a7, Scand1,* and *H2-Q2*). They are involved in the vitamin A metabolism (*Aldh1a1*), as a co-activator in transcriptional gene regulation (*Scand1*), or in so far unknown pathways (*Aldh1a7, H2-Q2*) and their role in adipogenesis will be discussed later (see 4.2.2 and 4.2.3; Babb & Bowen, 2003; Kathmann et al., 2000). Unfortunately, transcriptomic data on embryonic adipocytes are unavailable as a point of comparison. However, 399 DEGs were described in a similar analysis of E18.5 offspring's liver samples (Kelly et al., 2022). In contrast to this thesis and other studies, Kelly and coworkers omitted p-value correction for multiple testing (Savva et al., 2022). Here, correction for multiple testing caused a small number of DEGs but was performed to control the maximum experiment wise error rate to detect robustly regulated candidate genes (Bender & Lange, 2001). Additionally, the early time point in development investigated and the conservative mouse model used here might also contribute to the small number of genes as other studies described smaller changes earlier in development compared to later stages (Kelly et al., 2022).

In contrast to only few differentially expressed genes observed by RNA sequencing, proteomic analysis revealed dysregulated expression of more than 200 proteins by mat-HCD feeding in female adipocytes. These differences imply an important role of post-transcriptional regulation such as alternative splicing, translational efficiency, and mRNA stabilization in maternal obesity induced alterations in the offspring (Ghazalpour et al., 2011). Both, miRNAs and RNA binding proteins are key post-transcriptional regulators and are both described to be involved in regulating glucose and lipid homeostasis in adipocytes and impact metabolic disease (Kim &

Kyung Lee, 2012). Furthermore, maternal obesity causes differential miRNA expression in both placentas and offspring (Carreras-Badosa et al., 2017; Méndez-Mancilla et al., 2018). Moreover, nutrients like the fatty acids monounsaturated oleic (C18:1) and saturated palmitic acid (C16:0) can directly regulate gene expression on a post-transcriptional level and thereby affect offspring proteome (Distel et al., 1992; Lu et al., 2015). In sum, these results suggest that maternal obesity induces expression changes in offspring adipocytes primarily via post-transcriptional mechanisms, such as differentially expressed miRNAs and different fatty acid concentrations, rather than translational changes.

Proteomic analysis revealed differentially expressed proteins in mat-HCD female adipocytes enriched in GO Terms “fatty acid metabolic process” and “regulation of lipid metabolic process”. Interestingly, genes associated with “fatty acid metabolic process” were both up- and downregulated. Overall, data suggest an increased fatty acid breakdown in response to increased fatty acid supply by maternal HCD feeding as proteins related to beta oxidation and fatty acid degradation like ABCD2, ALDH3A2, and NAAA that were upregulated (Demozay et al., 2004; X. Liu et al., 2015; Tuo et al., 2017) and inhibitors of these processes like ACACB, FMO1, and DBI that were downregulated (Abu-Elheiga et al., 2012; Bravo-San Pedro et al., 2019; Veeravalli et al., 2014). Proteins involved in the transport of lipids within the cell like CPT1B, FABP5, and CES1D were reduced in mat-HCD adipocytes possibly impairing proper processing of increasingly supplied fatty acids (Li et al., 2022; Maples et al., 2015; Xu et al., 2022). Furthermore, a reduced expression of these proteins is associated with increased body weight and impaired glucose and lipid metabolism in mice and humans (Li et al., 2022; Maples et al., 2015). Furthermore, CYP2F2 and GSTP1, both involved in the detoxification of reactive molecules like small-chain aldehydes arising from fatty acid breakdown were upregulated in mat-HCD female adipocytes suggesting a response of these cells to an increased nutrient supply and metabolism (Dang et al., 2021; Ghosh Dastidar et al., 2018).

This data suggest that maternal obesity causes alterations in protein expression via an increased supply of nutrients already in E13.5 adipocytes leading to a dysregulated lipid metabolism priming the offspring to develop obesity and associated comorbidities in later life. This is further supported by the downregulation of different genes involved in DNL after mat-HCD exposure. Downregulation of ACSL3, GK, and especially SCD1, ACLY, and FASN indicate a reduced lipid synthesis via DNL in mat-HCD female adipocytes (Batchuluun et al., 2022; Klasson et al., 2022; Poudyal & Brown, 2011; Rahib et al., 2007; Wakil, 1989). Maternal obesity’s influence on offspring DNL extents to the epigenetic level, as Tetratricopeptide repeat domain 39B *(Ttc39b)* which decreases DNL via *Nr1h3* deactivation, was hypomethylated in addition to its increased protein expression in mat-HCD offspring adipocytes (Hsieh et al., 2016). This together together with increased fatty acid breakdown may contribute to the decreased adipocyte size phenotype in adult female mat-HCD offspring previously described

by my research group (Dahlhoff et al., 2014). Reduced expression of PNPLA2 in mat-HCD adipocytes further supports this notion as PNPLA2 is a key regulator of lipid droplet size. Previous data from my research group reveals upregulation of PNPLA2, FASN, and ACLY in adipocytes of female mat-HCD offspring to compensate for reduced adipocyte size in later life (Dahlhoff et al., 2014; unpublished data).

Epigenetic changes like altered DNA methylation are one of several mechanisms likely involved in fetal programming and studies revealed differential DNA methylation patterns cord blood of neonates from mothers with increased BMI (Catalano & Shankar, 2017). In this thesis, it was observed that maternal obesity causes changed DNA methylation in genes association with GO terms “fat cell differentiation” and “regulation of fat cell differentiation”. Interestingly, *Bmp2, Vstm2a,* and *Creb5* are all important for the commitment and maintenance of preadipocytes to the adipose lineage (Denton et al., 2019; Huang et al., 2009; Maekawa et al., 2010; Secco et al., 2017). In this process, *Bmp2* plays a key role as both *Vstm2a’s* and *Creb5’s* affect adipogenesis via *Bmp2* and *Pparg* dependent pathways (Maekawa et al., 2010; Secco et al., 2017). Additionally, maternal obesity impairs commitment to the adipogenic lineage via *Fbn1,* as an increased protein expression is revealed by proteomics in addition to an intron hypomethylation (Muthu et al., 2022). Hence, data suggest that maternal obesity affects the commitment of cells to the adipose lineage long term via epigenetic changes in DNA methylation. Furthermore, *Bmp2* expression was increased in *Aldh1a1* knockout cells suggesting a role of *Aldh1* in adipogenesis and fetal programming by maternal obesity (Nallamshetty et al., 2013). Overall, this data further strengthens epigenetic changes in DNA methylation as a mechanism involved in fetal programming.

These data further underline the need for early preventive strategies as intrauterine obesogenic environment impairs pathways associated with adipocyte commitment and lipid metabolism already in developing embryos. Reducing pre-pregnancy maternal weight is viewed as a promising strategy to prevent negative effects on offspring development, but introducing lifestyle changes to lose weight prior to pregnancy proofed to be difficult and can even cause harmful effects in offspring due to missing micronutrients (Hieronimus & Ensenauer, 2021). Therefore, dietary adjustments pre- and during pregnancy are proposed to ameliorate adverse effects on offspring. Previous work of my research group in NMRI mice revealed that improving HCD fatty acid composition by increasing omega-3 long-chain polyunsaturated fatty acid (n-3 LC PUFA) and medium-chain triglyceride (MCT) concentrations (FATMOD diet) without changing caloric density mitigated negative effects in offspring like decreased adipocyte size and body weight (Öner-Sieben et al, unpublished). However, n-3 LC-PUFA supplementation in a human study during pregnancy failed to improve offspring body composition at 5 years (Brei et al., 2016). Furthermore, fish oil supplementation, which is a source for n-3 LC-PUFAs especially docosahexaenoic (DHA) and eicosapentaenoic acid

(EPA), of mothers with overweight during pregnancy had no effect on body fat percentage of infants (Satokar et al., 2023). Additionally, maternal pre-pregnancy obesity weakens effectiveness of n-3 LC-PUFA supplementation during pregnancy depicted by reduced changes in plasma n-3 LC-PUFA concentrations complicating its use as a preventive strategy (Monthe-Dreze et al., 2018). Although, n-3 LC-PUFA supplementation reduced concentrations of oxidative stress markers in mothers' urine (Sley et al., 2020) and docosahexaenoic acid, an n-3 LC-PUFA, supplementation is associated with reduced pre-term risk by increasing pregnancy duration (Carlson et al., 2013; Simmonds et al., 2020). However, human dietary intervention studies are often influenced by numerous confounding factors that have not been adequately controlled in the past. Hence, further optimization of dietary strategies and study design is necessary to develop possible nutritional intervention targeting pregnant women. Additionally, further research in underlying mechanisms of fetal programming by maternal overweight during pregnancy is necessary to identify promising targets and outcomes for dietary intervention strategies.

4.2 Functional analyses of candidate genes in murine 3T3-L1 cells

4.2.1 Implementation of optimized 3T3-L1 differentiation protocol utilizing PPARG agonist rosiglitazone

Transcriptomic analysis of offspring adipocytes identified *Aldh1a1*, *Aldh1a7* and *Scand1* as target genes to further understand fetal programming by maternal obesity during pregnancy. To investigate their role in adipogenesis an *in vitro* model system for adipogenic differentiation the 3T3-L1 cell line was used, which is the most commonly used murine *in vitro*.

Adipogenic differentiation efficiency of 3T3-L1 cells was increased by adding *Pparg* agonist rosiglitazone to the differentiation cocktail consisting of insulin, dexamethasone, and IBMX (Zebisch et al., 2012). However, adipogenic differentiation success was assessed only phenotypically via lipid droplet staining. Hence, expression of different genes involved in adipogenesis during differentiation using this optimized protocol was investigated prior to using it to study the role of potential candidate genes in adipogenesis. *Pparg1, Pparg2, Cebpa, Acaca, Fasn, Nr1h3, Cidea, Fabp4, Cd36, Adipoq,* and *Mcp-1* expression during differentiation is similar between cells differentiated using rosiglitazone and previous results not using it supporting the use of rosiglitazone (Cordonier et al., 2016; Gao et al., 2017; Hallberg et al., 2008; Jackson et al., 2017; Krishna et al., 2018; Palhinha et al., 2019; Zhang et al., 2020). *Srebf1c* mRNA expression is described to increase during adipogenic differentiation which contrasts with it remaining unchanged when using rosiglitazone to induce adipogenesis (Payne et al., 2009). This indicates that direct *Pparg* activation by rosiglitazone diminishes *Srebf1c's Pparg*-dependent role in adipogenesis regulation rendering rosiglitazone unusable in studies investigating *Srebf1c* (Fajas et al., 1999). Similarly, *Pgc-1a* expression remains unchanged

and the protocol has to be adapted to mimic a more brown adipose tissue like phenotype to investigate its role in adipogenesis (Tanaka-Yachi et al., 2018). Furthermore, *Il-6* expression in 3T3-L1 is induced by inflammatory signals like Tumor necrosis factor *(Tnf)* and without such signals its expression remains unchanged as in my experiments (Fasshauer et al., 2003). Overall, the addition of rosiglitazone increases differentiation efficiency and induces similar gene expression profiles during differentiation as previous protocols for most investigated genes rendering it a suitable model for the investigation of murine adipogenesis. Lastly, *Pparg2, Acaca, Fasn, Cd36, Cidea, Fabp4,* and *Adiponectin* are suggested as markers for a successfully differentiation using rosiglitazone to adipogenically differentiate 3T3-L1 cells as they were significantly increased at the end of differentiation.

4.2.2 *Aldh1a1* and *Aldh1a7* regulates adipocyte development at different stages

The 3T3-L1 cell line was used as model for adipogenesis to further analyze *Aldh1a1* and *Aldh1a7*, whose gene expression was found to be downregulated in adipocytes of female murine embryos exposed to maternal obesity. Remarkably, *in vitro* analysis using murine 3T3-L1 cells revealed a regulatory role of *Aldh1a7* in adipogenesis. *Aldh1a7* knockdown inhibited adipogenesis assessed by lipid droplet formation and marker gene expression. Furthermore, its expression sharply increases during adipogenic differentiation of 3T3-L1 cells suggests a key role in regulation of adipogenesis. This is in line with an increasing *Aldh1a7* mRNA expression pattern previously described during early adipogenic differentiation of MEFs, which was shown to be thymoma viral proto-oncogene 1 *(Akt1*, also known as AKT serine/threonine kinase 1 in humans*)* dependent (Baudry et al., 2006). *Aldh1a7* has 92% protein sequence similarity with *Aldh1a1* (Black et al., 2009), but nevertheless, its enzymatic affinity and efficiency is much smaller and it is unable to catalyze the oxidation of retinaldehyde to retinoic acid, one of *Aldh1a1's* main enzymatic functions (Hsu et al., 1999; Kathmann et al., 2000; Reichert et al., 2011). This indicates that *Aldh1a7* might be a so called "dead enzyme", which are enzymes that lost catalytic activity but remain physiologically active (Jackson et al., 2015). They can affect their active counterpart, act as an allosteric modulator, interact with their natural substrate by binding it or other proteins as it is described for aldehyde dehydrogenase 16 family, member A1 *(Aldh16a1)* (Jackson et al., 2015). Hence, *Aldh1a7* might promote adipogenesis at early stages by binding retinaldehyde without oxidizing it but impairing its inhibiting effects on adipocyte differentiation previously described (Figure 27; Ziouzenkova et al., 2007). Its expression might be reduced in offspring's developing adipocytes exposed to an intrauterine obesogenic environment to compensate the increased energy supply and lipid droplet formation provided by maternal HCD feeding. Its downregulation in adipose tissue of adult female offspring of HCD fed dams presented here might contribute to the reduced adipocyte size seen in these mice (Dahlhoff et al., 2014). Hence, targeting *Aldh1a7* expression early in development using dietary interventions could promote adipocyte and adipose tissue

development and act as potential strategy to prevent dysregulated adipose tissue development in adult offspring described previously.

Even though experiments performed here do not indicate a role of *Aldh1a1* in adipogenesis, *Aldh1a1* is strongly expressed in murine adipocytes and is described to be involved in regulating fat tissue formation as *Aldh1a1* knockout mice are resistant to diet induced obesity and displayed smaller adipocytes and reduced adipogenesis (Reichert et al., 2011; Yasmeen et al., 2013; Ziouzenkova et al., 2007). Furthermore, *ex vivo* differentiated *Aldh1a1* knockout MEFs poorly differentiate into adipocytes in contrast to results presented here which were obtained utilizing 3T3-L1 cells (Reichert et al., 2011; K. Yang et al., 2017). Possible explanations for these differences include remaining *Aldh1a1* activity after incomplete and temporary *Aldh1a1* knockdown and the different model systems utilized here. Opposed to 3T3-L1 cells, MEFs are a heterogeneous cell populations including cells from diverse lineages such as muscle and bone, alongside those from the adipogenic lineage (Singhal et al., 2016). Hence, effects caused by *Aldh1a1* knockdown in cells other than preadipocytes might impair their adipogenic differentiation. Overall, the underlying mechanisms of how an *Aldh1a1* knockdown impairs adipogenesis have not yet been unraveled, but it was discussed to involve the vitamin A metabolism. During the vitamin A metabolism vitamin A is metabolized by alcohol dehydrogenase *(Adh)* family proteins into retinaldehyde which in turn is metabolized into retinoic acid mainly via *Aldh1a1* (Figure 27; Ziouzenkova et al., 2007). On the one hand, retinaldehyde inhibits adipocyte differentiation of 3T3-L1 cells (Ziouzenkova et al., 2007). On the other hand, adipogenesis is promoted by retinoic acid via activation of a signaling cascade involving zinc finger protein 423 *(Zfp423)* and *Pparg* (Reichert et al., 2011; Ziouzenkova et al., 2007). Therefore, it was postulated that MEF adipogenesis is reduced after *Aldh1a1* knockout due to reduced oxidation of retinaldehyde to retinoic acid by missing *Aldh1a1* causing increased retinaldehyde and decreased retinoic acid concentrations inhibiting adipocyte differentiation (Reichert et al., 2011). Nevertheless, adipogenesis inhibiting effects on adipogenesis of an *Aldh1a1* knockout emerge prior to it influencing retinaldehyde concentration, which indicates that *Aldh1a1* regulates adipocyte differentiation by pathways independent of vitamin A (D. Yang et al., 2017). However, after adding retinoic acid, the educt of *Aldh1a1,* to differentiating *Aldh1a1* knockout cells a rescuing effect regarding adipogenesis was observed (Reichert et al., 2011). Furthermore, increased retinoic acid synthesis during adipogenic differentiation by *Aldh1a1* was described to start at day 4 of differentiation. This suggests that *Aldh1a1* mainly regulates adipogenesis during later stages of differentiation via increased retinoic acid synthesis. This notion fits with data presented here of a siRNA mediated *Aldh1a1* knockdown during early phases not inhibiting adipogenesis. Furthermore, reduced expression of key adipogenesis markers *Pparg* and *Fabp4* was associated with reduced fat accumulation in visceral adipose tissue of *Aldh1a1* knockout mice. This is in line with a reduced

expression of *Aldh1a1* in combination with a reduced body fat ratio and adipocyte size in visceral adipose tissue of adult female offspring of HCD fed dams described previously (Dahlhoff et al., 2014). Overall, *Aldh1a1* dysregulation is associated with dysregulated adipose tissue development linked to fetal programming by an intrauterine obesogenic milieu, but the underlying mechanisms remain unclear as investigations regarding the involvement of the vitamin A metabolism in adipogenesis present conflicting results at this point.

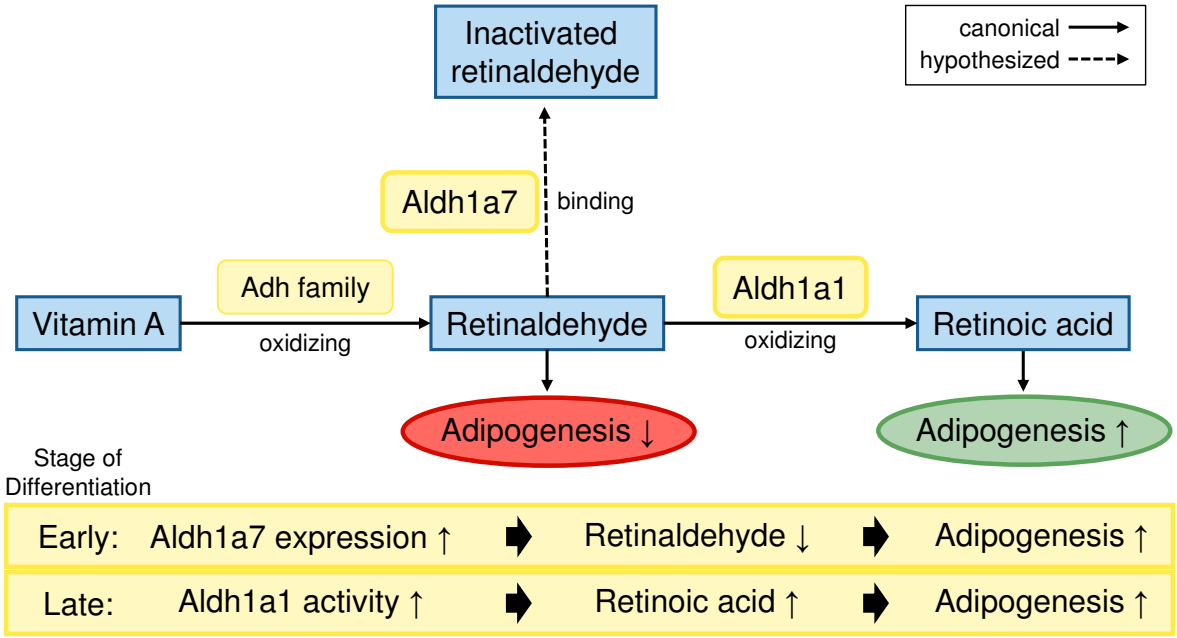

Figure 27: Hypothesized role of the vitamin A metabolism as well as *Aldh1a1* and *Aldh1a7* in adipogenesis regulation.
Different members of the alcohol dehydrogenase *(Adh)* family oxidize Vitamin A into retinaldehyde, which inhibits adipogenesis (Ziouzenkova et al., 2007). Next, mainly *Aldh1a1* oxidizes retinaldehyde to retinoic acid, which in turn promotes adipogenesis (Reichert et al., 2011). *Aldh1a7* might also bind retinaldehyde and thereby inhibiting it causing increased adipogenesis at early stages of adipogenic differentiation. *Aldh1a1* activity rises at later stages of adipogenic differentiation and might thereby promote adipogenesis via increased retinoic acid levels (Reichert et al., 2011). Canonical pathways are indicated by solid lines and hypothesized pathways by dashed lines. M. Schouwink generated this figure. *Adh* = Alcohol dehydrogenase; *Aldh1a1* = Aldehyde dehydrogenase family 1, subfamily A1; *Aldh1a7* = Aldehyde dehydrogenase family 1, subfamily A7

Cholesterol biosynthesis is another pathway regulated by *Aldh1a1* and poses as a possible alternative mechanism for *Aldh1a1's* regulation of adipogenesis as reduced cholesterol levels cause impaired insulin signaling in 3T3-L1 cells which in turn impairs adipocyte differentiation (Charkoftaki et al., 2019; Laviola et al., 2006; Parpal et al., 2001). Furthermore, *Aldh1a1* is also described to bind androgens, which inhibit commitment of precursor cells to the adipogenic lineage via Bone morphogenetic protein 4 *(Bmp4)* (Chazenbalk et al., 2013; Pereira et al., 1991). Hence, decreased *Aldh1a1* might lead to increased intracellular androgen levels causing decreased *Bmp4* signaling and commitment to the adipocyte lineage. Interestingly, an increased risk of insulin resistance and T2D is associated with increased concentrations of free androgens in women but with decreased concentrations in men (Navarro et al., 2015).

The underlying mechanisms and the role of adipose tissue in it are not yet resolved, but this indicates possible sex specific effects of altered *Aldh1a1* expression on offspring health development. Furthermore, a role of *Aldh1a1* in the adipogenic commitment of cells is further supported by the observation that constitutive *Aldh1a1* knockout persisting during the commitment phase inhibits adipogenesis in MEFs but *Aldh1a1* knockdown in the committed preadipocyte 3T3-L1 cell line performed in this thesis fails to reproduce this effect (Reichert et al., 2011; D. Yang et al., 2017; Ziouzenkova et al., 2007). This thesis produced conflicting results regarding the impact of maternal obesity on *Aldh1a1* expression in offsprings' fetal adipocytes as transcriptomics and western blot analysis revealed decreased *Aldh1a1* expression but proteomics analysis of similarly produced samples from a later cohort displayed an *Aldh1a1* upregulation. Hence, further studies are needed to delineate the impact of maternal obesity during pregnancy on *Aldh1a1* expression and its role in adipogenesis regulation. Nonetheless, data presented in this thesis suggest it plays a role in fetal programming by an intrauterine obesogenic milieu as its expression is dysregulated in both fetal as well as adult female adipocyte samples. Its dysregulation may therefore contribute to the altered adipose tissue phenotype of smaller adipocytes and less body fat percentage observed in adult female offspring exposed to maternal obesity (Dahlhoff et al., 2014).

There are only a few studies investigating *ALDH1* family members in human adipocyte differentiation, but *ALDH1A1* was described to be most expressed isoform in human adipose tissue (Reichert et al., 2011; Yasmeen et al., 2013). My analysis using SGBS cells, a human *in vitro* adipogenesis model, revealed a peak in expression of *ALDH1A1* and *ALDH1A3* late and early during adipogenesis, respectively, indicating a function in regulating adipogenesis. However, none of these isoforms displayed an expression pattern during adipogenesis comparable to murine *Aldh1a7,* to which no human orthologue exists. Hence, more research on the function of murine *Aldh1a7* and human *ALDH1A1* and *ALDH1A3* is necessary to determine whether they are functional orthologues regarding adipogenesis regulation.

Overall, further understanding of the influence of *Aldh1a* human and murine isoforms on adipocyte differentiation is needed to develop potential countermeasures to attenuate adverse effects of an obesogenic intrauterine environment on offspring development. *In vivo* mRNA delivery could be used to elevate expression of potential therapeutic target genes like *Aldh1a7* in adult offspring. Subcutaneous delivery of mRNA coding for fibroblast growth factor 21 *(Fgf21)* was able to ameliorate obesity and insulin resistance in diet-induced obese mice (Bartesaghi et al., 2022). Furthermore, subcutaneous mRNA delivery tests in humans reveal promising results in the field of regenerative angiogenesis to treat decreased vascularization caused e.g. by T2D (Gan et al., 2019). The administration of mRNA vaccines to millions of people during the Coronavirus disease 2019 (COVID-19) showed the short-term efficacy and safety of mRNA therapeutics (Qin et al., 2022). Long-term effect and safety of mRNA

therapeutics need to be investigated in future studies. On the contrary, antisense oligonucleotides (ASO) can be used to decrease target gene expression (Keating et al., 2022). They were successfully used to decrease body weight gain by targeting mitogen-activated protein kinase 8 *(Mapk8,* also known as *JNK1)* in mice obesity models (Yu et al., 2008). Furthermore, ASO targeting angiopoietin-like 8 *(Angptl8)* enhanced adipose lipid metabolism and ameliorated glucose intolerance after HCD feeding in C57BL/6 mice (Vatner et al., 2018). Even though research on ASO treatments for obesity are still at preclinical phase, clinical trials on treating e.g. leukemia, nonalcoholic steatohepatitis, or different kinds of tumors are currently running (Amanat et al., 2022). However, due to the unknown side effects, targeted interventions utilizing such mechanisms cannot be used in pregnant mothers and their developing offspring. Therefore, they are only an option for pre-pregnancy treatment of the mother or for treating adult offspring. Hence, development of preventive strategies in pregnant women should focus on nutritional internventions described above (4.1.2).

4.2.3 The role of *Scand1* during adipogenic differentiation remains ambiguous

Besides changed expression of *Aldh1a1* and *Aldh1a7* transcriptomic analysis displayed *Scand1,* also known as Pparg coactivator 2 *(Pgc-2)* to be upregulated in mat-HCD offspring. Hence, similarly to *Aldh1a1* and *Aldh1a7* the role of *Scand1* in adipogenesis was investigated, but remained unclear even though some evidence indicates its participation in regulating adipogenic differentiation.

RT-qPCR analysis including the same samples used for transcriptomic analysis revealed a reduced expression in contrast to an increased expression observed by RNA sequencing. Due to the three times bigger sample size of the RT-qPCR analysis it provides the more robust result indicating *Scand1* being downregulated in mat-HCD offspring. *Scand1* is able to bind SCAN domain-containing transcription factors like Zinc finger protein 202 *(Zfp202)* and non-SCAN domain-containing transcription factors like *Pparg,* which are both involved in regulation of lipid metabolism and adipocyte differentiation (Babb & Bowen, 2003). Via its action as a cofactor, it increases the transcriptional activity of *Pparg* and *Scand1* overexpression enhances adipogenesis (Castillo et al., 1999; Schmitz et al., 2004). Unexpectedly, analysis revealed *Scand1* expression being reduced during adipogenic differentiation of 3T3-L1 cells. This may indicate that murine *Scand1* expression is regulated by *Pparg* via a negative feedback loop as it is described for *Cebpb* regulation of Krüppel-like factor 4 *(Klf4)* in early adipogenesis (Birsoy et al., 2008). This way, induction of *Pparg* expression by rosiglitazone causes a reduced expression of *Scand1* during adipogenesis and further knockdown of *Scand1* using siRNA has only minor effects on adipogenesis as observed in this thesis. However, investigations of the role of *SCAND1* in human adipogenesis using SBGS cells revealed an opposing expression pattern compared to murine cells. This indicates differential expression regulation of human *SCAND1* compared to its murine orthologue as it was

previously described for Transformation related protein 53 *(Trp53)* and its role in cancer pathology (Fischer, 2021). Hence, further research is needed to identify *Scand1* role in regulation of adipogenesis especially regarding differences between human and murine adipogenesis.

4.3 Conclusion

Taken together, these results show maternal obesity-induced dysregulation on transcriptomic, proteomic and epigenetic levels in developing adipocytes from female E13.5 offspring embryos. They indicate a dysregulated adipocyte differentiation, commitment to the adipocyte lineage and fatty acid metabolism in offspring following exposure to maternal HCD feeding *in utero*. Proteomic analysis revealed alterations in lipid metabolism pathways generating a set of target genes to be investigated in future studies regarding their role in adipogenesis and fetal programming by maternal obesity. ALDH1A7 was identified as a strong regulator of murine adipogenesis with a reduced expression by maternal HCD feeding. Further understanding of this regulatory pathway and its translation into human adipocyte development could identify potential target genes for preventive strategies aiming at ameliorating obesity development in children exposed to an obesogenic intrauterine environment. It could help to optimize specific dietary changes and supplementation during pregnancy to improve offsprings' health trajectory regarding body composition and overweight development. Furthermore, drugs specifically targeting altered genes utilizing ASO or mRNA could be developed for treating women pre-pregnancy or adult offspring to improve offspring's health. Overall, results presented here further underline the importance of intrauterine fetal programming in offspring's development and the necessity to fully understand underlying mechanisms to develop preventing strategies.

In conclusion, this research underscores the urgency of implementing early life preventive strategies to mitigate the effects of maternal obesity on offspring development. By understanding the intricate molecular mechanisms underlying adipocyte development and dysregulation in the context of maternal obesity, preventive interventions aimed at disrupting this cycle and improving health of future generations can be developed.

5 References

Abu-Elheiga, L., Wu, H., Gu, Z., Bressler, R., & Wakil, S. J. (2012). Acetyl-CoA carboxylase 2-/- mutant mice are protected against fatty liver under high-fat, high-carbohydrate dietary and de novo lipogenic conditions. *J Biol Chem*, *287*(15), 12578-12588. https://doi.org/10.1074/jbc.M111.309559

Afshin, A., Forouzanfar, M. H., Reitsma, M. B., Sur, P., Estep, K., Lee, A., Marczak, L., Mokdad, A. H., Moradi-Lakeh, M., Naghavi, M., Salama, J. S., Vos, T., Abate, K. H., Abbafati, C., Ahmed, M. B., Al-Aly, Z., Alkerwi, A., Al-Raddadi, R., Amare, A. T., . . . Murray, C. J. L. (2017). Health Effects of Overweight and Obesity in 195 Countries over 25 Years. *N Engl J Med*, *377*(1), 13-27. https://doi.org/10.1056/NEJMoa1614362

Ahlqvist, E., Storm, P., Karajamaki, A., Martinell, M., Dorkhan, M., Carlsson, A., Vikman, P., Prasad, R. B., Aly, D. M., Almgren, P., Wessman, Y., Shaat, N., Spegel, P., Mulder, H., Lindholm, E., Melander, O., Hansson, O., Malmqvist, U., Lernmark, A., . . . Groop, L. (2018). Novel subgroups of adult-onset diabetes and their association with outcomes: a data-driven cluster analysis of six variables. *Lancet Diabetes Endocrinol*, *6*(5), 361-369. https://doi.org/10.1016/S2213-8587(18)30051-2

Akalin, A., Kormaksson, M., Li, S., Garrett-Bakelman, F. E., Figueroa, M. E., Melnick, A., & Mason, C. E. (2012). methylKit: a comprehensive R package for the analysis of genome-wide DNA methylation profiles. *Genome Biol*, *13*(10), R87. https://doi.org/10.1186/gb-2012-13-10-r87

Albers, L., Sobotzki, C., Kuß, O., Ajslev, T., Batista, R. F., Bettiol, H., Brabin, B., Buka, S. L., Cardoso, V. C., Clifton, V. L., Devereux, G., Gilman, S. E., Grzeskowiak, L. E., Heinrich, J., Hummel, S., Jacobsen, G. W., Jones, G., Koshy, G., Morgen, C. S., . . . von Kries, R. (2018). Maternal smoking during pregnancy and offspring overweight: is there a dose-response relationship? An individual patient data meta-analysis. *Int J Obes (Lond)*, *42*(7), 1249-1264. https://doi.org/10.1038/s41366-018-0050-0

Amanat, M., Nemeth, C. L., Fine, A. S., Leung, D. G., & Fatemi, A. (2022). Antisense Oligonucleotide Therapy for the Nervous System: From Bench to Bedside with Emphasis on Pediatric Neurology. *Pharmaceutics*, *14*(11). https://doi.org/10.3390/pharmaceutics14112389

Andermann, M. L., & Lowell, B. B. (2017). Toward a Wiring Diagram Understanding of Appetite Control. *Neuron*, *95*(4), 757-778. https://doi.org/10.1016/j.neuron.2017.06.014

Andersen, E., Ingerslev, L. R., Fabre, O., Donkin, I., Altintas, A., Versteyhe, S., Bisgaard, T., Kristiansen, V. B., Simar, D., & Barres, R. (2019). Preadipocytes from obese humans with type 2 diabetes are epigenetically reprogrammed at genes controlling adipose tissue function. *Int J Obes (Lond)*, *43*(2), 306-318. https://doi.org/10.1038/s41366-018-0031-3

Andres, A., Hull, H. R., Shankar, K., Casey, P. H., Cleves, M. A., & Badger, T. M. (2015). Longitudinal body composition of children born to mothers with normal weight, overweight, and obesity. *Obesity (Silver Spring)*, *23*(6), 1252-1258. https://doi.org/10.1002/oby.21078

Andrews, S. (2010). *FastQC: A quality control tool for high throughput sequence data*.

Babb, R., & Bowen, B. R. (2003). SDP1 is a peroxisome-proliferator-activated receptor gamma 2 co-activator that binds through its SCAN domain. *Biochem J*, *370*(Pt 2), 719-727. https://doi.org/10.1042/BJ20021378

Barsh, G. S., & Schwartz, M. W. (2002). Genetic approaches to studying energy balance: perception and integration. *Nature Reviews Genetics*, *3*(8), 589-600. https://doi.org/10.1038/nrg862

Bartesaghi, S., Wallenius, K., Hovdal, D., Liljeblad, M., Wallin, S., Dekker, N., Barlind, L., Davies, N., Seeliger, F., Winzell, M. S., Patel, S., Theisen, M., Brito, L., Bergenhem, N., Andersson, S., & Peng, X.-R. (2022). Subcutaneous delivery of FGF21 mRNA therapy reverses obesity, insulin resistance, and hepatic steatosis in diet-induced obese mice. *Molecular Therapy - Nucleic Acids*, *28*, 500-513. https://doi.org/10.1016/j.omtn.2022.04.010

Batchuluun, B., Pinkosky, S. L., & Steinberg, G. R. (2022). Lipogenesis inhibitors: therapeutic opportunities and challenges. *Nat Rev Drug Discov*, *21*(4), 283-305. https://doi.org/10.1038/s41573-021-00367-2

Baudry, A., Yang, Z. Z., & Hemmings, B. A. (2006). PKBalpha is required for adipose differentiation of mouse embryonic fibroblasts. *J Cell Sci*, *119*(Pt 5), 889-897. https://doi.org/10.1242/jcs.02792

Bender, R., & Lange, S. (2001). Adjusting for multiple testing--when and how? *J Clin Epidemiol*, *54*(4), 343-349. https://doi.org/10.1016/s0895-4356(00)00314-0

Birsoy, K., Chen, Z., & Friedman, J. (2008). Transcriptional regulation of adipogenesis by KLF4. *Cell Metab*, *7*(4), 339-347. https://doi.org/10.1016/j.cmet.2008.02.001

Black, W. J., Stagos, D., Marchitti, S. A., Nebert, D. W., Tipton, K. F., Bairoch, A., & Vasiliou, V. (2009). Human aldehyde dehydrogenase genes: alternatively spliced transcriptional variants and their

suggested nomenclature. *Pharmacogenet Genomics*, *19*(11), 893-902. https://doi.org/10.1097/FPC.0b013e3283329023

Brandao, B. B., Guerra, B. A., & Mori, M. A. (2017). Shortcuts to a functional adipose tissue: The role of small non-coding RNAs. *Redox Biol*, *12*, 82-102. https://doi.org/10.1016/j.redox.2017.01.020

Bravo-San Pedro, J. M., Sica, V., Martins, I., Anagnostopoulos, G., Maiuri, C., & Kroemer, G. (2019). Cell-autonomous, paracrine and neuroendocrine feedback regulation of autophagy by DBI/ACBP (diazepam binding inhibitor, acyl-CoA binding protein): the obesity factor. *Autophagy*, *15*(11), 2036-2038. https://doi.org/10.1080/15548627.2019.1662585

Brei, C., Stecher, L., Much, D., Karla, M. T., Amann-Gassner, U., Shen, J., Ganter, C., Karampinos, D. C., Brunner, S., & Hauner, H. (2016). Reduction of the n-6:n-3 long-chain PUFA ratio during pregnancy and lactation on offspring body composition: follow-up results from a randomized controlled trial up to 5 y of age. *Am J Clin Nutr*, *103*(6), 1472-1481. https://doi.org/10.3945/ajcn.115.128520

Byers, S. L., Wiles, M. V., Dunn, S. L., & Taft, R. A. (2012). Mouse estrous cycle identification tool and images. *PloS one*, *7*(4), e35538. https://doi.org/10.1371/journal.pone.0035538

Carlson, S. E., Colombo, J., Gajewski, B. J., Gustafson, K. M., Mundy, D., Yeast, J., Georgieff, M. K., Markley, L. A., Kerling, E. H., & Shaddy, D. J. (2013). DHA supplementation and pregnancy outcomes. *Am J Clin Nutr*, *97*(4), 808-815. https://doi.org/10.3945/ajcn.112.050021

Carreras-Badosa, G., Bonmatí, A., Ortega, F. J., Mercader, J. M., Guindo-Martínez, M., Torrents, D., Prats-Puig, A., Martinez-Calcerrada, J. M., de Zegher, F., Ibáñez, L., Fernandez-Real, J. M., Lopez-Bermejo, A., & Bassols, J. (2017). Dysregulation of Placental miRNA in Maternal Obesity Is Associated With Pre- and Postnatal Growth. *J Clin Endocrinol Metab*, *102*(7), 2584-2594. https://doi.org/10.1210/jc.2017-00089

Castillo, G., Brun, R. P., Rosenfield, J. K., Hauser, S., Park, C. W., Troy, A. E., Wright, M. E., & Spiegelman, B. M. (1999). An adipogenic cofactor bound by the differentiation domain of PPARgamma. *Embo j*, *18*(13), 3676-3687. https://doi.org/10.1093/emboj/18.13.3676

Castillo, H., Santos, I. S., & Matijasevich, A. (2015). Relationship between maternal pre-pregnancy body mass index, gestational weight gain and childhood fatness at 6-7 years by air displacement plethysmography. *Matern Child Nutr*, *11*(4), 606-617. https://doi.org/10.1111/mcn.12186

Catalano, P. M., & Shankar, K. (2017). Obesity and pregnancy: mechanisms of short term and long term adverse consequences for mother and child. *Bmj*, *356*, j1. https://doi.org/10.1136/bmj.j1

Cavalcante, R. G., & Sartor, M. A. (2017). annotatr: genomic regions in context. *Bioinformatics*, *33*(15), 2381-2383. https://doi.org/10.1093/bioinformatics/btx183

Charkoftaki, G., Thompson, D. C., Golla, J. P., Garcia-Milian, R., Lam, T. T., Engel, J., & Vasiliou, V. (2019). Integrated multi-omics approach reveals a role of ALDH1A1 in lipid metabolism in human colon cancer cells. *Chem Biol Interact*, *304*, 88-96. https://doi.org/10.1016/j.cbi.2019.02.030

Chazenbalk, G., Singh, P., Irge, D., Shah, A., Abbott, D. H., & Dumesic, D. A. (2013). Androgens inhibit adipogenesis during human adipose stem cell commitment to preadipocyte formation. *Steroids*, *78*(9), 920-926. https://doi.org/10.1016/j.steroids.2013.05.001

Chen, H., Yuan, R., Zhang, Y., Zhang, X., Chen, L., Zhou, X., Yuan, Z., Nie, Y., Li, M., Mo, D., & Chen, Y. (2016). ATF4 regulates SREBP1c expression to control fatty acids synthesis in 3T3-L1 adipocytes differentiation. *Biochim Biophys Acta*, *1859*(11), 1459-1469. https://doi.org/10.1016/j.bbagrm.2016.07.010

Collas, P. (2010). Programming differentiation potential in mesenchymal stem cells. *Epigenetics*, *5*(6), 476-482. https://doi.org/10.4161/epi.5.6.12517

Committee, A. D. A. P. P. (2021). 2. Classification and Diagnosis of Diabetes: Standards of Medical Care in Diabetes—2022. *Diabetes Care*, *45*(Supplement_1), S17-S38. https://doi.org/10.2337/dc22-S002

Cordonier, E. L., Jarecke, S. K., Hollinger, F. E., & Zempleni, J. (2016). Inhibition of acetyl-CoA carboxylases by soraphen A prevents lipid accumulation and adipocyte differentiation in 3T3-L1 cells. *Eur J Pharmacol*, *780*, 202-208. https://doi.org/10.1016/j.ejphar.2016.03.052

Dahlhoff, M., Pfister, S., Blutke, A., Rozman, J., Klingenspor, M., Deutsch, M. J., Rathkolb, B., Fink, B., Gimpfl, M., Hrabe de Angelis, M., Roscher, A. A., Wolf, E., & Ensenauer, R. (2014). Peri-conceptional obesogenic exposure induces sex-specific programming of disease susceptibilities in adult mouse offspring. *Biochim Biophys Acta*, *1842*(2), 304-317, Article Journal Article Research Support, Non-U.S. Gov't Journal Article Research Support, Non-U.S. Gov't. https://doi.org/10.1016/j.bbadis.2013.11.021

Dang, T. T. H., Choi, M., Pham, H. G., & Yun, J. W. (2021). Cytochrome P450 2F2 (CYP2F2) negatively regulates browning in 3T3-L1 white adipocytes. *Eur J Pharmacol*, *908*, 174318. https://doi.org/10.1016/j.ejphar.2021.174318

Dastagir, K., Reimers, K., Lazaridis, A., Jahn, S., Maurer, V., Strauss, S., Dastagir, N., Radtke, C., Kampmann, A., Bucan, V., & Vogt, P. M. (2014). Murine embryonic fibroblast cell lines differentiate into three mesenchymal lineages to different extents: new models to investigate differentiation processes. *Cellular reprogramming*, *16*(4), 241-252. https://doi.org/10.1089/cell.2014.0005

Demozay, D., Rocchi, S., Mas, J.-C., Grillo, S., Pirola, L., Chavey, C., & Van Obberghen, E. (2004). Fatty Aldehyde Dehydrogenase: POTENTIAL ROLE IN OXIDATIVE STRESS PROTECTION AND REGULATION OF ITS GENE EXPRESSION BY INSULIN*. *Journal of Biological Chemistry*, *279*(8), 6261-6270. https://doi.org/https://doi.org/10.1074/jbc.M312062200

Denton, N. F., Eghleilib, M., Al-Sharifi, S., Todorcevic, M., Neville, M. J., Loh, N., Drakesmith, A., Karpe, F., & Pinnick, K. E. (2019). Bone morphogenetic protein 2 is a depot-specific regulator of human adipogenesis. *Int J Obes (Lond)*, *43*(12), 2458-2468. https://doi.org/10.1038/s41366-019-0421-1

Deutsche Adipositas-Gesellschaft e.V., D. (2014). Interdisziplinäre Leitlinie der Qualität S3 zur „Prävention und Therapie der Adipositas". In (Vol. 8, pp. 179-221).

Dias, M. D. S., Matijasevich, A., Barros, A. J., Menezes, A. M. B., Schneider, B. C., Hartwig, F. P., Barros, F. C., Wehrmeister, F. C., Goncalves, H., Santos, I. S., Assuncao, M. C. F., & Horta, B. L. (2021). Influence of maternal pre-pregnancy nutritional status on offspring anthropometric measurements and body composition in three Brazilian Birth Cohorts. *Public Health Nutr*, *24*(5), 882-894. https://doi.org/10.1017/S1368980020004887

Distel, R. J., Robinson, G. S., & Spiegelman, B. M. (1992). Fatty acid regulation of gene expression. Transcriptional and post-transcriptional mechanisms. *Journal of Biological Chemistry*, *267*(9), 5937-5941. https://doi.org/https://doi.org/10.1016/S0021-9258(18)42645-2

Dufau, J., Shen, J. X., Couchet, M., De Castro Barbosa, T., Mejhert, N., Massier, L., Griseti, E., Mouisel, E., Amri, E. Z., Lauschke, V. M., Ryden, M., & Langin, D. (2021). In vitro and ex vivo models of adipocytes. *American journal of physiology. Cell physiology*, *320*(5), C822-C841. https://doi.org/10.1152/ajpcell.00519.2020

Eisenberg, D., Shikora, S. A., Aarts, E., Aminian, A., Angrisani, L., Cohen, R. V., de Luca, M., Faria, S. L., Goodpaster, K. P. S., Haddad, A., Himpens, J. M., Kow, L., Kurian, M., Loi, K., Mahawar, K., Nimeri, A., O'Kane, M., Papasavas, P. K., Ponce, J., . . . Kothari, S. N. (2023). 2022 American Society of Metabolic and Bariatric Surgery (ASMBS) and International Federation for the Surgery of Obesity and Metabolic Disorders (IFSO) Indications for Metabolic and Bariatric Surgery. *Obes Surg*, *33*(1), 3-14. https://doi.org/10.1007/s11695-022-06332-1

El Hajj, N., Pliushch, G., Schneider, E., Dittrich, M., Muller, T., Korenkov, M., Aretz, M., Zechner, U., Lehnen, H., & Haaf, T. (2013). Metabolic programming of MEST DNA methylation by intrauterine exposure to gestational diabetes mellitus. *Diabetes*, *62*(4), 1320-1328. https://doi.org/10.2337/db12-0289

Ensenauer, R., Brandlhuber, L., Burgmann, M., Sobotzki, C., Zwafink, C., Anzill, S., Holdt, L., Teupser, D., Hasbargen, U., Netz, H., Roscher, A. A., & von Kries, R. (2015). Obese Nondiabetic Pregnancies and High Maternal Glycated Hemoglobin at Delivery as an Indicator of Offspring and Maternal Postpartum Risks: The Prospective PEACHES Mother-Child Cohort. *Clin Chem*, *61*(11), 1381-1390. https://doi.org/10.1373/clinchem.2015.242206

Ensenauer, R., Chmitorz, A., Riedel, C., Fenske, N., Hauner, H., Nennstiel-Ratzel, U., & von Kries, R. (2013). Effects of suboptimal or excessive gestational weight gain on childhood overweight and abdominal adiposity: results from a retrospective cohort study. *Int J Obes (Lond)*, *37*(4), 505-512. https://doi.org/10.1038/ijo.2012.226

Fajas, L., Schoonjans, K., Gelman, L., Kim, J. B., Najib, J., Martin, G., Fruchart, J. C., Briggs, M., Spiegelman, B. M., & Auwerx, J. (1999). Regulation of peroxisome proliferator-activated receptor gamma expression by adipocyte differentiation and determination factor 1/sterol regulatory element binding protein 1: implications for adipocyte differentiation and metabolism. *Mol Cell Biol*, *19*(8), 5495-5503. https://doi.org/10.1128/MCB.19.8.5495

Fasshauer, M., & Bluher, M. (2015). Adipokines in health and disease. *Trends Pharmacol Sci*, *36*(7), 461-470. https://doi.org/10.1016/j.tips.2015.04.014

Fasshauer, M., Klein, J., Lossner, U., & Paschke, R. (2003). Interleukin (IL)-6 mRNA Expression is Stimulated by Insulin, Isoproterenol, Tumour Necrosis Factor Alpha, Growth Hormone, and IL-6 in 3T3-L1 Adipocytes. *Horm Metab Res*, *35*(03), 147-152.

Fischer-Posovszky, P., Newell, F. S., Wabitsch, M., & Tornqvist, H. E. (2008). Human SGBS cells - a unique tool for studies of human fat cell biology. *Obes Facts*, *1*(4), 184-189. https://doi.org/10.1159/000145784

Fischer, M. (2021). Mice Are Not Humans: The Case of p53. *Trends in Cancer*, *7*(1), 12-14. https://doi.org/https://doi.org/10.1016/j.trecan.2020.08.007

Frayling, T. M., Timpson, N. J., Weedon, M. N., Zeggini, E., Freathy, R. M., Lindgren, C. M., Perry, J. R., Elliott, K. S., Lango, H., Rayner, N. W., Shields, B., Harries, L. W., Barrett, J. C., Ellard, S., Groves, C. J., Knight, B., Patch, A. M., Ness, A. R., Ebrahim, S., . . . McCarthy, M. I. (2007). A common variant in the FTO gene is associated with body mass index and predisposes to childhood and adult obesity. *Science*, *316*(5826), 889-894. https://doi.org/10.1126/science.1141634

Friedman, J. M. (2019). Leptin and the endocrine control of energy balance. *Nat Metab*, *1*(8), 754-764. https://doi.org/10.1038/s42255-019-0095-y

Furuhashi, M., Saitoh, S., Shimamoto, K., & Miura, T. (2014). Fatty Acid-Binding Protein 4 (FABP4): Pathophysiological Insights and Potent Clinical Biomarker of Metabolic and Cardiovascular Diseases. *Clin Med Insights Cardiol*, *8*(Suppl 3), 23-33, Article Journal Article Review Journal Article Review. https://doi.org/10.4137/CMC.S17067

Gan, L.-M., Lagerström-Fermér, M., Carlsson, L. G., Arfvidsson, C., Egnell, A.-C., Rudvik, A., Kjaer, M., Collén, A., Thompson, J. D., Joyal, J., Chialda, L., Koernicke, T., Fuhr, R., Chien, K. R., & Fritsche-Danielson, R. (2019). Intradermal delivery of modified mRNA encoding VEGF-A in patients with type 2 diabetes. *Nature Communications*, *10*(1), 871. https://doi.org/10.1038/s41467-019-08852-4

Gao, H., Li, D., Yang, P., Zhao, L., Wei, L., Chen, Y., & Ruan, X. Z. (2017). Suppression of CD36 attenuates adipogenesis with a reduction of P2X7 expression in 3T3-L1 cells. *Biochem Biophys Res Commun*, *491*(1), 204-208. https://doi.org/10.1016/j.bbrc.2017.07.077

Gauster, M., Hiden, U., van Poppel, M., Frank, S., Wadsack, C., Hauguel-de Mouzon, S., & Desoye, G. (2011). Dysregulation of placental endothelial lipase in obese women with gestational diabetes mellitus. *Diabetes*, *60*(10), 2457-2464. https://doi.org/10.2337/db10-1434

Gaytán-Pacheco, N., Lima-Rogel, V., Méndez-Mancilla, A., Escalante-Padrón, F., Toro-Ortíz, J. C., Jiménez-Capdeville, M. E., Zaga-Clavellina, V., Portales-Pérez, D. P., Noyola, D. E., & Salgado-Bustamante, M. (2021). Changes in PPAR-γ Expression Are Associated with microRNA Profiles during Fetal Programming due to Maternal Overweight and Obesity. *Gynecol Obstet Invest*, *86*(5), 415-426. https://doi.org/10.1159/000517116

Gemma, C., Sookoian, S., Alvariñas, J., García, S. I., Quintana, L., Kanevsky, D., González, C. D., & Pirola, C. J. (2009). Maternal pregestational BMI is associated with methylation of the PPARGC1A promoter in newborns. *Obesity (Silver Spring)*, *17*(5), 1032-1039. https://doi.org/10.1038/oby.2008.605

Ghaben, A. L., & Scherer, P. E. (2019). Adipogenesis and metabolic health. *Nat Rev Mol Cell Biol*, *20*(4), 242-258. https://doi.org/10.1038/s41580-018-0093-z

Ghazalpour, A., Bennett, B., Petyuk, V. A., Orozco, L., Hagopian, R., Mungrue, I. N., Farber, C. R., Sinsheimer, J., Kang, H. M., Furlotte, N., Park, C. C., Wen, P. Z., Brewer, H., Weitz, K., Camp, D. G., 2nd, Pan, C., Yordanova, R., Neuhaus, I., Tilford, C., . . . Lusis, A. J. (2011). Comparative analysis of proteome and transcriptome variation in mouse. *PLoS Genet*, *7*(6), e1001393. https://doi.org/10.1371/journal.pgen.1001393

Ghosh Dastidar, S., Jagatheesan, G., Haberzettl, P., Shah, J., Hill, B. G., Bhatnagar, A., & Conklin, D. J. (2018). Glutathione S-transferase P deficiency induces glucose intolerance via JNK-dependent enhancement of hepatic gluconeogenesis. *Am J Physiol Endocrinol Metab*, *315*(5), E1005-e1018. https://doi.org/10.1152/ajpendo.00345.2017

Gillman, M. W. (2005). Developmental origins of health and disease. *N Engl J Med*, *353*(17), 1848-1850. https://doi.org/10.1056/NEJMe058187

Gimpfl, M., Rozman, J., Dahlhoff, M., Kubeck, R., Blutke, A., Rathkolb, B., Klingenspor, M., Hrabe de Angelis, M., Oner-Sieben, S., Seibt, A., Roscher, A. A., Wolf, E., & Ensenauer, R. (2017). Modification of the fatty acid composition of an obesogenic diet improves the maternal and placental metabolic environment in obese pregnant mice. *Biochim Biophys Acta Mol Basis Dis*, *1863*(6), 1605-1614, Article Journal Article Research Support, Non-U.S. Gov't Journal Article Research Support, Non-U.S. Gov't. https://doi.org/10.1016/j.bbadis.2017.02.021

Gomes, D., Le, L., Perschbacher, S., Haas, N. A., Netz, H., Hasbargen, U., Delius, M., Lange, K., Nennstiel, U., Roscher, A. A., Mansmann, U., & Ensenauer, R. (2022). Predicting the earliest deviation in weight gain in the course towards manifest overweight in offspring exposed to obesity in pregnancy: a longitudinal cohort study. *BMC Med*, *20*(1), 156. https://doi.org/10.1186/s12916-022-02318-z

Gomes, D., von Kries, R., Delius, M., Mansmann, U., Nast, M., Stubert, M., Langhammer, L., Haas, N. A., Netz, H., Obermeier, V., Kuhle, S., Holdt, L. M., Teupser, D., Hasbargen, U., Roscher, A. A., & Ensenauer, R. (2018). Late-pregnancy dysglycemia in obese pregnancies after negative testing for gestational diabetes and risk of future childhood overweight: An interim analysis from

a longitudinal mother-child cohort study. *PLoS Med*, *15*(10), e1002681. https://doi.org/10.1371/journal.pmed.1002681

Green, H., & Kehinde, O. (1974). Sublines of mouse 3T3 cells that accumulate lipid. *Cell*, *1*(3), 113-116. https://doi.org/10.1016/0092-8674(74)90126-3

Griffiths, S. K., & Campbell, J. P. (2014). Placental structure, function and drug transfer. *Continuing Education in Anaesthesia Critical Care & Pain*, *15*(2), 84-89. https://doi.org/10.1093/bjaceaccp/mku013

Hallberg, M., Morganstein, D. L., Kiskinis, E., Shah, K., Kralli, A., Dilworth, S. M., White, R., Parker, M. G., & Christian, M. (2008). A functional interaction between RIP140 and PGC-1alpha regulates the expression of the lipid droplet protein CIDEA. *Mol Cell Biol*, *28*(22), 6785-6795. https://doi.org/10.1128/MCB.00504-08

Hellemans, J., Mortier, G., De Paepe, A., Speleman, F., & Vandesompele, J. (2007). qBase relative quantification framework and software for management and automated analysis of real-time quantitative PCR data. *Genome Biol*, *8*(2), R19. https://doi.org/10.1186/gb-2007-8-2-r19

Heni, M. (2024). The insulin resistant brain: impact on whole-body metabolism and body fat distribution. *Diabetologia*. https://doi.org/10.1007/s00125-024-06104-9

Heslehurst, N., Vieira, R., Akhter, Z., Bailey, H., Slack, E., Ngongalah, L., Pemu, A., & Rankin, J. (2019). The association between maternal body mass index and child obesity: A systematic review and meta-analysis. *PLoS Med*, *16*(6), e1002817. https://doi.org/10.1371/journal.pmed.1002817

Hieronimus, B., & Ensenauer, R. (2021). Influence of maternal and paternal pre-conception overweight/obesity on offspring outcomes and strategies for prevention. *Eur J Clin Nutr*, *75*(12), 1735-1744. https://doi.org/10.1038/s41430-021-00920-7

Hsieh, J., Koseki, M., Molusky, M. M., Yakushiji, E., Ichi, I., Westerterp, M., Iqbal, J., Chan, R. B., Abramowicz, S., Tascau, L., Takiguchi, S., Yamashita, S., Welch, C. L., Di Paolo, G., Hussain, M. M., Lefkowitch, J. H., Rader, D. J., & Tall, A. R. (2016). TTC39B deficiency stabilizes LXR reducing both atherosclerosis and steatohepatitis. *Nature*, *535*(7611), 303-307. https://doi.org/10.1038/nature18628

Hsu, L. C., Chang, W. C., Hoffmann, I., & Duester, G. (1999). Molecular analysis of two closely related mouse aldehyde dehydrogenase genes: identification of a role for Aldh1, but not Aldh-pb, in the biosynthesis of retinoic acid. *Biochem J*, *339 (Pt 2)*(Pt 2), 387-395. https://www.ncbi.nlm.nih.gov/pubmed/10191271

Hu, Z., Tylavsky, F. A., Han, J. C., Kocak, M., Fowke, J. H., Davis, R. L., Lewinn, K., Bush, N. R., & Zhao, Q. (2019). Maternal metabolic factors during pregnancy predict early childhood growth trajectories and obesity risk: the CANDLE Study. *International Journal of Obesity*, *43*(10), 1914-1922. https://doi.org/10.1038/s41366-019-0326-z

Huang, H., Song, T. J., Li, X., Hu, L., He, Q., Liu, M., Lane, M. D., & Tang, Q. Q. (2009). BMP signaling pathway is required for commitment of C3H10T1/2 pluripotent stem cells to the adipocyte lineage. *Proc Natl Acad Sci U S A*, *106*(31), 12670-12675. https://doi.org/10.1073/pnas.0906266106

Hwang, H. H., Moon, P. G., Lee, J. E., Kim, J. G., Lee, W., Ryu, S. H., & Baek, M. C. (2011). Identification of the target proteins of rosiglitazone in 3T3-L1 adipocytes through proteomic analysis of cytosolic and secreted proteins. *Mol Cells*, *31*(3), 239-246. https://doi.org/10.1007/s10059-011-0026-6

International Diabetes Federation, I. (2021). *IDF Diabetes Atlas, 10th edn.*

IQTIG. (2023). *Bundesauswertung zum Erfassungsjahr 2022 Perinatalmedizin: Geburtshilfe*.

Jackson, B. C., Thompson, D. C., Charkoftaki, G., & Vasiliou, V. (2015). Dead enzymes in the aldehyde dehydrogenase gene family: role in drug metabolism and toxicology. *Expert Opin Drug Metab Toxicol*, *11*(12), 1839-1847. https://doi.org/10.1517/17425255.2016.1108406

Jackson, R. M., Griesel, B. A., Gurley, J. M., Szweda, L. I., & Olson, A. L. (2017). Glucose availability controls adipogenesis in mouse 3T3-L1 adipocytes via up-regulation of nicotinamide metabolism. *J Biol Chem*, *292*(45), 18556-18564. https://doi.org/10.1074/jbc.M117.791970

Jais, A., & Brüning, J. C. (2022). Arcuate Nucleus-Dependent Regulation of Metabolism-Pathways to Obesity and Diabetes Mellitus. *Endocr Rev*, *43*(2), 314-328. https://doi.org/10.1210/endrev/bnab025

Jastreboff, A. M., Aronne, L. J., Ahmad, N. N., Wharton, S., Connery, L., Alves, B., Kiyosue, A., Zhang, S., Liu, B., Bunck, M. C., & Stefanski, A. (2022). Tirzepatide Once Weekly for the Treatment of Obesity. *N Engl J Med*, *387*(3), 205-216. https://doi.org/10.1056/NEJMoa2206038

Jastreboff, A. M., Kaplan, L. M., Frías, J. P., Wu, Q., Du, Y., Gurbuz, S., Coskun, T., Haupt, A., Milicevic, Z., & Hartman, M. L. (2023). Triple-Hormone-Receptor Agonist Retatrutide for Obesity - A Phase 2 Trial. *N Engl J Med*, *389*(6), 514-526. https://doi.org/10.1056/NEJMoa2301972

Jiang, Y., Berry, D. C., Tang, W., & Graff, J. M. (2014). Independent stem cell lineages regulate adipose organogenesis and adipose homeostasis. *Cell reports*, *9*(3), 1007-1022. https://doi.org/10.1016/j.celrep.2014.09.049

Joseph, S. B., Laffitte, B. A., Patel, P. H., Watson, M. A., Matsukuma, K. E., Walczak, R., Collins, J. L., Osborne, T. F., & Tontonoz, P. (2002). Direct and indirect mechanisms for regulation of fatty acid synthase gene expression by liver X receptors. *J Biol Chem*, *277*(13), 11019-11025. https://doi.org/10.1074/jbc.M111041200

Kajimoto, K., Takayanagi, S., Sasaki, S., Akita, H., & Harashima, H. (2012). RNA interference-based silencing reveals the regulatory role of fatty acid-binding protein 4 in the production of IL-6 and vascular endothelial growth factor in 3T3-L1 adipocytes. *Endocrinology*, *153*(11), 5629-5636. https://doi.org/10.1210/en.2012-1456

Kathmann, E. C., Naylor, S., & Lipsky, J. J. (2000). Rat liver constitutive and phenobarbital-inducible cytosolic aldehyde dehydrogenases are highly homologous proteins that function as distinct isozymes. *Biochemistry*, *39*(36), 11170-11176. https://doi.org/10.1021/bi001120m

Kaur, Y., de Souza, R. J., Gibson, W. T., & Meyre, D. (2017). A systematic review of genetic syndromes with obesity. *Obesity reviews : an official journal of the International Association for the Study of Obesity*, *18*(6), 603-634. https://doi.org/10.1111/obr.12531

Kawai, T., Autieri, M. V., & Scalia, R. (2021). Adipose tissue inflammation and metabolic dysfunction in obesity. *American journal of physiology. Cell physiology*, *320*(3), C375-C391. https://doi.org/10.1152/ajpcell.00379.2020

Keating, M. F., Drew, B. G., & Calkin, A. C. (2022). Antisense Oligonucleotide Technologies to Combat Obesity and Fatty Liver Disease. *Front Physiol*, *13*, 839471. https://doi.org/10.3389/fphys.2022.839471

Kelly, A. C., F, J. R., Chan, J., Cox, L. A., Powell, T. L., & Jansson, T. (2022). Transcriptomic responses are sex-dependent in the skeletal muscle and liver in offspring of obese mice. *Am J Physiol Endocrinol Metab*, *323*(4), E336-E353. https://doi.org/10.1152/ajpendo.00263.2021

Kheniser, K., Saxon, D. R., & Kashyap, S. R. (2021). Long-Term Weight Loss Strategies for Obesity. *J Clin Endocrinol Metab*, *106*(7), 1854-1866. https://doi.org/10.1210/clinem/dgab091

Kim, W., & Kyung Lee, E. (2012). Post-transcriptional regulation in metabolic diseases. *RNA Biology*, *9*(6), 772-780. https://doi.org/10.4161/rna.20091

Klasson, T. D., LaGory, E. L., Zhao, H., Huynh, S. K., Papandreou, I., Moon, E. J., & Giaccia, A. J. (2022). ACSL3 regulates lipid droplet biogenesis and ferroptosis sensitivity in clear cell renal cell carcinoma. *Cancer Metab*, *10*(1), 14. https://doi.org/10.1186/s40170-022-00290-z

Koch, C. M., Chiu, S. F., Akbarpour, M., Bharat, A., Ridge, K. M., Bartom, E. T., & Winter, D. R. (2018). A Beginner's Guide to Analysis of RNA Sequencing Data. *Am J Respir Cell Mol Biol*, *59*(2), 145-157. https://doi.org/10.1165/rcmb.2017-0430TR

Könner, A. C., Janoschek, R., Plum, L., Jordan, S. D., Rother, E., Ma, X., Xu, C., Enriori, P., Hampel, B., Barsh, G. S., Kahn, C. R., Cowley, M. A., Ashcroft, F. M., & Brüning, J. C. (2007). Insulin action in AgRP-expressing neurons is required for suppression of hepatic glucose production. *Cell Metab*, *5*(6), 438-449. https://doi.org/10.1016/j.cmet.2007.05.004

Krishna, M. S., Aneesh Kumar, A., & Abdul Jaleel, K. A. (2018). Time-dependent alterations in mRNA, protein and microRNA during in vitro adipogenesis. *Mol Cell Biochem*, *448*(1-2), 1-8. https://doi.org/10.1007/s11010-018-3307-y

Krueger, F. (2010). *Trim Galore!*

Krueger, F., & Andrews, S. R. (2011). Bismark: a flexible aligner and methylation caller for Bisulfite-Seq applications. *Bioinformatics*, *27*(11), 1571-1572. https://doi.org/10.1093/bioinformatics/btr167

Kubota, M., Yamamoto, K., & Yoshiyama, S. (2023). Effect on Hemoglobin A1c (HbA1c) and Body Weight After Discontinuation of Tirzepatide, a Novel Glucose-Dependent Insulinotropic Peptide (GIP) and Glucagon-Like Peptide-1 (GLP-1) Receptor Agonist: A Single-Center Case Series Study. *Cureus*, *15*(10), e46490. https://doi.org/10.7759/cureus.46490

Kuntz, B., Zeiher, J., Starker, A., Prütz, F., & Lampert, T. (2018). Rauchen in der Schwangerschaft – Querschnittergebnisse aus KiGGS Welle 2 und Trends. In (Vol. 3): Robert Koch-Institut, Epidemiologie und Gesundheitsberichterstattung.

Kusunoki, J., Kanatani, A., & Moller, D. E. (2006). Modulation of fatty acid metabolism as a potential approach to the treatment of obesity and the metabolic syndrome. *Endocrine*, *29*(1), 91-100. https://doi.org/10.1385/ENDO:29:1:91

Lahti-Pulkkinen, M., Bhattacharya, S., Wild, S. H., Lindsay, R. S., Raikkonen, K., Norman, J. E., Bhattacharya, S., & Reynolds, R. M. (2019). Consequences of being overweight or obese during pregnancy on diabetes in the offspring: a record linkage study in Aberdeen, Scotland. *Diabetologia*, *62*(8), 1412-1419. https://doi.org/10.1007/s00125-019-4891-4

Langenberg, C., Sharp, S. J., Franks, P. W., Scott, R. A., Deloukas, P., Forouhi, N. G., Froguel, P., Groop, L. C., Hansen, T., Palla, L., Pedersen, O., Schulze, M. B., Tormo, M.-J., Wheeler, E., Agnoli, C., Arriola, L., Barricarte, A., Boeing, H., Clarke, G. M., . . . Wareham, N. J. (2014). Gene-Lifestyle Interaction and Type 2 Diabetes: The EPIC InterAct Case-Cohort Study. *PLoS medicine*, *11*(5), e1001647. https://doi.org/10.1371/journal.pmed.1001647

Laurencikiene, J., & Ryden, M. (2012). Liver X receptors and fat cell metabolism. *Int J Obes (Lond)*, *36*(12), 1494-1502. https://doi.org/10.1038/ijo.2012.21

Lavebratt, C., Almgren, M., & Ekstrom, T. J. (2012). Epigenetic regulation in obesity. *Int J Obes (Lond)*, *36*(6), 757-765. https://doi.org/10.1038/ijo.2011.178

Laviola, L., Perrini, S., Cignarelli, A., & Giorgino, F. (2006). Insulin signalling in human adipose tissue. *Archives of Physiology and Biochemistry*, *112*(2), 82-88. https://doi.org/10.1080/13813450600736174

Le Moullec, N., Fianu, A., Maillard, O., Chazelle, E., Naty, N., Schneebeli, C., Gérardin, P., Huiart, L., Charles, M. A., & Favier, F. (2018). Sexual dimorphism in the association between gestational diabetes mellitus and overweight in offspring at 5-7 years: The OBEGEST cohort study. *PloS one*, *13*(4), e0195531. https://doi.org/10.1371/journal.pone.0195531

Lecoutre, S., Maqdasy, S., Lambert, M., & Breton, C. (2023). The Impact of Maternal Obesity on Adipose Progenitor Cells. *Biomedicines*, *11*(12). https://doi.org/10.3390/biomedicines11123252

Leon-Garcia, S. M., Roeder, H. A., Nelson, K. K., Liao, X., Pizzo, D. P., Laurent, L. C., Parast, M. M., & LaCoursiere, D. Y. (2016). Maternal obesity and sex-specific differences in placental pathology. *Placenta*, *38*, 33-40. https://doi.org/10.1016/j.placenta.2015.12.006

Li, G., Li, X., Yang, L., Wang, S., Dai, Y., Fekry, B., Veillon, L., Tan, L., Berdeaux, R., Eckel-Mahan, K., Lorenzi, P. L., Zhao, Z., Lehner, R., & Sun, K. (2022). Adipose tissue-specific ablation of Ces1d causes metabolic dysregulation in mice. *Life Sci Alliance*, *5*(8). https://doi.org/10.26508/lsa.202101209

Li, S., Zhu, Y., Yeung, E., Chavarro, J. E., Yuan, C., Field, A. E., Missmer, S. A., Mills, J. L., Hu, F. B., & Zhang, C. (2017). Offspring risk of obesity in childhood, adolescence and adulthood in relation to gestational diabetes mellitus: a sex-specific association. *Int J Epidemiol*, *46*(5), 1533-1541. https://doi.org/10.1093/ije/dyx151

Liu, P., Li, G., Wu, J., Zhou, X., Wang, L., Han, W., Lv, Y., & Sun, C. (2015). Vaspin promotes 3T3-L1 preadipocyte differentiation. *Exp Biol Med (Maywood)*, *240*(11), 1520-1527. https://doi.org/10.1177/1535370214565081

Liu, X., Liu, J., Lester, J. D., Pijut, S. S., & Graf, G. A. (2015). ABCD2 identifies a subclass of peroxisomes in mouse adipose tissue. *Biochemical and Biophysical Research Communications*, *456*(1), 129-134. https://doi.org/https://doi.org/10.1016/j.bbrc.2014.11.046

Loos, R. J. F., & Yeo, G. S. H. (2022). The genetics of obesity: from discovery to biology. *Nat Rev Genet*, *23*(2), 120-133. https://doi.org/10.1038/s41576-021-00414-z

Lu, S., Mott, J. L., & Harrison-Findik, D. D. (2015). Saturated Fatty Acids Induce Post-transcriptional Regulation of HAMP mRNA via AU-rich Element-binding Protein, Human Antigen R (HuR)*. *Journal of Biological Chemistry*, *290*(40), 24178-24189. https://doi.org/https://doi.org/10.1074/jbc.M115.648212

MacLennan, N. K., James, S. J., Melnyk, S., Piroozi, A., Jernigan, S., Hsu, J. L., Janke, S. M., Pham, T. D., & Lane, R. H. (2004). Uteroplacental insufficiency alters DNA methylation, one-carbon metabolism, and histone acetylation in IUGR rats. *Physiol Genomics*, *18*(1), 43-50. https://doi.org/10.1152/physiolgenomics.00042.2004

Maekawa, T., Jin, W., & Ishii, S. (2010). The role of ATF-2 family transcription factors in adipocyte differentiation: antiobesity effects of p38 inhibitors. *Mol Cell Biol*, *30*(3), 613-625. https://doi.org/10.1128/MCB.00685-09

Mannino, A., Sarapis, K., & Moschonis, G. (2022). The Effect of Maternal Overweight and Obesity Pre-Pregnancy and During Childhood in the Development of Obesity in Children and Adolescents: A Systematic Literature Review. *Nutrients*, *14*(23). https://doi.org/10.3390/nu14235125

Maples, J. M., Brault, J. J., Witczak, C. A., Park, S., Hubal, M. J., Weber, T. M., Houmard, J. A., & Shewchuk, B. M. (2015). Differential epigenetic and transcriptional response of the skeletal muscle carnitine palmitoyltransferase 1B (CPT1B) gene to lipid exposure with obesity. *Am J Physiol Endocrinol Metab*, *309*(4), E345-356. https://doi.org/10.1152/ajpendo.00505.2014

Masuyama, H., & Hiramatsu, Y. (2012). Effects of a High-Fat Diet Exposure in Utero on the Metabolic Syndrome-Like Phenomenon in Mouse Offspring through Epigenetic Changes in Adipocytokine Gene Expression. *Endocrinology*, *153*(6), 2823-2830. https://doi.org/10.1210/en.2011-2161

Matikainen-Ankney, B. A., & Kravitz, A. V. (2018). Persistent effects of obesity: a neuroplasticity hypothesis. *Ann N Y Acad Sci*, *1428*(1), 221-239. https://doi.org/10.1111/nyas.13665

Méndez-Mancilla, A., Lima-Rogel, V., Toro-Ortíz, J. C., Escalante-Padrón, F., Monsiváis-Urenda, A. E., Noyola, D. E., & Salgado-Bustamante, M. (2018). Differential expression profiles of circulating microRNAs in newborns associated to maternal pregestational overweight and obesity. *Pediatr Obes*, *13*(3), 168-174. https://doi.org/10.1111/ijpo.12247

Monthe-Dreze, C., Penfield-Cyr, A., Smid, M. C., & Sen, S. (2018). Maternal Pre-Pregnancy Obesity Attenuates Response to Omega-3 Fatty Acids Supplementation During Pregnancy. *Nutrients*, *10*(12), 1908. https://doi.org/10.3390/nu10121908

Moseti, D., Regassa, A., & Kim, W. K. (2016). Molecular Regulation of Adipogenesis and Potential Anti-Adipogenic Bioactive Molecules. *Int J Mol Sci*, *17*(1). https://doi.org/10.3390/ijms17010124

Mota de Sa, P., Richard, A. J., Hang, H., & Stephens, J. M. (2017). Transcriptional Regulation of Adipogenesis. *Compr Physiol*, *7*(2), 635-674. https://doi.org/10.1002/cphy.c160022

Müller, T. D., Finan, B., Bloom, S. R., D'Alessio, D., Drucker, D. J., Flatt, P. R., Fritsche, A., Gribble, F., Grill, H. J., Habener, J. F., Holst, J. J., Langhans, W., Meier, J. J., Nauck, M. A., Perez-Tilve, D., Pocai, A., Reimann, F., Sandoval, D. A., Schwartz, T. W., . . . Tschöp, M. H. (2019). Glucagon-like peptide 1 (GLP-1). *Mol Metab*, *30*, 72-130. https://doi.org/10.1016/j.molmet.2019.09.010

Muthu, M. L., Tiedemann, K., Fradette, J., Komarova, S., & Reinhardt, D. P. (2022). Fibrillin-1 regulates white adipose tissue development, homeostasis, and function. *Matrix Biol*, *110*, 106-128. https://doi.org/10.1016/j.matbio.2022.05.002

Nallamshetty, S., Wang, H., Rhee, E. J., Kiefer, F. W., Brown, J. D., Lotinun, S., Le, P., Baron, R., Rosen, C. J., & Plutzky, J. (2013). Deficiency of retinaldehyde dehydrogenase 1 induces BMP2 and increases bone mass in vivo. *PloS one*, *8*(8), e71307. https://doi.org/10.1371/journal.pone.0071307

Narayan, K. M., Boyle, J. P., Thompson, T. J., Gregg, E. W., & Williamson, D. F. (2007). Effect of BMI on lifetime risk for diabetes in the U.S. *Diabetes Care*, *30*(6), 1562-1566. https://doi.org/10.2337/dc06-2544

National Research Council, N. (2009). *Weight Gain During Pregnancy: Reexaming the Guidelines*. National Academies Press (US), Copyright © 2009, National Academy of Sciences. https://doi.org/10.17226/12584

Navarro, G., Allard, C., Xu, W., & Mauvais-Jarvis, F. (2015). The role of androgens in metabolism, obesity, and diabetes in males and females. *Obesity*, *23*(4), 713-719. https://doi.org/https://doi.org/10.1002/oby.21033

Nehring, I., Chmitorz, A., Reulen, H., von Kries, R., & Ensenauer, R. (2013). Gestational diabetes predicts the risk of childhood overweight and abdominal circumference independent of maternal obesity. *Diabet Med*, *30*(12), 1449-1456. https://doi.org/10.1111/dme.12286

Niculescu, M. D., Lupu, D. S., & Craciunescu, C. N. (2013). Perinatal manipulation of α-linolenic acid intake induces epigenetic changes in maternal and offspring livers. *FASEB J*, *27*(1), 350-358. https://doi.org/10.1096/fj.12-210724

Nowotny, B., Zahiragic, L., Krog, D., Nowotny, P. J., Herder, C., Carstensen, M., Yoshimura, T., Szendroedi, J., Phielix, E., Schadewaldt, P., Schloot, N. C., Shulman, G. I., & Roden, M. (2013). Mechanisms underlying the onset of oral lipid-induced skeletal muscle insulin resistance in humans. *Diabetes*, *62*(7), 2240-2248. https://doi.org/10.2337/db12-1179

O'Brien, P. E., Hindle, A., Brennan, L., Skinner, S., Burton, P., Smith, A., Crosthwaite, G., & Brown, W. (2019). Long-Term Outcomes After Bariatric Surgery: a Systematic Review and Meta-analysis of Weight Loss at 10 or More Years for All Bariatric Procedures and a Single-Centre Review of 20-Year Outcomes After Adjustable Gastric Banding. *Obes Surg*, *29*(1), 3-14. https://doi.org/10.1007/s11695-018-3525-0

Palhinha, L., Liechocki, S., Hottz, E. D., Pereira, J., de Almeida, C. J., Moraes-Vieira, P. M. M., Bozza, P. T., & Maya-Monteiro, C. M. (2019). Leptin Induces Proadipogenic and Proinflammatory Signaling in Adipocytes. *Front Endocrinol (Lausanne)*, *10*, 841. https://doi.org/10.3389/fendo.2019.00841

Parpal, S., Karlsson, M., Thorn, H., & Strålfors, P. (2001). Cholesterol depletion disrupts caveolae and insulin receptor signaling for metabolic control via insulin receptor substrate-1, but not for mitogen-activated protein kinase control. *J Biol Chem*, *276*(13), 9670-9678. https://doi.org/10.1074/jbc.M007454200

Patro Golab, B., Santos, S., Voerman, E., Lawlor, D. A., Jaddoe, V. W. V., & Gaillard, R. (2018). Influence of maternal obesity on the association between common pregnancy complications and risk of childhood obesity: an individual participant data meta-analysis. *Lancet Child Adolesc Health*, *2*(11), 812-821. https://doi.org/10.1016/s2352-4642(18)30273-6

Payne, V. A., Au, W. S., Lowe, C. E., Rahman, S. M., Friedman, J. E., O'Rahilly, S., & Rochford, J. J. (2009). C/EBP transcription factors regulate SREBP1c gene expression during adipogenesis. *Biochem J*, *425*(1), 215-223. https://doi.org/10.1042/BJ20091112

Pereira, F., Rosenmann, E., Nylen, E., Kaufman, M., Pinsky, L., & Wrogemann, K. (1991). The 56 kDa androgen binding protein is an aldehyde dehydrogenase. *Biochem Biophys Res Commun*, *175*(3), 831-838. https://doi.org/10.1016/0006-291x(91)91640-x

Perschbacher, S., Eckel, N., Gomes, D., & Ensenauer, R. (2022). Mütterliche Adipositas und langfristige Auswirkungen auf die Nachkommen. In A. Strauss & C. Strauss (Eds.), *Praxisbuch Adipositas in der Geburtshilfe* (pp. 277-295). Springer Berlin Heidelberg. https://doi.org/10.1007/978-3-662-61906-3_15

Phelps, N. H., Singleton, R. K., Zhou, B., Heap, R. A., Mishra, A., Bennett, J. E., Paciorek, C. J., Lhoste, V. P. F., Carrillo-Larco, R. M., Stevens, G. A., Rodriguez-Martinez, A., Bixby, H., Bentham, J., Di Cesare, M., Danaei, G., Rayner, A. W., Barradas-Pires, A., Cowan, M. J., Savin, S., . . . Ezzati, M. (2024). Worldwide trends in underweight and obesity from 1990 to 2022: a pooled analysis of 3663 population-representative studies with 222 million children, adolescents, and adults. *The Lancet*. https://doi.org/https://doi.org/10.1016/S0140-6736(23)02750-2

Poudyal, H., & Brown, L. (2011). Stearoyl-CoA desaturase: a vital checkpoint in the development and progression of obesity. *Endocr Metab Immune Disord Drug Targets*, *11*(3), 217-231. https://doi.org/10.2174/187153011796429826

Puigserver, P., Wu, Z., Park, C. W., Graves, R., Wright, M., & Spiegelman, B. M. (1998). A cold-inducible coactivator of nuclear receptors linked to adaptive thermogenesis. *Cell*, *92*(6), 829-839. https://doi.org/10.1016/s0092-8674(00)81410-5

Puri, V., Ranjit, S., Konda, S., Nicoloro, S. M., Straubhaar, J., Chawla, A., Chouinard, M., Lin, C., Burkart, A., Corvera, S., Perugini, R. A., & Czech, M. P. (2008). Cidea is associated with lipid droplets and insulin sensitivity in humans. *Proc Natl Acad Sci U S A*, *105*(22), 7833-7838. https://doi.org/10.1073/pnas.0802063105

Qin, S., Tang, X., Chen, Y., Chen, K., Fan, N., Xiao, W., Zheng, Q., Li, G., Teng, Y., Wu, M., & Song, X. (2022). mRNA-based therapeutics: powerful and versatile tools to combat diseases. *Signal Transduction and Targeted Therapy*, *7*(1), 166. https://doi.org/10.1038/s41392-022-01007-w

Rahib, L., MacLennan, N. K., Horvath, S., Liao, J. C., & Dipple, K. M. (2007). Glycerol kinase deficiency alters expression of genes involved in lipid metabolism, carbohydrate metabolism, and insulin signaling. *Eur J Hum Genet*, *15*(6), 646-657. https://doi.org/10.1038/sj.ejhg.5201801

Ranadive, S. A., & Vaisse, C. (2008). Lessons from extreme human obesity: monogenic disorders. *Endocrinol Metab Clin North Am*, *37*(3), 733-751, x. https://doi.org/10.1016/j.ecl.2008.07.003

Reichert, B., Yasmeen, R., Jeyakumar, S. M., Yang, F., Thomou, T., Alder, H., Duester, G., Maiseyeu, A., Mihai, G., Harrison, E. H., Rajagopalan, S., Kirkland, J. L., & Ziouzenkova, O. (2011). Concerted action of aldehyde dehydrogenases influences depot-specific fat formation. *Mol Endocrinol*, *25*(5), 799-809. https://doi.org/10.1210/me.2010-0465

Reitzle, L., Schmidt, C., Heidemann, C., Icks, A., Kaltheuner, M., Ziese, T., & Scheidt-Nave, C. (2021). Gestational diabetes in Germany: Development of screening participation and prevalence. *J Health Monit*, *6*(2), 3-18. https://doi.org/10.25646/8325

Riedel, C., von Kries, R., Buyken, A. E., Diethelm, K., Keil, T., Grabenhenrich, L., Müller, M. J., & Plachta-Danielzik, S. (2014). Overweight in adolescence can be predicted at age 6 years: a CART analysis in German cohorts. *PloS one*, *9*(3), e93581. https://doi.org/10.1371/journal.pone.0093581

Romero-Calvo, I., Ocon, B., Martinez-Moya, P., Suarez, M. D., Zarzuelo, A., Martinez-Augustin, O., & de Medina, F. S. (2010). Reversible Ponceau staining as a loading control alternative to actin in Western blots. *Anal Biochem*, *401*(2), 318-320. https://doi.org/10.1016/j.ab.2010.02.036

Rosenbauer, J., Neu, A., Rothe, U., Seufert, J., & Holl, R. W. (2019). Diabetestypen sind nicht auf Altersgruppen beschränkt: Typ-1-Diabetes bei Erwachsenen und Typ-2-Diabetes bei Kindern und Jugendlichen. *Journal of Health Monitoring*, *4*(2), 31--53. https://doi.org/http://dx.doi.org/10.25646/5981

Rosenfeld, C. S. (2015). Sex-Specific Placental Responses in Fetal Development. *Endocrinology*, *156*(10), 3422-3434. https://doi.org/10.1210/en.2015-1227

Ruijter, J. M., Ramakers, C., Hoogaars, W. M., Karlen, Y., Bakker, O., van den Hoff, M. J., & Moorman, A. F. (2009). Amplification efficiency: linking baseline and bias in the analysis of quantitative PCR data. *Nucleic Acids Res*, *37*(6), e45. https://doi.org/10.1093/nar/gkp045

Şanlı, E., & Kabaran, S. (2019). Maternal Obesity, Maternal Overnutrition and Fetal Programming: Effects of Epigenetic Mechanisms on the Development of Metabolic Disorders. *Curr Genomics*, *20*(6), 419-427. https://doi.org/10.2174/1389202920666191030092225

Satokar, V. V., Derraik, J. G. B., Harwood, M., Okesene-Gafa, K., Beck, K., Cameron-Smith, D., Garg, M. L., O'Sullivan, J. M., Sundborn, G., Pundir, S., Mason, R. P., Cutfield, W. S., & Albert, B. B. (2023). Fish oil supplementation during pregnancy and postpartum in mothers with overweight and obesity to improve body composition and metabolic health during infancy: A double-blind randomized controlled trial. *Am J Clin Nutr*, *117*(5), 883-895. https://doi.org/10.1016/j.ajcnut.2023.02.007

Savva, C., Helguero, L. A., Gonzalez-Granillo, M., Couto, D., Melo, T., Li, X., Angelin, B., Domingues, M. R., Kutter, C., & Korach-Andre, M. (2021). Obese mother offspring have hepatic lipidic modulation that contributes to sex-dependent metabolic adaptation later in life. *Commun Biol*, *4*(1), 14. https://doi.org/10.1038/s42003-020-01513-z

Savva, C., Helguero, L. A., Gonzalez-Granillo, M., Melo, T., Couto, D., Buyandelger, B., Gustafsson, S., Liu, J., Domingues, M. R., Li, X., & Korach-Andre, M. (2022). Maternal high-fat diet programs white and brown adipose tissue lipidome and transcriptome in offspring in a sex- and tissue-dependent manner in mice. *Int J Obes (Lond)*, *46*(4), 831-842. https://doi.org/10.1038/s41366-021-01060-5

Scheidl, T. B., Brightwell, A. L., Easson, S. H., & Thompson, J. A. (2023). Maternal obesity and programming of metabolic syndrome in the offspring: searching for mechanisms in the adipocyte progenitor pool. *BMC Med*, *21*(1), 50. https://doi.org/10.1186/s12916-023-02730-z

Schmitz, G., Heimerl, S., & Langmann, T. (2004). Zinc finger protein ZNF202 structure and function in transcriptional control of HDL metabolism. *Curr Opin Lipidol*, *15*(2), 199-208. https://doi.org/10.1097/00041433-200404000-00013

Scholtens, D. M., Kuang, A., Lowe, L. P., Hamilton, J., Lawrence, J. M., Lebenthal, Y., Brickman, W. J., Clayton, P., Ma, R. C., McCance, D., Tam, W. H., Catalano, P. M., Linder, B., Dyer, A. R., Lowe, W. L., Jr., & Metzger, B. E. (2019). Hyperglycemia and Adverse Pregnancy Outcome Follow-up Study (HAPO FUS): Maternal Glycemia and Childhood Glucose Metabolism. *Diabetes Care*, *42*(3), 381-392. https://doi.org/10.2337/dc18-2021

Schoonejans, J. M., Blackmore, H. L., Ashmore, T. J., Pantaleao, L. C., Pellegrini Pisani, L., Dearden, L., Tadross, J. A., Aiken, C. E., Fernandez-Twinn, D. S., & Ozanne, S. E. (2022). Sex-specific effects of maternal metformin intervention during glucose-intolerant obese pregnancy on body composition and metabolic health in aged mouse offspring. *Diabetologia*, *65*(12), 2132-2145. https://doi.org/10.1007/s00125-022-05789-0

Schoonejans, J. M., & Ozanne, S. E. (2021). Developmental programming by maternal obesity: Lessons from animal models. *Diabet Med*, *38*(12), e14694. https://doi.org/10.1111/dme.14694

Schulman, A. R., & Thompson, C. C. (2017). Complications of Bariatric Surgery: What You Can Expect to See in Your GI Practice. *The American Journal of Gastroenterology*, *112*(11), 1640-1655. https://doi.org/https://doi.org/10.1038/ajg.2017.241

Secco, B., Camire, E., Briere, M. A., Caron, A., Billong, A., Gelinas, Y., Lemay, A. M., Tharp, K. M., Lee, P. L., Gobeil, S., Guimond, J. V., Patey, N., Guertin, D. A., Stahl, A., Haddad, E., Marsolais, D., Bosse, Y., Birsoy, K., & Laplante, M. (2017). Amplification of Adipogenic Commitment by VSTM2A. *Cell reports*, *18*(1), 93-106. https://doi.org/10.1016/j.celrep.2016.12.015

Seneviratne, S. N., & Rajindrajith, S. (2022). Fetal programming of obesity and type 2 diabetes. *World J Diabetes*, *13*(7), 482-497. https://doi.org/10.4239/wjd.v13.i7.482

Simmonds, L. A., Sullivan, T. R., Skubisz, M., Middleton, P. F., Best, K. P., Yelland, L. N., Quinlivan, J., Zhou, S. J., Liu, G., McPhee, A. J., Gibson, R. A., & Makrides, M. (2020). Omega-3 fatty acid supplementation in pregnancy-baseline omega-3 status and early preterm birth: exploratory analysis of a randomised controlled trial. *BJOG*, *127*(8), 975-981. https://doi.org/10.1111/1471-0528.16168

Simmonds, M., Llewellyn, A., Owen, C. G., & Woolacott, N. (2016). Predicting adult obesity from childhood obesity: a systematic review and meta-analysis. *Obesity reviews : an official journal of the International Association for the Study of Obesity*, *17*(2), 95-107. https://doi.org/10.1111/obr.12334

Singhal, P. K., Sassi, S., Lan, L., Au, P., Halvorsen, S. C., Fukumura, D., Jain, R. K., & Seed, B. (2016). Mouse embryonic fibroblasts exhibit extensive developmental and phenotypic diversity. *Proc Natl Acad Sci U S A*, *113*(1), 122-127. https://doi.org/10.1073/pnas.1522401112

Sley, E. G., Rosen, E. M., van 't Erve, T. J., Sathyanarayana, S., Barrett, E. S., Nguyen, R. H. N., Bush, N. R., Milne, G. L., Swan, S. H., & Ferguson, K. K. (2020). Omega-3 fatty acid supplement use and oxidative stress levels in pregnancy. *PloS one*, *15*(10), e0240244. https://doi.org/10.1371/journal.pone.0240244

Smemo, S., Tena, J. J., Kim, K. H., Gamazon, E. R., Sakabe, N. J., Gómez-Marín, C., Aneas, I., Credidio, F. L., Sobreira, D. R., Wasserman, N. F., Lee, J. H., Puviindran, V., Tam, D., Shen, M., Son, J. E., Vakili, N. A., Sung, H. K., Naranjo, S., Acemel, R. D., . . . Nóbrega, M. A. (2014).

Obesity-associated variants within FTO form long-range functional connections with IRX3. *Nature*, *507*(7492), 371-375. https://doi.org/10.1038/nature13138

Smith, J., Cianflone, K., Biron, S., Hould, F. S., Lebel, S., Marceau, S., Lescelleur, O., Biertho, L., Simard, S., Kral, J. G., & Marceau, P. (2009). Effects of Maternal Surgical Weight Loss in Mothers on Intergenerational Transmission of Obesity. *The Journal of Clinical Endocrinology & Metabolism*, *94*(11), 4275-4283. https://doi.org/10.1210/jc.2009-0709

Spiegel, K., Tasali, E., Leproult, R., Scherberg, N., & Van Cauter, E. (2011). Twenty-four-hour profiles of acylated and total ghrelin: relationship with glucose levels and impact of time of day and sleep. *J Clin Endocrinol Metab*, *96*(2), 486-493. https://doi.org/10.1210/jc.2010-1978

Steinert, R. E., Feinle-Bisset, C., Asarian, L., Horowitz, M., Beglinger, C., & Geary, N. (2017). Ghrelin, CCK, GLP-1, and PYY(3–36): Secretory Controls and Physiological Roles in Eating and Glycemia in Health, Obesity, and After RYGB. *Physiol Rev*, *97*(1), 411-463. https://doi.org/10.1152/physrev.00031.2014

Suyama, S., Maekawa, F., Maejima, Y., Kubota, N., Kadowaki, T., & Yada, T. (2016). Glucose level determines excitatory or inhibitory effects of adiponectin on arcuate POMC neuron activity and feeding. *Sci Rep*, *6*, 30796. https://doi.org/10.1038/srep30796

Szendroedi, J., Saxena, A., Weber, K. S., Strassburger, K., Herder, C., Burkart, V., Nowotny, B., Icks, A., Kuss, O., Ziegler, D., Al-Hasani, H., Müssig, K., Roden, M., & The, G. D. S. G. (2016). Cohort profile: the German Diabetes Study (GDS). *Cardiovascular Diabetology*, *15*(1), 59. https://doi.org/10.1186/s12933-016-0374-9

Tanaka-Yachi, R., Shirasaki, M., Otsu, R., Takahashi-Muto, C., Inoue, H., Aoki, Y., Koike, T., & Kiyose, C. (2018). delta-Tocopherol promotes thermogenic gene expression via PGC-1alpha upregulation in 3T3-L1 cells. *Biochem Biophys Res Commun*, *506*(1), 53-59. https://doi.org/10.1016/j.bbrc.2018.10.021

Taylor, R., Barnes, A. C., Hollingsworth, K. G., Irvine, K. M., Solovyova, A. S., Clark, L., Kelly, T., Martin-Ruiz, C., Romeres, D., Koulman, A., Meek, C. M., Jenkins, B., Cobelli, C., & Holman, R. R. (2023). Aetiology of Type 2 diabetes in people with a 'normal' body mass index: testing the personal fat threshold hypothesis. *Clin Sci (Lond)*, *137*(16), 1333-1346. https://doi.org/10.1042/CS20230586

Toschke, A. M., Montgomery, S. M., Pfeiffer, U., & von Kries, R. (2003). Early intrauterine exposure to tobacco-inhaled products and obesity. *Am J Epidemiol*, *158*(11), 1068-1074. https://doi.org/10.1093/aje/kwg258

Tuo, W., Leleu-Chavain, N., Spencer, J., Sansook, S., Millet, R., & Chavatte, P. (2017). Therapeutic Potential of Fatty Acid Amide Hydrolase, Monoacylglycerol Lipase, and N-Acylethanolamine Acid Amidase Inhibitors. *Journal of Medicinal Chemistry*, *60*(1), 4-46. https://doi.org/10.1021/acs.jmedchem.6b00538

Turcot, V., Lu, Y., Highland, H. M., Schurmann, C., Justice, A. E., Fine, R. S., Bradfield, J. P., Esko, T., Giri, A., Graff, M., Guo, X., Hendricks, A. E., Karaderi, T., Lempradl, A., Locke, A. E., Mahajan, A., Marouli, E., Sivapalaratnam, S., Young, K. L., . . . Sattar, N. (2018). Protein-altering variants associated with body mass index implicate pathways that control energy intake and expenditure in obesity. *Nat Genet*, *50*(1), 26-41. https://doi.org/10.1038/s41588-017-0011-x

Vandesompele, J., De Preter, K., Pattyn, F., Poppe, B., Van Roy, N., De Paepe, A., & Speleman, F. (2002). Accurate normalization of real-time quantitative RT-PCR data by geometric averaging of multiple internal control genes. *Genome Biol*, *3*(7), RESEARCH0034. https://doi.org/10.1186/gb-2002-3-7-research0034

Vatner, D. F., Goedeke, L., Camporez, J. G., Lyu, K., Nasiri, A. R., Zhang, D., Bhanot, S., Murray, S. F., Still, C. D., Gerhard, G. S., Shulman, G. I., & Samuel, V. T. (2018). Angptl8 antisense oligonucleotide improves adipose lipid metabolism and prevents diet-induced NAFLD and hepatic insulin resistance in rodents. *Diabetologia*, *61*(6), 1435-1446. https://doi.org/10.1007/s00125-018-4579-1

Veeravalli, S., Omar, B. A., Houseman, L., Hancock, M., Gonzalez Malagon, S. G., Scott, F., Janmohamed, A., Phillips, I. R., & Shephard, E. A. (2014). The phenotype of a flavin-containing monooyxgenase knockout mouse implicates the drug-metabolizing enzyme FMO1 as a novel regulator of energy balance. *Biochem Pharmacol*, *90*(1), 88-95. https://doi.org/10.1016/j.bcp.2014.04.007

Voerman, E., Santos, S., Patro Golab, B., Amiano, P., Ballester, F., Barros, H., Bergström, A., Charles, M. A., Chatzi, L., Chevrier, C., Chrousos, G. P., Corpeleijn, E., Costet, N., Crozier, S., Devereux, G., Eggesbø, M., Ekström, S., Fantini, M. P., Farchi, S., . . . Jaddoe, V. W. V. (2019). Maternal body mass index, gestational weight gain, and the risk of overweight and obesity across childhood: An individual participant data meta-analysis. *PLoS Med*, *16*(2), e1002744. https://doi.org/10.1371/journal.pmed.1002744

von Kries, R., Chmitorz, A., Rasmussen, K. M., Bayer, O., & Ensenauer, R. (2013). Late pregnancy reversal from excessive gestational weight gain lowers risk of childhood overweight--a cohort study. *Obesity (Silver Spring)*, *21*(6), 1232-1237. https://doi.org/10.1002/oby.20197

Wabitsch, M., Brenner, R. E., Melzner, I., Braun, M., Moller, P., Heinze, E., Debatin, K. M., & Hauner, H. (2001). Characterization of a human preadipocyte cell strain with high capacity for adipose differentiation. *Int J Obes Relat Metab Disord*, *25*(1), 8-15. https://doi.org/10.1038/sj.ijo.0801520

Wakil, S. J. (1989). Fatty acid synthase, a proficient multifunctional enzyme. *Biochemistry*, *28*(11), 4523-4530, Article Journal Article Research Support, Non-U.S. Gov't Research Support, U.S. Gov't, P.H.S. Review. https://doi.org/10.1021/bi00437a001

Wang, J., Pan, L., Liu, E., Liu, H., Liu, J., Wang, S., Guo, J., Li, N., Zhang, C., & Hu, G. (2019). Gestational diabetes and offspring's growth from birth to 6 years old. *Int J Obes (Lond)*, *43*(4), 663-672. https://doi.org/10.1038/s41366-018-0193-z

Wang, Q., Liu, C., Uchida, A., Chuang, J. C., Walker, A., Liu, T., Osborne-Lawrence, S., Mason, B. L., Mosher, C., Berglund, E. D., Elmquist, J. K., & Zigman, J. M. (2014). Arcuate AgRP neurons mediate orexigenic and glucoregulatory actions of ghrelin. *Mol Metab*, *3*(1), 64-72. https://doi.org/10.1016/j.molmet.2013.10.001

Waterland, R. A., & Jirtle, R. L. (2004). Early nutrition, epigenetic changes at transposons and imprinted genes, and enhanced susceptibility to adult chronic diseases. *Nutrition*, *20*(1), 63-68. https://doi.org/10.1016/j.nut.2003.09.011

Wilding, J. P. H., Batterham, R. L., Calanna, S., Davies, M., Van Gaal, L. F., Lingvay, I., McGowan, B. M., Rosenstock, J., Tran, M. T. D., Wadden, T. A., Wharton, S., Yokote, K., Zeuthen, N., & Kushner, R. F. (2021). Once-Weekly Semaglutide in Adults with Overweight or Obesity. *N Engl J Med*, *384*(11), 989-1002. https://doi.org/10.1056/NEJMoa2032183

Wilding, J. P. H., Batterham, R. L., Davies, M., Van Gaal, L. F., Kandler, K., Konakli, K., Lingvay, I., McGowan, B. M., Oral, T. K., Rosenstock, J., Wadden, T. A., Wharton, S., Yokote, K., & Kushner, R. F. (2022). Weight regain and cardiometabolic effects after withdrawal of semaglutide: The STEP 1 trial extension. *Diabetes Obes Metab*, *24*(8), 1553-1564. https://doi.org/10.1111/dom.14725

World Health Organization, W. (2023). *International Classification of Diseases, Eleventh Revision (ICD-11) (Version 01/2023)*. Retrieved 06.02.2024 from https://icd.who.int/browse11.

Wu, T., Hu, E., Xu, S., Chen, M., Guo, P., Dai, Z., Feng, T., Zhou, L., Tang, W., Zhan, L., Fu, X., Liu, S., Bo, X., & Yu, G. (2021). clusterProfiler 4.0: A universal enrichment tool for interpreting omics data. *Innovation (Camb)*, *2*(3), 100141. https://doi.org/10.1016/j.xinn.2021.100141

Xourafa, G., Korbmacher, M., & Roden, M. (2024). Inter-organ crosstalk during development and progression of type 2 diabetes mellitus. *Nature Reviews Endocrinology*, *20*(1), 27-49. https://doi.org/10.1038/s41574-023-00898-1

Xu, B., Chen, L., Zhan, Y., Marquez, K. N. S., Zhuo, L., Qi, S., Zhu, J., He, Y., Chen, X., Zhang, H., Shen, Y., Chen, G., Gu, J., Guo, Y., Liu, S., & Xie, T. (2022). The Biological Functions and Regulatory Mechanisms of Fatty Acid Binding Protein 5 in Various Diseases. *Front Cell Dev Biol*, *10*, 857919. https://doi.org/10.3389/fcell.2022.857919

Yang, D., Krois, C. R., Huang, P., Wang, J., Min, J., Yoo, H. S., Deng, Y., & Napoli, J. L. (2017). Raldh1 promotes adiposity during adolescence independently of retinal signaling. *PloS one*, *12*(11), e0187669. https://doi.org/10.1371/journal.pone.0187669

Yang, K., Adin, C., Shen, Q., Lee, L. J., Yu, L., Fadda, P., Samogyi, A., Ham, K., Xu, L., Gilor, C., & Ziouzenkova, O. (2017). Aldehyde dehydrogenase 1 a1 regulates energy metabolism in adipocytes from different species. *Xenotransplantation*, *24*(5). https://doi.org/10.1111/xen.12318

Yang, Q. Y., Liang, J. F., Rogers, C. J., Zhao, J. X., Zhu, M. J., & Du, M. (2013). Maternal obesity induces epigenetic modifications to facilitate Zfp423 expression and enhance adipogenic differentiation in fetal mice. *Diabetes*, *62*(11), 3727-3735. https://doi.org/10.2337/db13-0433

Yasmeen, R., Reichert, B., Deiuliis, J., Yang, F., Lynch, A., Meyers, J., Sharlach, M., Shin, S., Volz, K. S., Green, K. B., Lee, K., Alder, H., Duester, G., Zechner, R., Rajagopalan, S., & Ziouzenkova, O. (2013). Autocrine function of aldehyde dehydrogenase 1 as a determinant of diet- and sex-specific differences in visceral adiposity. *Diabetes*, *62*(1), 124-136. https://doi.org/10.2337/db11-1779

Yu, X. X., Murray, S. F., Watts, L., Booten, S. L., Tokorcheck, J., Monia, B. P., & Bhanot, S. (2008). Reduction of JNK1 expression with antisense oligonucleotide improves adiposity in obese mice. *Am J Physiol Endocrinol Metab*, *295*(2), E436-445. https://doi.org/10.1152/ajpendo.00629.2007

Zebisch, K., Voigt, V., Wabitsch, M., & Brandsch, M. (2012). Protocol for effective differentiation of 3T3-L1 cells to adipocytes. *Anal Biochem*, *425*(1), 88-90, Article Journal Article Research Support,

Non-U.S. Gov't Journal Article Research Support, Non-U.S. Gov't. https://doi.org/10.1016/j.ab.2012.03.005

Zhang, H., Li, C., Xin, Y., Cui, X., Cui, J., & Zhou, G. (2020). Suppression of NSDHL attenuates adipogenesis with a downregulation of LXR-SREBP1 pathway in 3T3-L1 cells. *Biosci Biotechnol Biochem*, *84*(5), 980-988. https://doi.org/10.1080/09168451.2020.1719823

Zhang, Y., & Chua, S., Jr. (2017). Leptin Function and Regulation. *Compr Physiol*, *8*(1), 351-369. https://doi.org/10.1002/cphy.c160041

Ziouzenkova, O., Orasanu, G., Sharlach, M., Akiyama, T. E., Berger, J. P., Viereck, J., Hamilton, J. A., Tang, G., Dolnikowski, G. G., Vogel, S., Duester, G., & Plutzky, J. (2007). Retinaldehyde represses adipogenesis and diet-induced obesity. *Nat Med*, *13*(6), 695-702. https://doi.org/10.1038/nm1587

6 List of Abbreviations

ABCD2	ATP-binding cassette sub-family D member 2
ABHD1	Abhydrolase domain containing 1
Acaa1b	Acetyl-Coenzyme A acyltransferase 1B
Acaca	Acetyl-CoA carboxylase 1
ACACB	Acetyl-CoA carboxylase 2
ACBP	Acyl-CoA-binding protein
Ache	Acetylcholinesterase
ACLY	ATP-citrate synthase
ACN	Acetonitrile
ACOD1	Acyl-CoA desaturase 1
ACSL3	Acyl-CoA synthetase long-chain family member 3
ACSL3	Fatty acid CoA ligase Acsl3
ACSL6	Acyl-CoA synthetase long-chain family member 6
ACSM3	Acyl-coenzyme A synthetase ACSM3
Actb	actin beta
Adh	Alcohol dehydrogenase
ADH7	All-trans-retinol dehydrogenase
Adipoq	Adiponectin, C1Q and collagen domain containing
AGC	Automatic gain control
AGRP	Agouti-related protein
Aldh1a1	Aldehyde dehydrogenase family 1, subfamily A1
Aldh1a2	Aldehyde dehydrogenase family 1, subfamily A2
Aldh1a3	Aldehyde dehydrogenase family 1, subfamily A3
Aldh1a7	Aldehyde dehydrogenase family 1, subfamily A7
ALDH1L2	Mitochondrial 10-formyltetrahydrofolate dehydrogenase
ALDH3A2	Aldehyde dehydrogenase family 3 member A2
ANOVA	Analysis of variance
AUC	Area under curve
ASO	Antisense oligonucleotides
B2m	beta-2 microglobulin
Bbs2	Bardet-Biedl syndrome 2
BG	blood glucose
BMI	Body mass index
Bmp2	Bone morphogenetic protein 2
Bmp4	Bone morphogenetic protein 4
C3	Complement C3
CCK	Cholecystokinin
CD	Control diet
CD36	Cluster of differentiation 36
cDNA	complementary DANN
Cebpa	CCAAT/enhancer-binding protein alpha
CES1D	Carboxylesterase 1D
CHP1	Calcineurin B homologous protein 1
Cidea	Cell death-inducing DNA fragmentation factor, alpha subunit-like effector A
Cntnap2	Contactin associated protein-like 2
Col	Collagenase D
COVID-19	Coronavirus disease 2019
CPT1B	Carnitine O-palmitoyltransferase 1
Creb5	cAMP responsive element binding protein 5
CYP2F2	Cytochrome P450 2F2
DAB2	Disabled homolog 2
DBI	Diazepam binding inhibitor
DEG	Differentially expressed gene
Disp	Dispase II

DMEM	Dulbecco’s Modified Eagle Medium
DOGaD	Developmental origins of health and disease
DPBS	Dulbecco's phosphate buffered saline
DTT	Dithiothreitol
E%	Energy percent
E13.5	Embryonic age 13.5 days
Entpd6	Ectonucleoside triphosphate diphosphohydrolase
EPHX2	Bifunctional epoxide hydrolase 2
Fabp4	Fatty acid binding protein 4
FABP5	Fatty acid-binding protein 5
FADS3	Fatty acid desaturase 3
FAIMS	High field asymmetric waveform ion mobility spectrometry
Fasn	Fatty acid synthase
FASN	Fatty acid synthase
Fbn1	Fibrillin 1
FBS	Fetal bovine serum
FDR	False discovery rate
Fgf21	Fibroblast growth factor 21
FMC1	Protein FMC1 homolog
FMO1	Flavin-containing monooxygenase 1
Fto	FTO alpha-ketoglutarate dependent dioxygenase
Gapdh	glyceraldehyde-3-phosphate dehydrogenase
GDM	Gestational diabetes mellitus
GGT5	Glutathione hydrolase 5 proenzyme
GK	Glycerol kinase
GLP-1	Glucagon-like peptide 1
GO	Gene ontology
GSTP1	Glutathione S-transferase P 1
GWAS	Genome-wide association study
GWG	Gestional weight gain
H2-Q2	histocompatibility 2, Q region locus 2
HCD	High-caloric diet
Hprt	hypoxanthine guanine phosphoribosyl transferase
IBMX	3-isobutyl-1-methylxanthine
Il6	Interleukin 6
ipGTT	intraperitoneal glucose tolerance test
IVD	Isovaleryl coenzyme A dehydrogenase
Kdm5C	Lysine demethylase 5C
Kdm5D	Lysine demethylase 5D
Lep	Leptin
Mapk8	Mitogen-activated protein kinase 8
mat-CD	maternal control diet
mat-HCD	maternal high-caloric diet
Mc4r	Melanocortin 4 receptor
Mcp1	Monocyte Chemoattractant Protein-1
MCT	Medium-chain triglyceride
MEF	Mouse embryonic fibroblast
miRNA	micro RNA
MS	Mass spectroscopy
MYO5A	Unconventional myosin-Va
n-3 LC-PUFA	Omega-3 long-chain polyunstaturated fatty acid
NAAA	N-acylethanolamine-hydrolyzing acid amidase
NBCS	Newborn calf serum
Ncor2	Nuclear receptor co-repressor 2
NMRI	Naval Medical Research Institute

Nr1h3	nuclear receptor subfamily 1, group H, member 3
OR	Odds ratio
ORA	Over representation analysis
PCK1	Phosphoenolpyruvate carboxykinase
PDK1	Pyruvate dehydrogenase kinase isozyme 1
PFA	Formaldehyde
Pgc-1a	Peroxisome proliferative activated receptor, gamma, coactivator 1 alpha
Pgc-2	Pparg coactivator 2
PLPL2	Patatin-like phospholipase domain-containing protein 2
PLPL3	1-acylglycerol-3-phosphate O-acyltransferase Pnpla3
Pnpla3	Patatin-like phospholipase domain containing 3
POMC	Pro-opiomelanocortin
Pparg1	Peroxisome proliferator-activated receptor gamma 1
Pparg2	Peroxisome proliferator-activated receptor gamma 2
Rora	RAR-related orphan receptor alpha
RPKM	Reads per kilobase million
RPMI	Roswell Park Memorial Institute
RRBS	Reduced representation bisulfite sequencing
RT-qPCR	Reverse transcriptase quantitative polymerase chain reaction
SAT	Subcutaneous adipose tissue
Scand1	SCAN domain-containing 1
Scd1	Stearoyl-Coenzyme A desaturase 1
SDS	Sodium dodecyl sulfate
SEM	Standard error of the mean
siAldh1a1	Small interfering RNA knockdown of Aldehyde dehydrogenase family 1, subfamily A1
siAldh1a7	Small interfering RNA knockdown of Aldehyde dehydrogenase family 1, subfamily A7
siRNA	Small interfering RNA
siScand1	Small interfering RNA knockdown of SCAN domain-containing 1
Srebf1c	sterol regulatory element binding transcription factor 1c
T1D	Type 1 diabetes mellitus
T2D	Type 2 diabetes mellitus
Tbp	TATA box binding protein
THIKB	3-ketoacyl-CoA thiolase B
THNSL2	Threonine synthase-like 2
Tnf	Tumor necrosis factor
Trp53	Transformation related protein 53
Ttc39b	Tetratricopeptide repeat domain 39B
Ube2d2a	ubiquitin-conjugating enzyme E2D 2A
Ucp1	uncoupling protein 1
UDI	unique dual indexing
VAT	Visceral adipose tissue
Vstm2a	V-set and transmembrane domain containing 2A
WHO	World health organization
Zbtb7c	Zinc finger and BTB domain containing 7C
Zfp202	Zinc finger protein 202
Zfp423	Zinc finger protein 423

7 List of Figures

8 Acknowledgments

I express my gratitude to my supervisor Regina Ensenauer for granting me the opportunity to conduct research within your research group, and for your valuable scientific guidance and oversight.

Additionally, I extend my gratitude to Hadi Al-Hasani for serving as my first referee and for providing helpful insights and engaging discussions.

Furthermore, I would like to thank Soner Öner-Sieben for the great support, everyday talks, and mentoring you have provided. You helped me to keep going. I also want to thank the other members of our research group, Liesa Schumacher, Maximiliane Fritz, Thomas Hautzinger, and Angelina Markshausen for helpful chats and good laughs. My thanks go to all the people on our laboratory floor and especially Anette Seibt for all your help.

I also want to thank Bengt-Frederik Belgardt and his team Celina Uhlemeyer, Marlene Piribauer, Michael Rieck, Caroline Schlegel, Jennifer Kuboth, Anna Heusch, and Tim Dorweiler for welcoming me wholeheartedly to your team, for the support in the laboratory and helpful discussions. Special thanks go to Celina Uhlemeyer for your invaluable help, all the talks that helped to survive the long hours with the mice and the “vivid-wusel-weeks” and your ongoing friendship.

Many thanks go to every “VIVID” member for the good talks and laughs we shared at different get-togethers and retreats.

Next, I want to express my gratitude to all the collaboration partners Patrick Petzsch and Karl Köhrer from the Biological and Medical Research Center for the transcriptomic analysis, Sonja Hartwig and Stefan Lehr from the Proteome Analysis Unit for the proteomic analysis and Martin Wabitsch and his team for providing the SGBS cell line. Thank you for your contribution to this thesis.

Finally, I would like to thank my friends and family for all your encouragement and support. You always had an open ear for me, were understanding, and helped me to keep a life outside of work and science.

9 Declarations

Erklärung

Ich versichere an Eides Statt, dass die Dissertation von mir selbständig und ohne unzulässige fremde Hilfe unter Beachtung der „Grundsätze zur Sicherung guter wissenschaftlicher Praxis an der Heinrich-Heine-Universität Düsseldorf“ erstellt worden ist. Die aus fremden Quellen direkt oder indirekt übernommenen Gedanken sind ausnahmslos als solche kenntlich gemacht.

Die vorliegende Arbeit wurde weder in dieser noch in ähnlicher Form bei einer anderen akademischen Institution eingereicht.

Marten Schouwink

Düsseldorf, den 26. Mai 2024

Declaration

I hereby declare that I have written the present thesis independently, without assistance from external parties, and without the use of other resources than those indicated. The ideas taken directly or indirectly from external sources are duly acknowledged in the text.

The work, either in full or in part, has not been previously submitted to any other academic institution.

Marten Schouwink

Düsseldorf, 26th of June 2024

10 Further publications

Averdunk L, Huetzen MA, Moreno-Andrés D, Kalb R, McKee S, Hsieh TC, Seibt A, **Schouwink M**, Lalani S, Faqeih EA, Brunet T, Boor P, Neveling K, Hoischen A, Hildebrandt B, Graf E, Lu L, Jin W, Schaper J, Omer JA, Demaret T, Fleischer N, Schindler D, Krawitz P, Mayatepek E, Wieczorek D, Wang LL, Antonin W, Jachimowicz RD, von Felbert V, Distelmaier F. Biallelic variants in CRIPT cause a Rothmund-Thomson-like syndrome with increased cellular senescence. Genet Med. 2023 Jul;25(7):100836. doi:10.1016/j.gim.2023.100836. Epub 2023 Mar 31. PMID: 37013901

Jonuscheit M*, Uhlemeyer C*, Korzekwa B, **Schouwink M**, Öner-Sieben S, Ensenauer R, Roden M, Belgardt BF, Schrauwen-Hinderling VB. Post mortem analysis of hepatic volume and lipid content by magnetic resonance imaging and spectroscopy in fixed murine neonates. NMR Biomed. (accepted 14 February 2024), Original research article, *equally contributed

11 Supplementary Information

Supplementary Table S1: UDI indices used for demultiplexing of the respective samples UDI = unique dual indexing.

Sample ID	UDI_ID	i7 sequence	i5 sequence
002_0405_001	6	GCTTGTCA	GTATGTTC
002_0405_002	7	CAAGCTAG	CGCTATGT
002_0405_003	8	TGGATCGA	TATCGCAC
002_0405_004	9	AGTTCAGG	TCTGTTGG
002_0405_005	10	GACCTGAA	CTCACCAA
002_0405_006	11	TCTCTACT	GAACCGCG
002_0405_007	13	CCAAGTCT	TCATCCTT
002_0405_008	14	TTGGACTC	CTGCTTCC
002_0405_009	17	TAATACAG	GTGAATAT
002_0405_010	18	CGGCGTGA	ACAGGCGC

Overall information regarding the full length western blot pictures.

Each blot was imaged twice. Once to detect the chemiluminescent bands of the probed proteins and once to detect the size marker. To check the size of the detected bands the images were merged. For the protein quantification, the picture of only the chemiluminescent bands was used.

Protein standards used are indicated in the figure legends. PageRuler Plus Prestained Protein Ladder 10 to 250 kDa (Thermo Scientific) band sizes from high to low are 190, 115, 80, 70, 50, 30, 25, 15, 10 kDa. HiMark Pre-Stained HMW Protein Standard (Invitrogen) band sizes from high to low are 460, 268, 238, 171, 117, 71, 55, 41, 31 kDa.

Regarding Supplementary Figure S4 to Supplementary Figure S22: The experiment was repeated in three independent runs and samples were taken at the days 0, 2, 4, 7, 11, and 15 of differentiation. Samples in the different lanes will be indicated using the following pattern: run 1 – day 0 = 1-0. Furthermore, a positive control was run, which consisted of a protein lysate from the murine liver.

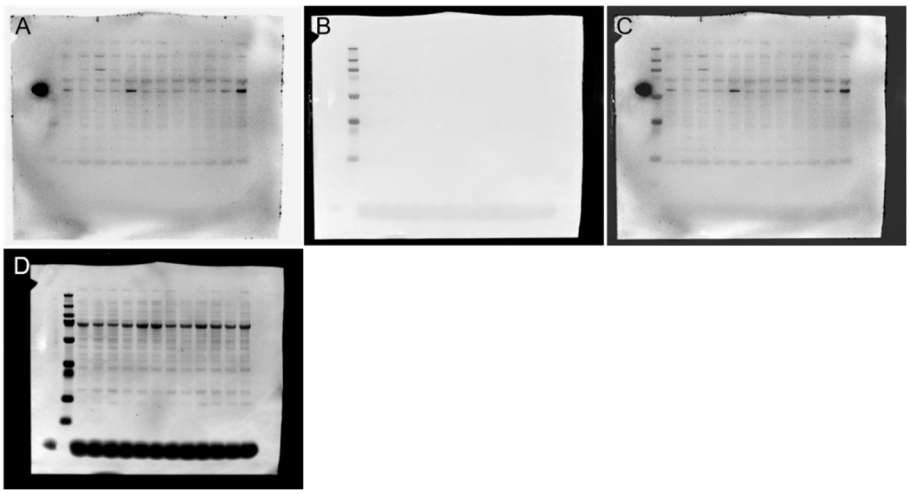

Supplementary Figure S1: Full length western blots – Blot 1.
Lanes: Liver, PageRuler Plus, mat-CD-1, mat-HCD-1, mat-HCD-2, mat-CD-2, mat-CD3, mat-HCD-3, mat-HCD-4, mat-CD-4, mat-CD-5, mat-HCD-5, mat-HCD-6, mat-CD6; A-B: probed for ALDH1A1; D: Ponceau S staining

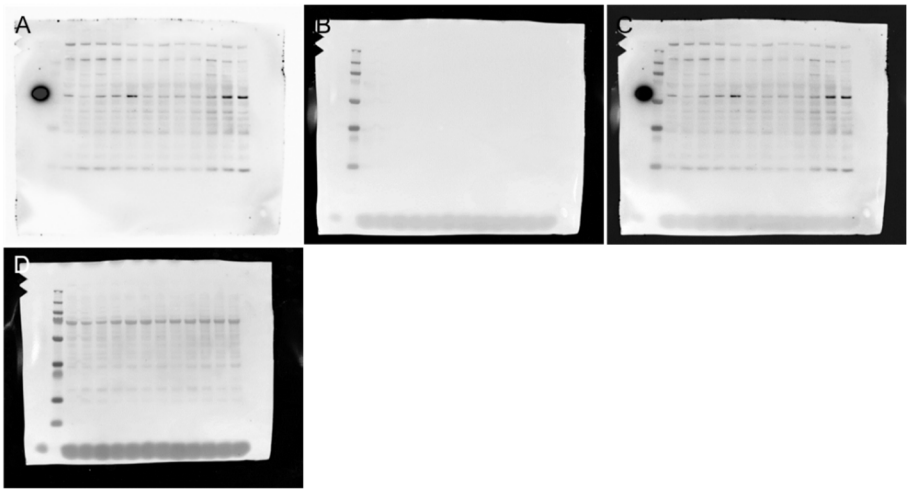

Supplementary Figure S2: Full length western blots – Blot 2.
Lanes: Liver, PageRuler Plus, mat-CD-1, mat-HCD-1, mat-HCD-2, mat-CD-2, mat-CD3, mat-HCD-3, mat-HCD-4, mat-CD-4, mat-CD-5, mat-HCD-5, mat-HCD-6, mat-CD6; A-B: probed for ALDH1A1; D: Ponceau S staining

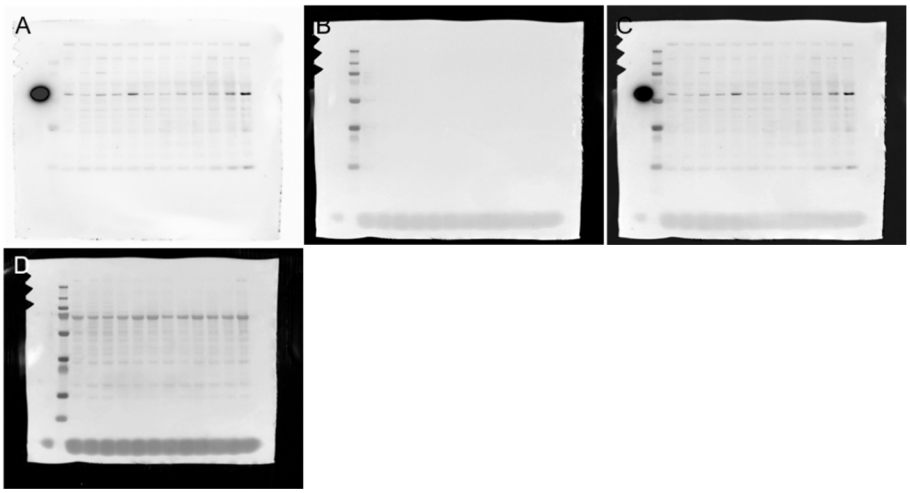

Supplementary Figure S3: Full length western blots – Blot 3.
Lanes: Liver, PageRuler Plus, mat-CD-1, mat-HCD-1, mat-HCD-2, mat-CD-2, mat-CD3, mat-HCD-3, mat-HCD-4, mat-CD-4, mat-CD-5, mat-HCD-5, mat-HCD-6, mat-CD6; A-B: probed for ALDH1A1; D: Ponceau S staining

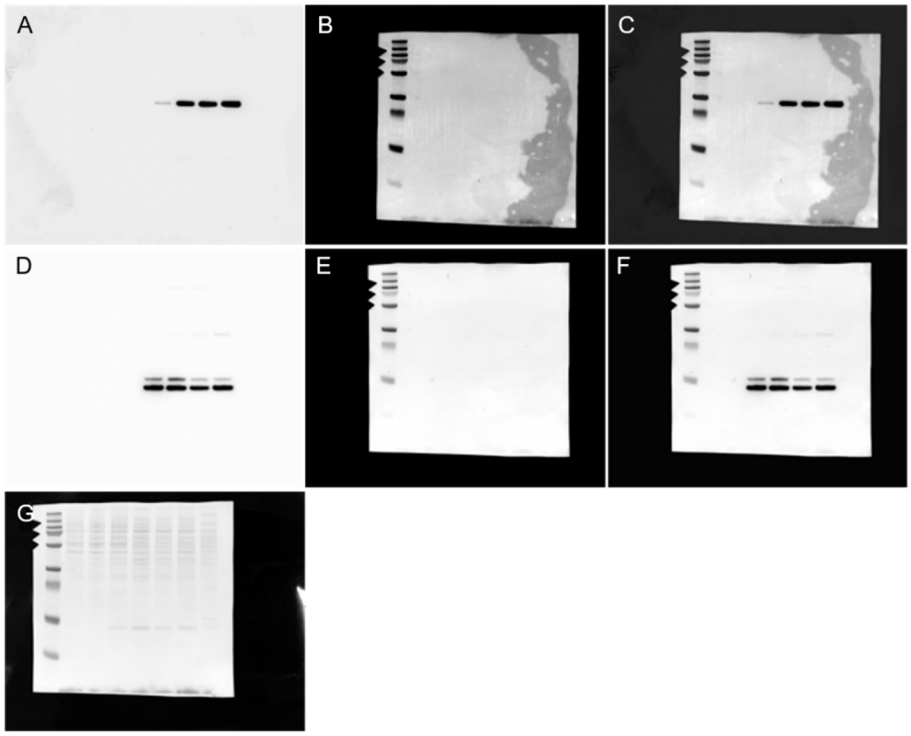

Supplementary Figure S4: Full length western blots – Blot 4.
Lanes: PageRuler Plus, 3-0, 3-2, 3-4, 3-7, 3-11, 3-15, positive control; A-C: probed for ADIPONECTIN; D-F: probed for FABP4, G: Ponceau S staining

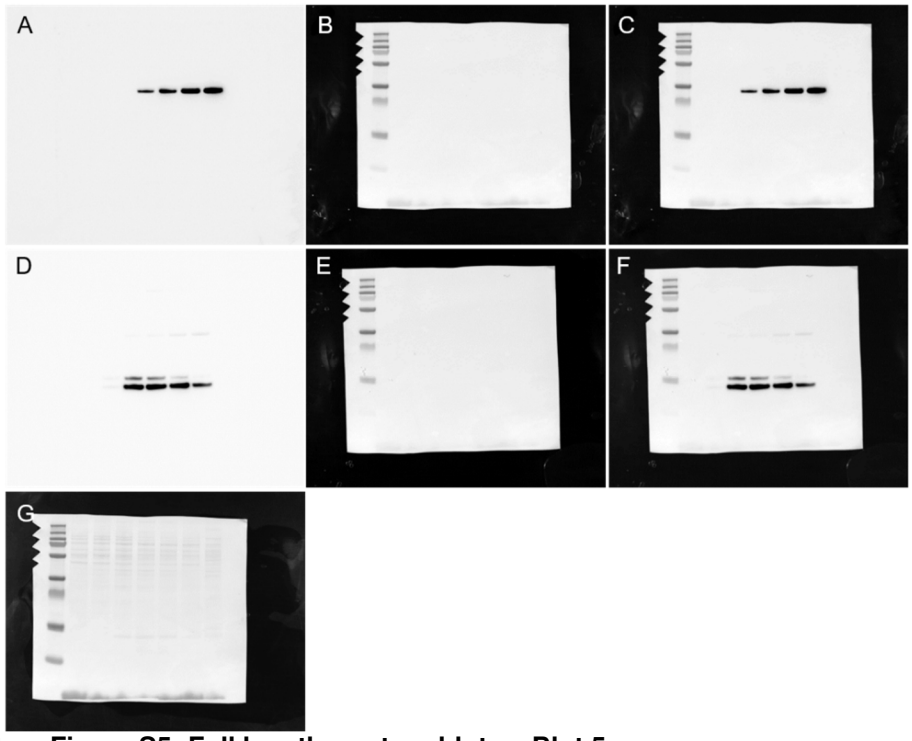

Supplementary Figure S5: Full length western blots – Blot 5.
Lanes: PageRuler Plus, 1-0, 1-2, 1-4, 1-7, 1-11, 1-15, positive control; A-C: probed for ADIPONECTIN; D-F: probed for FABP4, G: Ponceau S staining

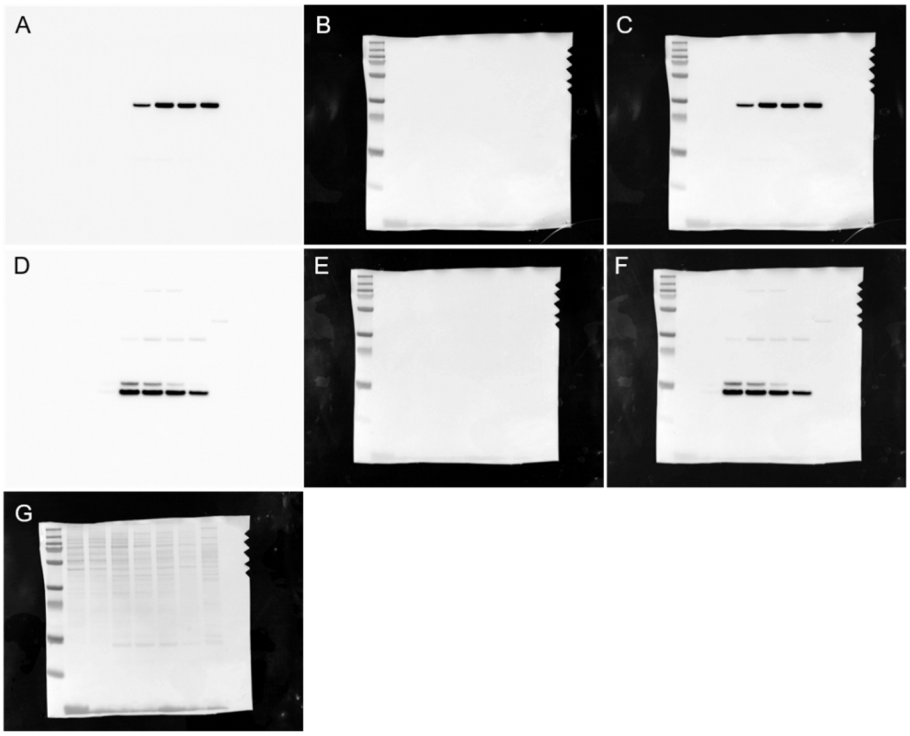

Supplementary Figure S6: Full length western blots – Blot 6.
Lanes: PageRuler Plus, 2-0, 2-2, 2-4, 2-7, 2-11, 2-15, positive control; A-C: probed for ADIPONECTIN; D-F: probed for FABP4, G: Ponceau S staining

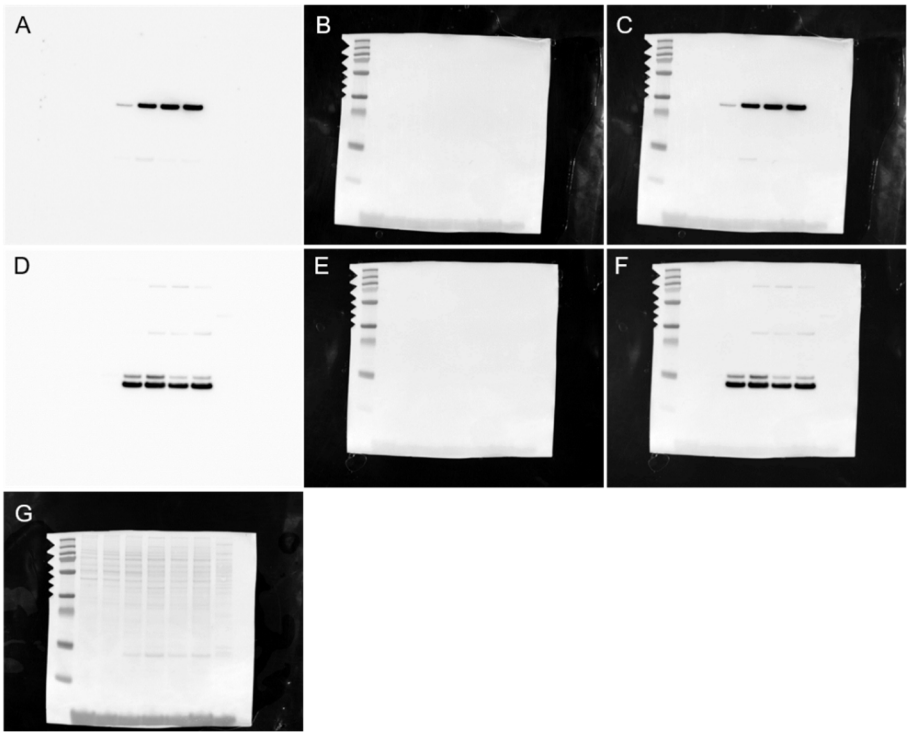

Supplementary Figure S7: Full length western blots – Blot 7.
Lanes: PageRuler Plus, 3-0, 3-2, 3-4, 3-7, 3-11, 3-15, positive control; A-C: probed for ADIPONECTIN; D-F: probed for FABP4, G: Ponceau S staining

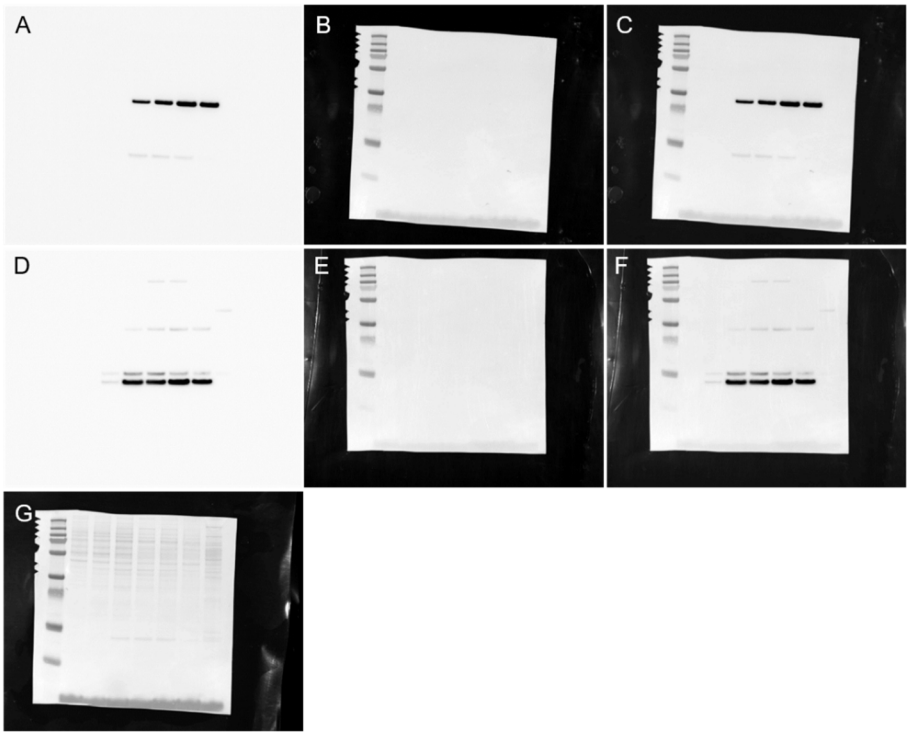

Supplementary Figure S8: Full length western blots – Blot 8.
Lanes: PageRuler Plus, 1-0, 1-2, 1-4, 1-7, 1-11, 1-15, positive control; A-C: probed for ADIPONECTIN; D-F: probed for FABP4, G: Ponceau S staining

Supplementary Figure S9: Full length western blots – Blot 9.
Lanes: PageRuler Plus, 2-0, 2-2, 2-4, 2-7, 2-11, 2-15, positive control; A-C: probed for ADIPONECTIN; D-F: probed for FABP4, G: Ponceau S staining

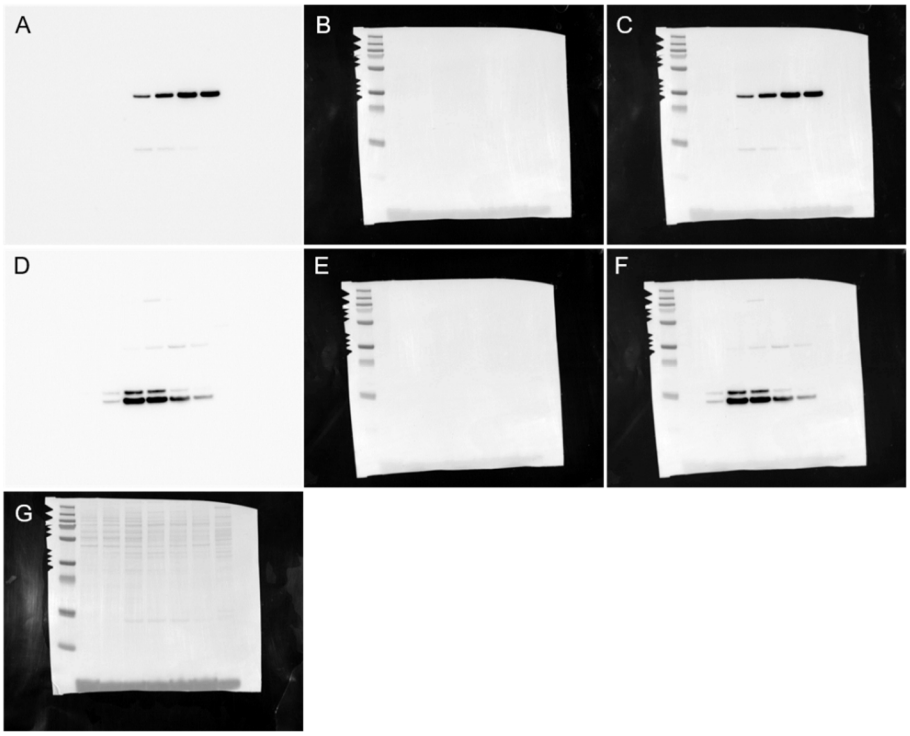

Supplementary Figure S10: Full length western blots – Blot 10.
Lanes: PageRuler Plus, 1-0, 1-2, 1-4, 1-7, 1-11, 1-15, positive control; A-C: probed for ADIPONECTIN; D-F: probed for FABP4, G: Ponceau S staining

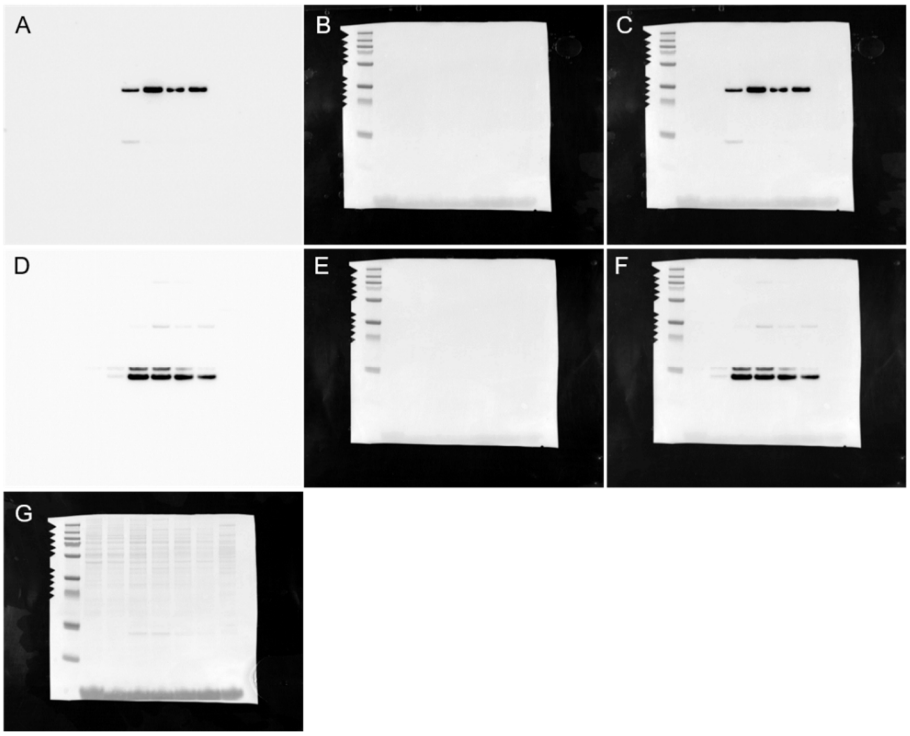

Supplementary Figure S11: Full length western blots – Blot 11.
Lanes: PageRuler Plus, 2-0, 2-2, 2-4, 2-7, 2-11, 2-15, positive control; A-C: probed for ADIPONECTIN; D-F: probed for FABP4, G: Ponceau S staining

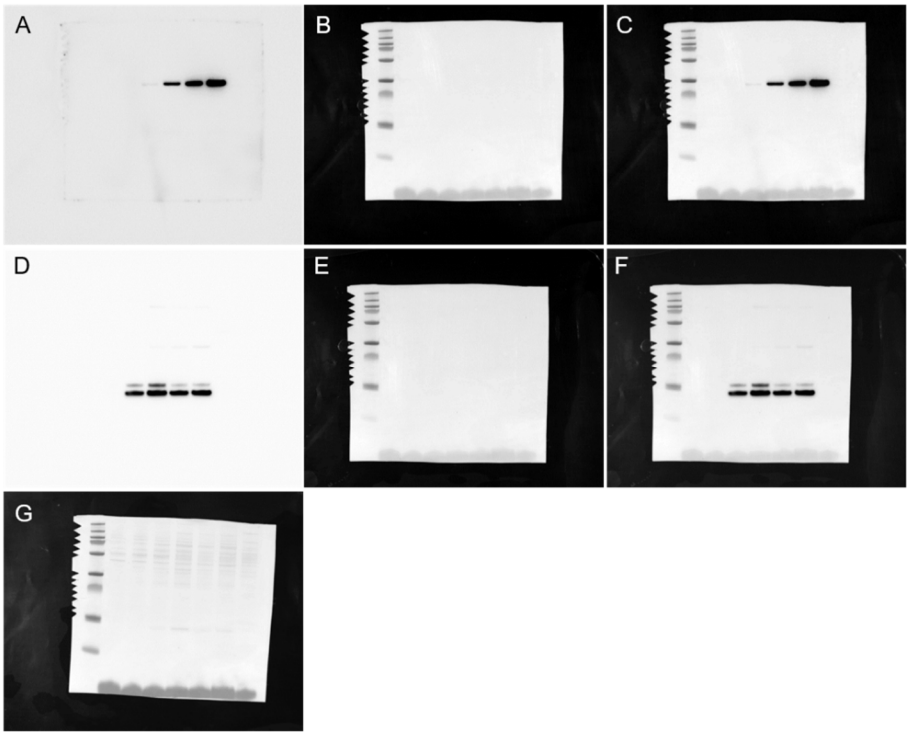

Supplementary Figure S12: Full length western blots – Blot 12.
Lanes: PageRuler Plus, 3-0, 3-2, 3-4, 3-7, 3-11, 3-15, positive control; A-C: probed for ADIPONECTIN; D-F: probed for FABP4, G: Ponceau S staining

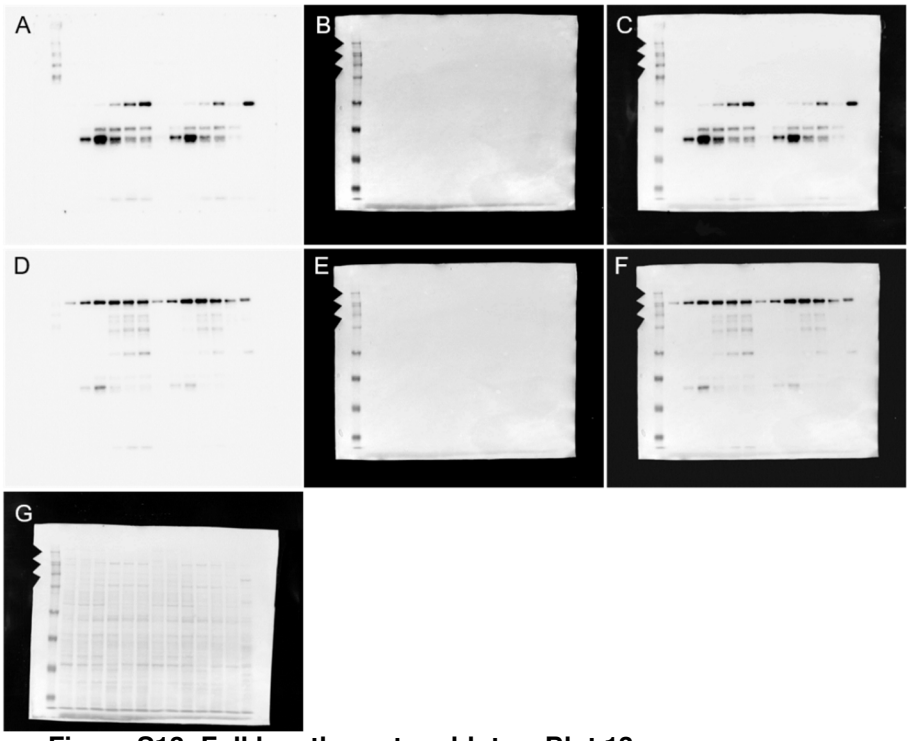

Supplementary Figure S13: Full length western blots – Blot 13.
Lanes: HiMark, 3-0, 3-2, 3-4, 3-7, 3-11, 3-15, 1-0, 1-2, 1-4, 1-7, 1-11, 1-15, positive control; A-C: probed for PPARG; D-F: probed for ACACA; G: Ponceau S staining

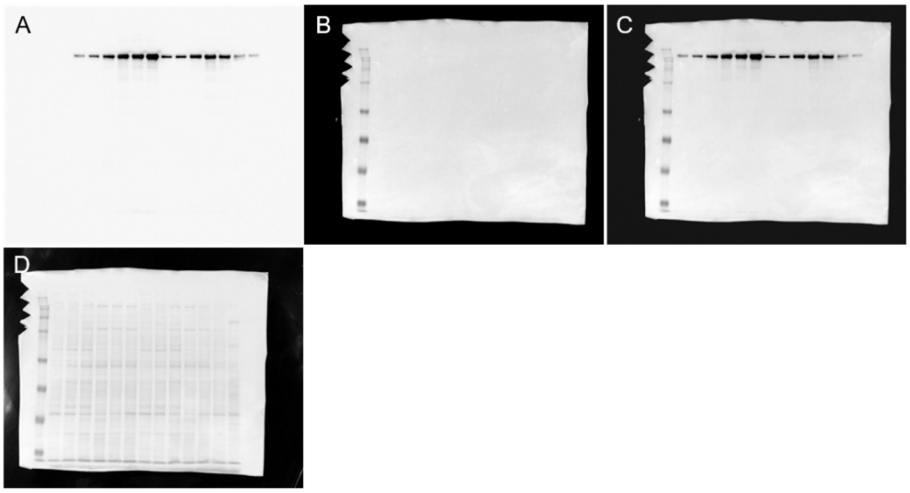

Supplementary Figure S14: Full length western blots – Blot 14.
Lanes: HiMark, 3-0, 3-2, 3-4, 3-7, 3-11, 3-15, 1-0, 1-2, 1-4, 1-7, 1-11, 1-15, positive control; A-C: probed for FASN; D: Ponceau S staining

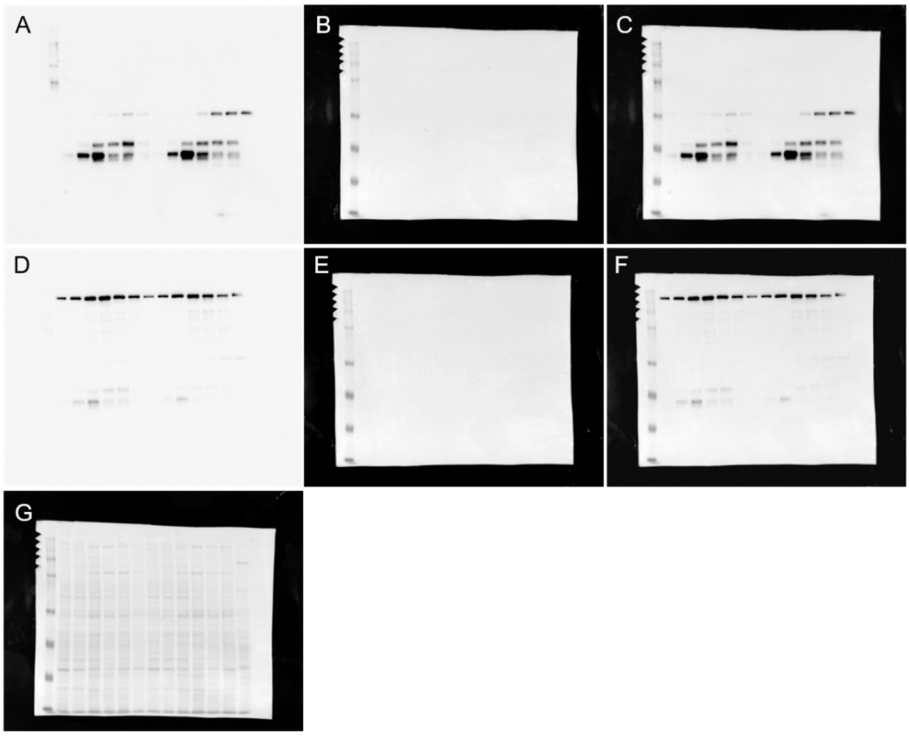

Supplementary Figure S15: Full length western blots – Blot 15.
Lanes: HiMark, 2-0, 2-2, 2-4, 2-7, 2-11, 2-15, 3-0, 3-2, 3-4, 3-7, 3-11, 3-15, positive control; A-C: probed for PPARG; D-F: probed for ACACA, G: Ponceau S staining

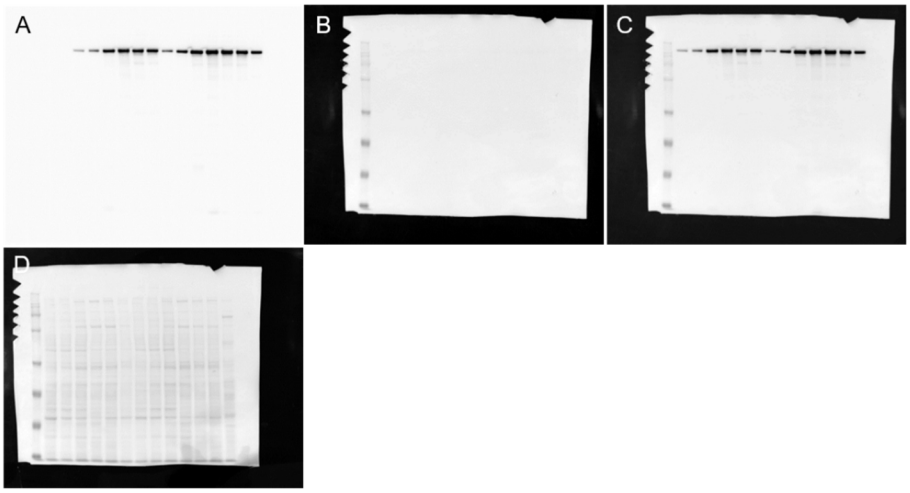

Supplementary Figure S16: Full length western blots – Blot 16.
Lanes: HiMark, 2-0, 2-2, 2-4, 2-7, 2-11, 2-15, 3-0, 3-2, 3-4, 3-7, 3-11, 3-15, positive control; A-C: probed for FASN; D: Ponceau S staining

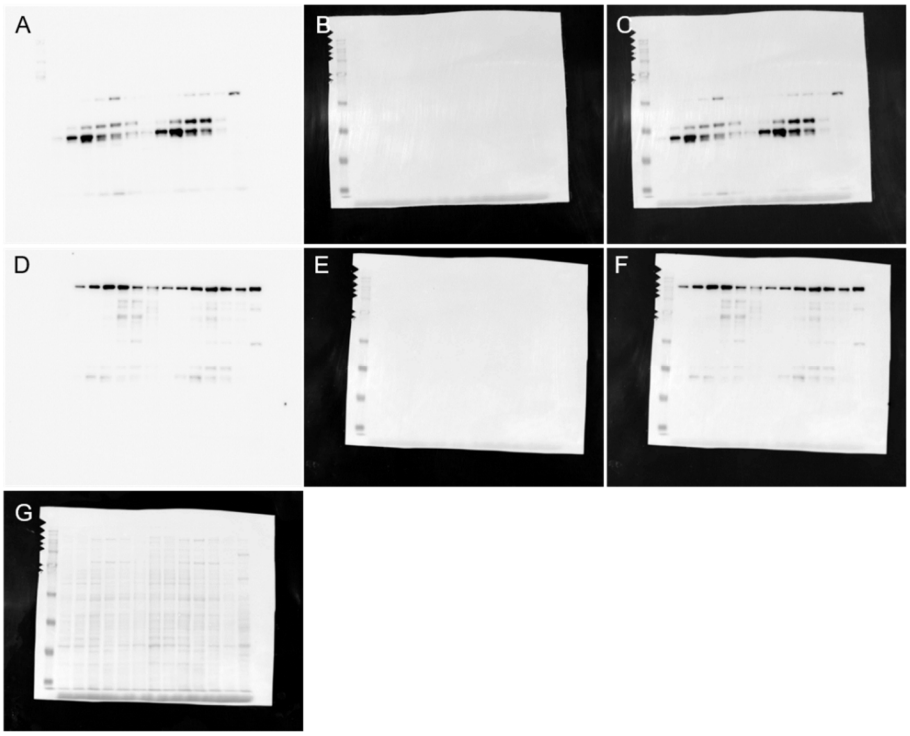

Supplementary Figure S17: Full length western blots – Blot 17.
Lanes: HiMark, 1-0, 1-2, 1-4, 1-7, 1-11, 1-15, 2-0, 2-2, 2-4, 2-7, 2-11, 2-15, positive control; A-C: probed for PPARG; D-F: probed for ACACA, G: Ponceau S staining

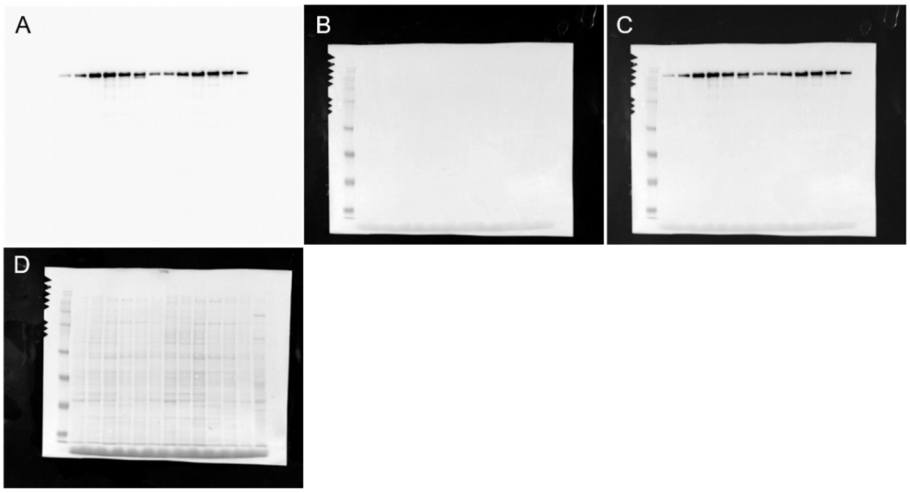

Supplementary Figure S18: Full length western blots – Blot 18.
Lanes: HiMark, 1-0, 1-2, 1-4, 1-7, 1-11, 1-15, 2-0, 2-2, 2-4, 2-7, 2-11, 2-15, positive control; A-C: probed for FASN; D: Ponceau S staining

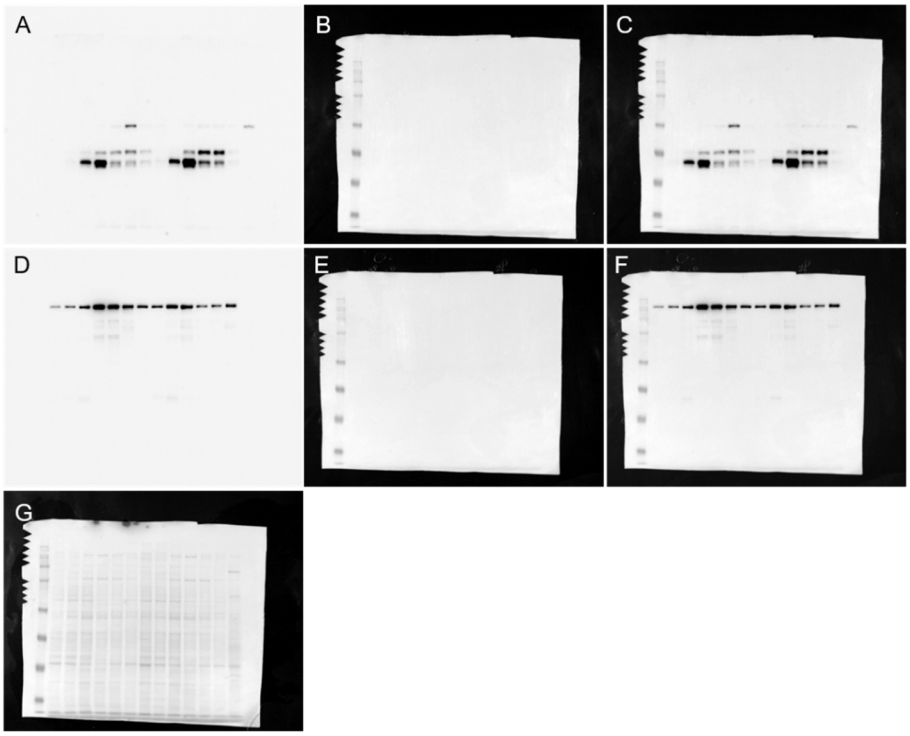

Supplementary Figure S19: Full length western blots – Blot 19.
Lanes: HiMark, 1-0, 1-2, 1-4, 1-7, 1-11, 1-15, 2-0, 2-2, 2-4, 2-7, 2-11, 2-15, positive control; A-C: probed for PPARG; D-F: probed for ACACA, G: Ponceau S staining

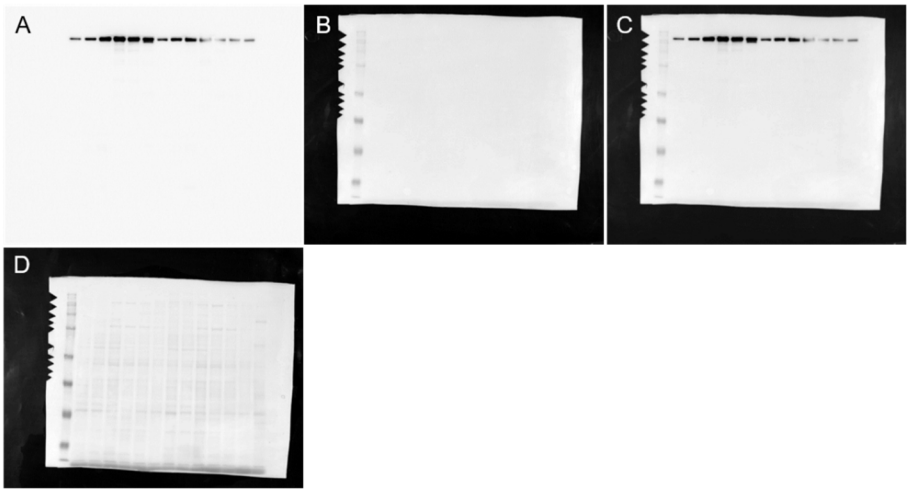

Supplementary Figure S20: Full length western blots – Blot 20.
Lanes: HiMark, 1-0, 1-2, 1-4, 1-7, 1-11, 1-15, 2-0, 2-2, 2-4, 2-7, 2-11, 2-15, positive control; A-C: probed for FASN; D: Ponceau S staining

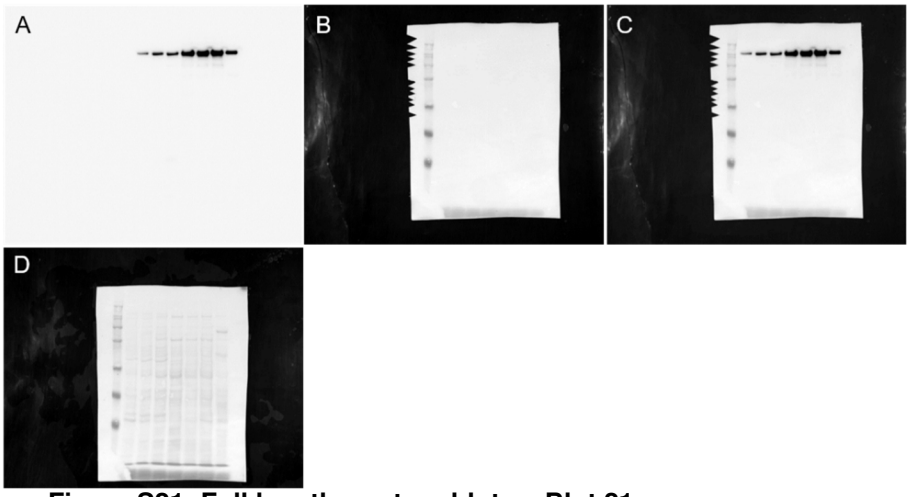

Supplementary Figure S21: Full length western blots – Blot 21.
Lanes: HiMark, 3-0, 3-2, 3-4, 3-7, 3-11, 3-15, positive control; A-C: probed for FASN; D: Ponceau S staining

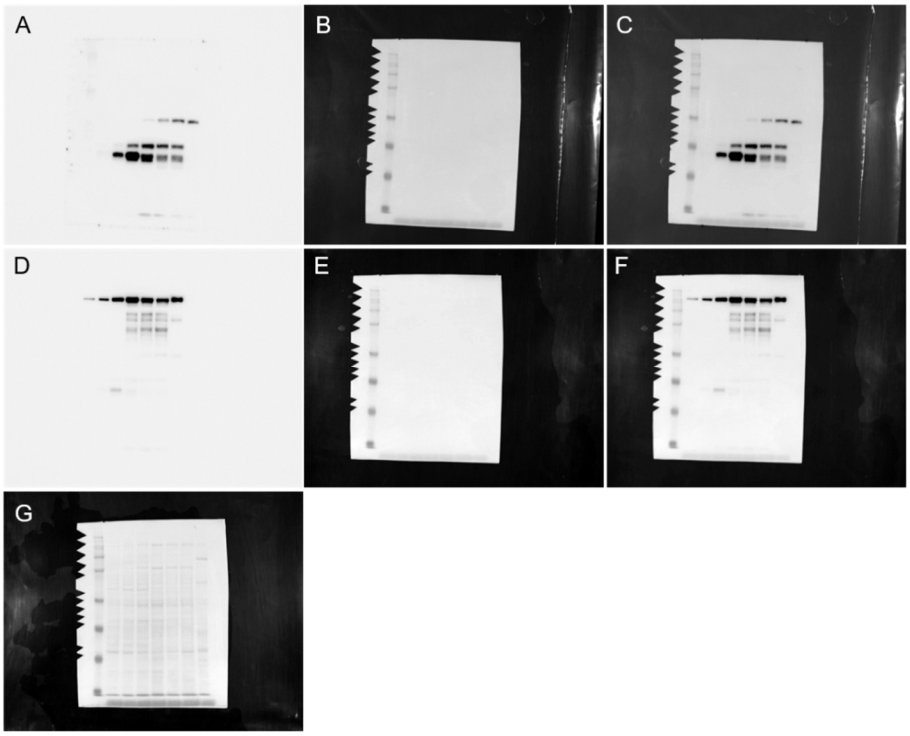

Supplementary Figure S22: Full length western blots – Blot 22.
Lanes: HiMark, 3-0, 3-2, 3-4, 3-7, 3-11, 3-15, positive control; A-C: probed for PPARG; D-F: probed for ACACA, G: Ponceau S staining

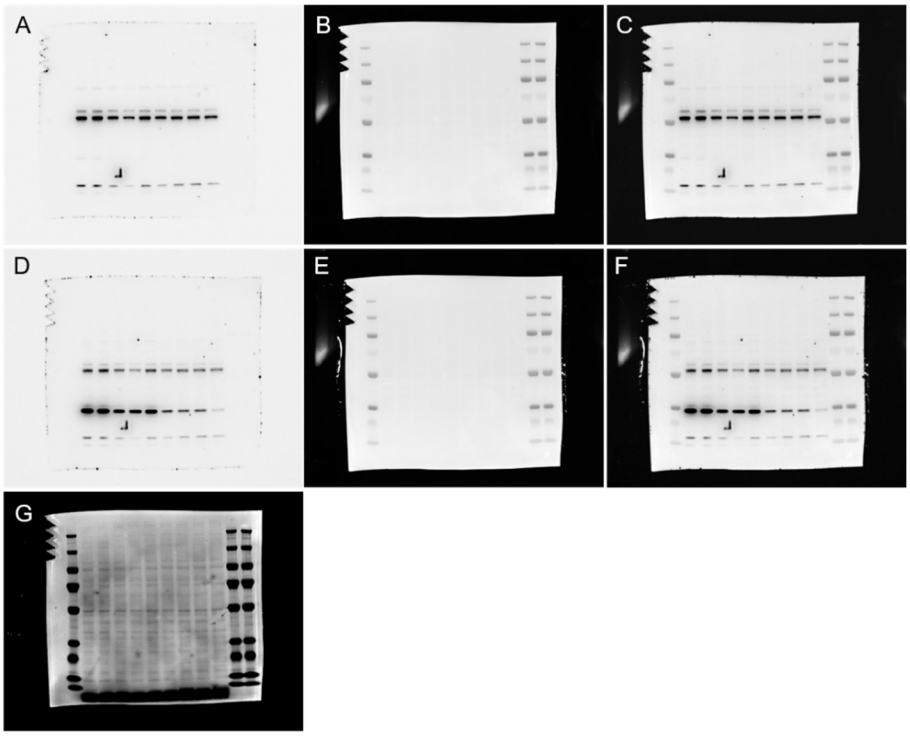

Supplementary Figure S23: Full length western blots – Blot 23.
Lanes: PageRuler Plus, Control-1, Control-2, Control-3, siAldh1a1-1, siAldh1a1-2, siAldh1a1-3, siAldh1a7-1, siAldh1a7-2, siAldh1a7-3, PageRuler Plus, PageRuler Plus; A-C: probed for PPARG; D-F: probed for ADIPONECTIN, G: Ponceau S staining

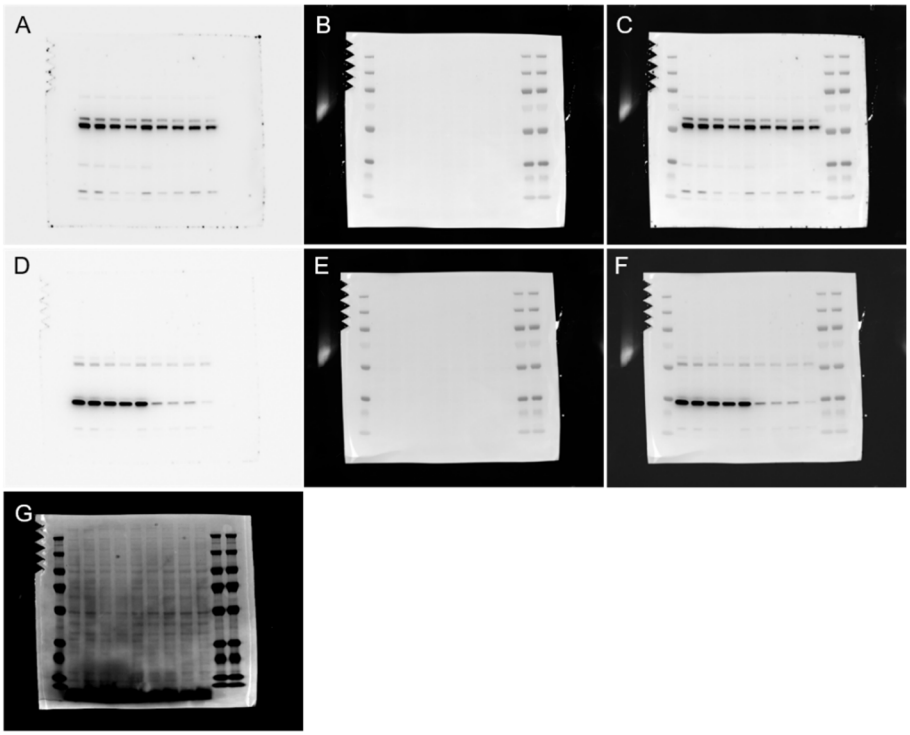

Supplementary Figure S24: Full length western blots – Blot 24.
Lanes: PageRuler Plus, Control-1, Control-2, Control-3, siAldh1a1-1, siAldh1a1-2, siAldh1a1-3, siAldh1a7-1, siAldh1a7-2, siAldh1a7-3, PageRuler Plus, PageRuler Plus; A-C: probed for PPARG; D-F: probed for ADIPONECTIN, G: Ponceau S staining

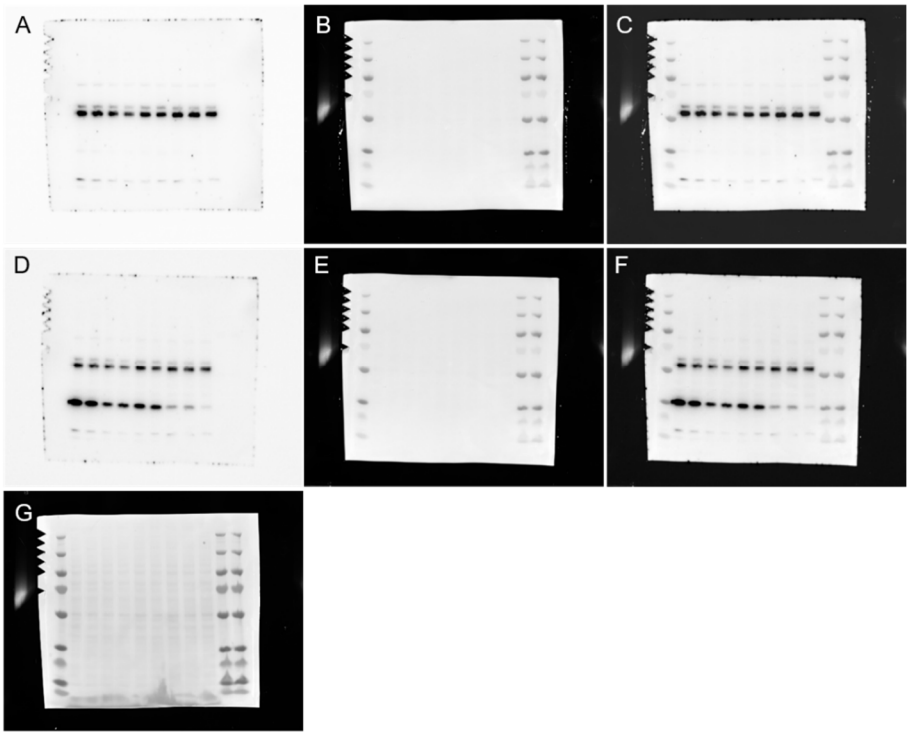

Supplementary Figure S25: Full length western blots – Blot 25.
Lanes: PageRuler Plus, Control-1, Control-2, Control-3, siAldh1a1-1, siAldh1a1-2, siAldh1a1-3, siAldh1a7-1, siAldh1a7-2, siAldh1a7-3, PageRuler Plus, PageRuler Plus; A-C: probed for PPARG; D-F: probed for ADIPONECTIN, G: Ponceau S staining

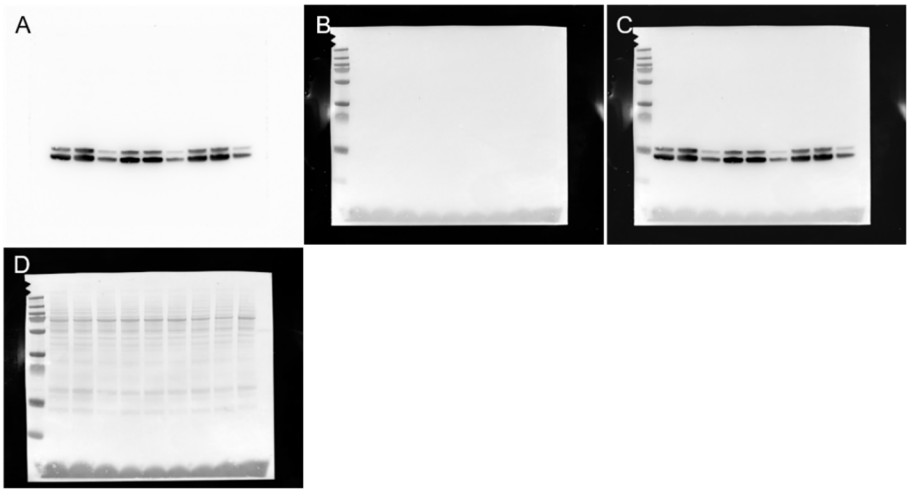

Supplementary Figure S26: Full length western blots – Blot 26.
Lanes: PageRuler Plus, Control-1, siAldh1a1-1, siAldh1a7-1, Control-2, siAldh1a1-2, siAldh1a7-2, Control-3, siAldh1a1-3, siAldh1a7-3; A-C: probed for FABP4; D: Ponceau S staining

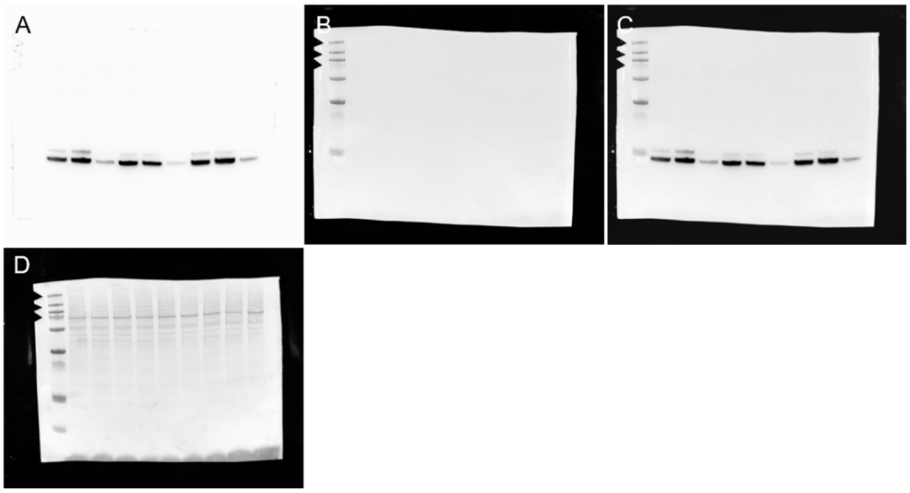

Supplementary Figure S27: Full length western blots – Blot 27.
Lanes: PageRuler Plus, Control-1, siAldh1a1-1, siAldh1a7-1, Control-2, siAldh1a1-2, siAldh1a7-2, Control-3, siAldh1a1-3, siAldh1a7-3; A-C: probed for FABP4; D: Ponceau S staining

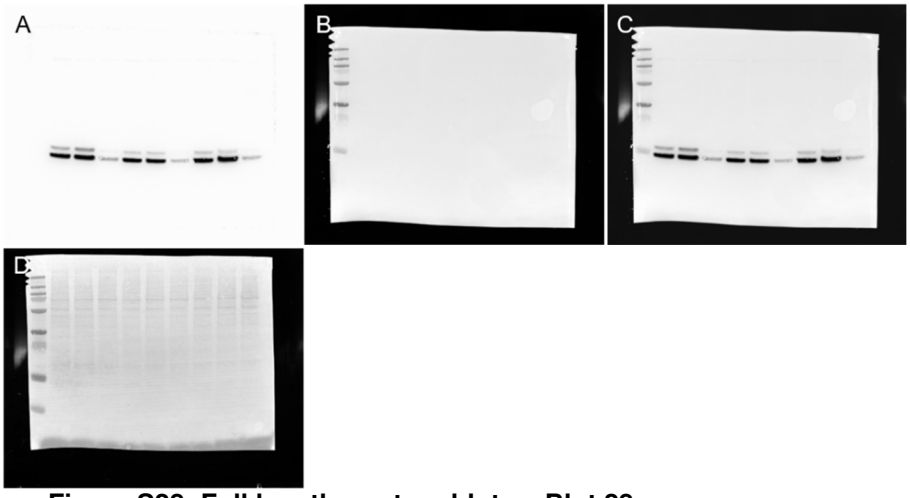

Supplementary Figure S28: Full length western blots – Blot 28.
Lanes: PageRuler Plus, Control-1, siAldh1a1-1, siAldh1a7-1, Control-2, siAldh1a1-2, siAldh1a7-2, Control-3, siAldh1a1-3, siAldh1a7-3; A-C: probed for FABP4; D: Ponceau S staining

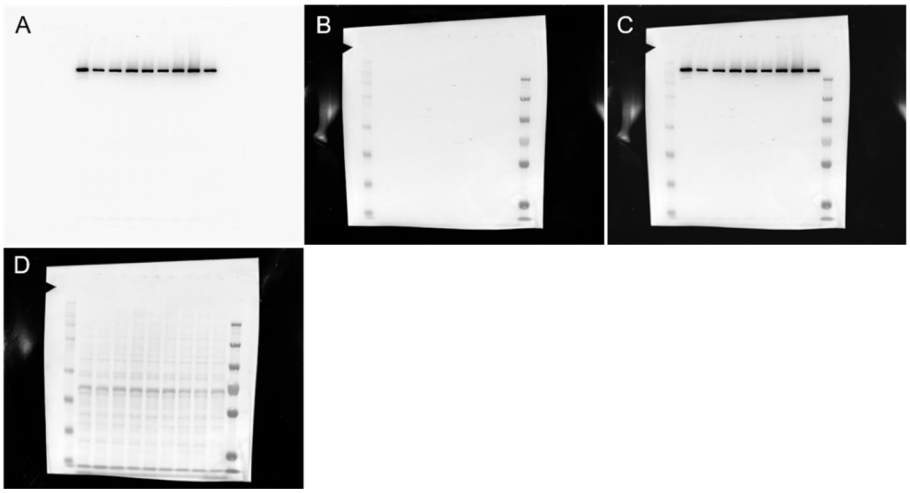

Supplementary Figure S29: Full length western blots – Blot 29.
Lanes: HiMark, Control-1, siAldh1a1-1, siAldh1a7-1, Control-2, siAldh1a1-2, siAldh1a7-2, Control-3, siAldh1a1-3, siAldh1a7-3, PageRuler Plus; A-C: probed for FABP4; D: Ponceau S staining

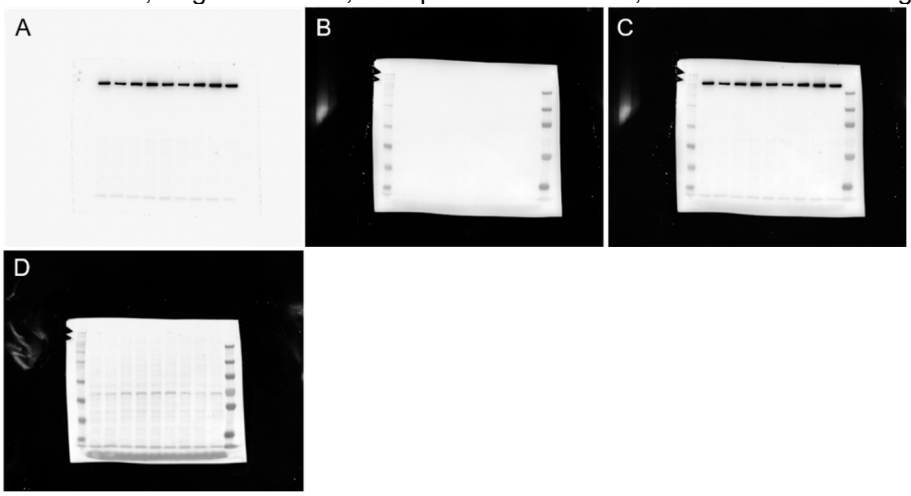

Supplementary Figure S30: Full length western blots – Blot 30.
Lanes: HiMark, Control-1, siAldh1a1-1, siAldh1a7-1, Control-2, siAldh1a1-2, siAldh1a7-2, Control-3, siAldh1a1-3, siAldh1a7-3, PageRuler Plus; A-C: probed for FABP4; D: Ponceau S staining

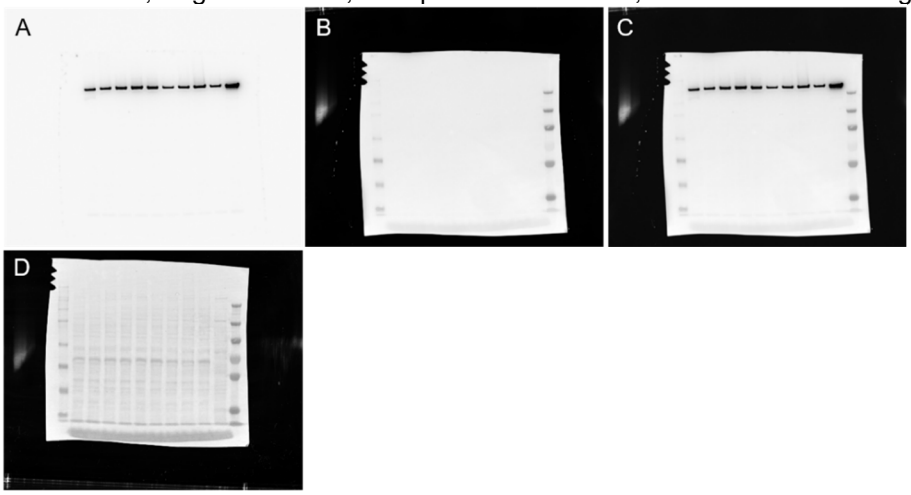

Supplementary Figure S31: Full length western blots – Blot 31.
Lanes: HiMark, Control-1, siAldh1a1-1, siAldh1a7-1, Control-2, siAldh1a1-2, siAldh1a7-2, Control-3, siAldh1a1-3, siAldh1a7-3, PageRuler Plus; A-C: probed for FABP4; D: Ponceau S staining